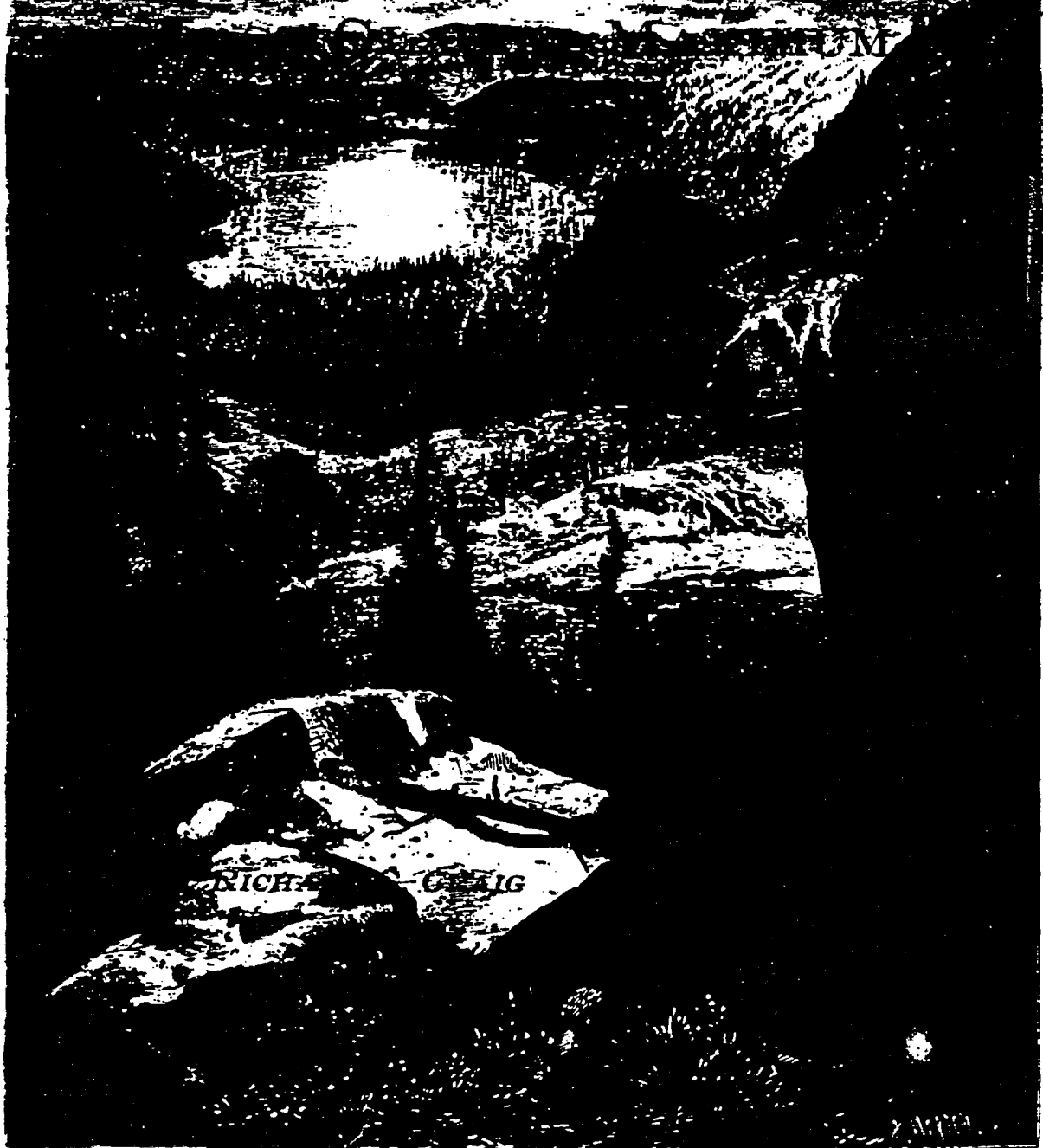


1404

Craig

(please put
in SCP
file)

CLIMATES AND LAKES
OF THE
DEATH VALLEY DRAINAGE SYSTEM
DURING THE
CENozoIC PERIOD



8803300262 880308
PDR WASTE PDR
WM-11

CLIMATES AND LAKES
OF THE
DEATH VALLEY DRAINAGE SYSTEM
DURING THE
LAST GLACIAL MAXIMUM

by

Richard G. Craig

with contributions from
Barry L. Roberts and Michael P. Singer

Department of Geology
Kent State University
Kent, Ohio 44242

Executive Summary

This report describes long-range climate models useful in studying the stability of the Nevada Test Site as a geologic repository for disposal of nuclear wastes. The long half-lives of transuranic elements that are a part of such wastes necessitate the consideration of stability for at least 10,000 years. During such a time span climate change is likely. Thus it becomes imperative to develop means of estimating the effects of such climate change upon the waste package.

We present a set of predictions of temperature, precipitation, evapotranspiration and runoff typical of a climatic extreme such as occurred in the recent geologic past (about 18,000 years ago). These are made for a large region surrounding the Nevada Test Site. Important tests of the reasonableness of these predictions are made. Lake configurations predicted under our 'model' climate are compared to those observed at present, on the one hand, and to those preserved in the geologic record (for 18,000 years ago) on the other. Both of these, as well as other tests, suggest our predictions are in accord with the actual conditions.

The procedure is briefly summarized; it has been described in detail in two previous reports to Battelle. The equations are derived from observed climate data using stepwise regression. Variables used can reflect other global climatic regimes such as a glaciation. We suggest future work that would enhance the applicability of this model to the nuclear waste assessment problem.

Specific conclusions from this study are as follows:

- . Quite precise estimates of the modern local climate on a detailed monthly basis are possible. About 65% to 95% of the variability of climate in this time range can be predicted.
- . Reasonably precise estimates of the local climate can also be made for conditions analogous to the last glacial maximum at which time a number of large lakes existed in the Southwest U.S.
- . Lakes comparable to those known from the geologic record are predicted for these climatic conditions. This provides some confidence in the detailed predictions.
- . Such a climate extreme will be characterized by 90% increase in precipitation. In areas presently arid, runoff will change very little, however, because of continued high evapotranspiration.
- . The most significant precipitation change is the dramatic increase in the Sierra Nevada Mountains. Runoff from these mountains will cause growth of lakes in a chain extending to the Panamint Valley. No significant lake is forecast for Death Valley.
- . Changes in temperature will be small and erratic. Increases will occur, as will decreases. Changes are highly site specific.
- . If lake evaporation rates also decrease by 27% a major lake will form in Death Valley. This agrees with previous geologic studies.
- . Such a climate change as forecast by our equations is likely to be accompanied by increased recharge rates. Groundwater flow conditions may be modified accordingly. Site stability could be influenced by these changes.

TABLE OF CONTENTS

	<u>Page</u>
Executive Summary	i
Table of Contents	iii
List of Tables -----	iv
List of Figures -----	v
Introduction -----	1
The Method of Climate Predictions -----	7
Predictions of Modern Climate -----	17
Temperature -----	17
Precipitation -----	35
Application to Other Geologic Boundary Conditions -	53
Predictions of Last Glacial Maximum Climate -----	58
Temperature -----	59
Precipitation -----	76
Solution of Total Runoff -----	85
Solution of Lake Configurations -----	102
Modern -----	102
Last Glacial Maximum -----	108
Pluvial Maximum -----	118
Conclusions -----	125
Future Work -----	129
Acknowledgements -----	136
References -----	140
Appendix -----	143

LIST OF TABLES

<u>Table</u>		<u>Page</u>
1.	Listing of all independent variables defined in the study of climate and available for stepwise regression predictions of precipitation and temperature -----	12
2.	Results of stepwise regressions to predict monthly mean temperatures -----	13
3.	Results of stepwise regressions to predict monthly mean precipitation -----	14
4.	Values of percent variance explained (adjusted R^2) and the standard errors for each of the regression equations -----	15
5.	Number of months for which the observed value at a station exceeds the predicted value by two standard errors (>2) and by three standard errors (>3) of the regression equation -----	18
6.	Measures of skewness (g_1) and kurtosis (g_2) of the residuals from the equations to predict temperature and precipitation -----	19
7.	Summary of our estimates of temperature change in the Southwest at the Last Glacial Maximum -----	75
8.	Summary of our estimates of precipitation change in the Southwest at the Last Glacial Maximum -----	81
9.	Statistical summary of regression testing for a linear relation between mean monthly change in the precipitation and the standard deviation of that change -----	83
10.	Values of the consumptive use coefficient, K , used in the Blaney-Criddle equation to estimate evapotranspiration -----	86
11.	Estimates of change in climate at the time of the last maximum pluvial event as reported in the literature -----	122

LIST OF FIGURES

<u>Figure</u>		<u>Page</u>
1.	Areas of interest in this study -----	2
2.	Configuration of lakes in the Death Valley drainage system at their last maximum stand in the Late Pleistocene -----	5
3.	Location of the 124 climate stations for which data were available -----	8
4.	Schematic illustration of the predictor variables defined for use in the climate equations -----	10
	Predicted temperatures for the entire level II area obtained using the regression equations. Predictions for each month are given as well as that for mean annual temperature. The top map in each figure is the prediction for modern conditions. The lower map is the prediction for the last glacial maximum conditions.	
5.	January modern (top) and last glacial maximum (bottom) temperatures -----	20
6.	February modern (top) and last glacial maximum (bottom) temperatures -----	21
7.	March modern (top) and last glacial maximum (bottom) temperatures -----	22
8.	April modern (top) and last glacial maximum (bottom) temperatures -----	23
9.	May modern (top) and last glacial maximum (bottom) temperatures -----	24
10.	June modern (top) and last glacial maximum (bottom) temperatures -----	25
11.	July modern (top) and last glacial maximum (bottom) temperatures -----	26
12.	August modern (top) and last glacial maximum (bottom) temperatures -----	27

LIST OF FIGURES (continued)

<u>Figure</u>		<u>Page</u>
13.	September modern (top) and last glacial maximum (bottom) temperatures -----	28
14.	October modern (top) and last glacial maximum (bottom) temperatures -----	29
15.	November modern (top) and last glacial maximum (bottom) temperatures -----	30
16.	December modern (top) and last glacial maximum (bottom) temperatures -----	31
17.	Mean annual modern (top) and last glacial maximum (bottom) temperatures -----	32
	Predicted precipitation, using the equations described, applied to the level II area. Predictions for each month are given as well as the total annual precipitation. The top map is the prediction based upon modern boundary conditions. The bottom map is the prediction for the last glacial maximum boundary conditions.	
18.	January modern (top) and last glacial maximum (bottom) precipitation -----	36
19.	February modern (top) and last glacial maximum (bottom) precipitation -----	37
20.	March modern (top) and last glacial maximum (bottom) precipitation -----	38
21.	April modern (top) and last glacial maximum (bottom) precipitation -----	39
22.	May modern (top) and last glacial maximum (bottom) precipitation -----	40
23.	June modern (top) and last glacial maximum (bottom) precipitation -----	41
24.	July modern (top) and last glacial maximum (bottom) precipitation -----	42

LIST OF FIGURES (continued)

<u>Figure</u>		<u>Page</u>
25.	August modern (top) and last glacial maximum (bottom) precipitation -----	43
26.	September modern (top) and last glacial maximum (bottom) precipitation -----	44
27.	October modern (top) and last glacial maximum (bottom) precipitation -----	45
28.	November modern (top) and last glacial maximum (bottom) precipitation -----	46
29.	December modern (top) and last glacial maximum (bottom) precipitation -----	47
30.	Total annual modern (top) and last glacial maximum (bottom) precipitation -----	48
	Change in temperature (top) and in precipitation (bottom) for each month of the year and for the yearly value. Comparison is made between the present and the last glacial maximum (18,000 yr BP) with positive values indicating an increase in the value at the last glacial maximum over that predicted for today.	
31.	January temperature change (top) and precipitation change (bottom) -----	62
32.	February temperature change (top) and precipitation change (bottom) -----	63
33.	March temperature change (top) and precipitation change (bottom) -----	64
34.	April temperature change (top) and precipitation change (bottom) -----	65
35.	May temperature change (top) and precipitation change (bottom) -----	66
36.	June temperature change (top) and precipitation change (bottom) -----	67

LIST OF FIGURES (continued)

<u>Figure</u>		<u>Page</u>
37.	July temperature change (top) and precipitation change (bottom) -----	68
38.	August temperature change (top) and precipitation change (bottom) -----	69
39.	September temperature change (top) and precipitation change (bottom) -----	70
40.	October temperature change (top) and precipitation change (bottom) -----	71
41.	November temperature change (top) and precipitation change (bottom) -----	72
42.	December temperature change (top) and precipitation change (bottom) -----	73
43.	Annual temperature change (top) and precipitation change (bottom) -----	75
44.	Relation between the monthly mean change in precipitation and the standard deviation of that change -----	82
	Predicted potential evapotranspiration obtained from the Blaney-Criddle equation. Predictions for February and August are given as well as the annual total. The top map is the prediction based upon predicted modern temperatures. The bottom map is the prediction based upon predicted temperatures at the last glacial maximum.	
45.	February modern (top) and last glacial maximum (bottom) evapotranspiration -----	87
46.	August modern (top) and last glacial maximum (bottom) evapotranspiration -----	88
47.	Annual modern (top) and last glacial maximum (bottom) evapotranspiration -----	89
48.	Relation between evapotranspiration and depth to the water table (from: Tanner, 1957, figure 7) -----	91

LIST OF FIGURES (continued)

<u>Figure</u>		<u>Page</u>
49.	Annual potential evapotranspiration for the area as reported by the Department of Commerce (1968, Plate 2) -----	92
	Predicted runoff in the level II area. Predictions for February and August are given as well as the annual total. The top map is predicted modern runoff. The bottom map is the predicted last glacial maximum runoff. Runoff is computed as precipitation minus evapotranspiration and set equal to zero where deficits occur.	
50.	February modern (top) and last glacial maximum (bottom) runoff -----	96
51.	August modern (top) and last glacial maximum (bottom) runoff -----	97
52.	Annual total modern (top) and last glacial maximum (bottom) runoff -----	98
53.	Observed values of runoff under present climatic conditions in the Southwest -----	99
54.	Convergence to an equilibrium configuration of lakes illustrated by the water surface elevation of Lake Owens at each 10 year time step of a 1000 year simulation -----	103
55.	Configuration of lakes in the Death Valley drainage system that are in equilibrium with the estimated modern runoff computed with our climate equations -----	104
56.	Relation between lake evaporation and elevation. These values are from Mifflin and Wheat (1979) -----	105
57.	Observed modern lake configurations (dark shading) in the Death Valley drainage system -----	106
58.	Change in total annual runoff between the present and the last glacial maximum -----	112

LIST OF FIGURES (continued)

<u>Figure</u>		<u>Page</u>
59.	Convergence to an equilibrium configuration of lakes illustrated by the water surface elevation of Lake Searles at each 10 year time step of a 1000 year simulation -----	114
60.	Configuration of lakes in the Death Valley drainage system that are in equilibrium with the estimated last glacial maximum runoff -----	115
61.	Configuration of lakes in the Death Valley drainage system that are in equilibrium with the estimated last glacial maximum runoff coupled with a 30% reduction in lake evaporation rates -----	119

INTRODUCTION

The primary objective of this study is to define a method capable of specifying the boundary conditions controlling the behaviour of the groundwater system in the area of Yucca Mountain, Nevada (Figure 1). With such a specification available it will be possible to model groundwater flow through the repository and estimate the effects of such flow upon the stability of the site.

Of greatest interest as an external control upon the hydrogeologic system is the amount of recharge to be expected. Because recharge varies significantly throughout the area, and because this variability itself influences the configuration and behaviour of that system, it is necessary to specify these recharge values at a large number of points within the area. Since a finite difference approach is being used to model groundwater flow, it is most helpful to have recharge specified at each node of a large and detailed grid.

Recharge rate is largely a function of the amount of precipitation falling on the area. It is also decreased through evapotranspiration, itself controlled by temperature. Thus good estimates of recharge require accurate predictions of the precipitation and temperature within the region.

Both of these vary with elevation. This is the so-called orographic effect. Another aspect of the orographic

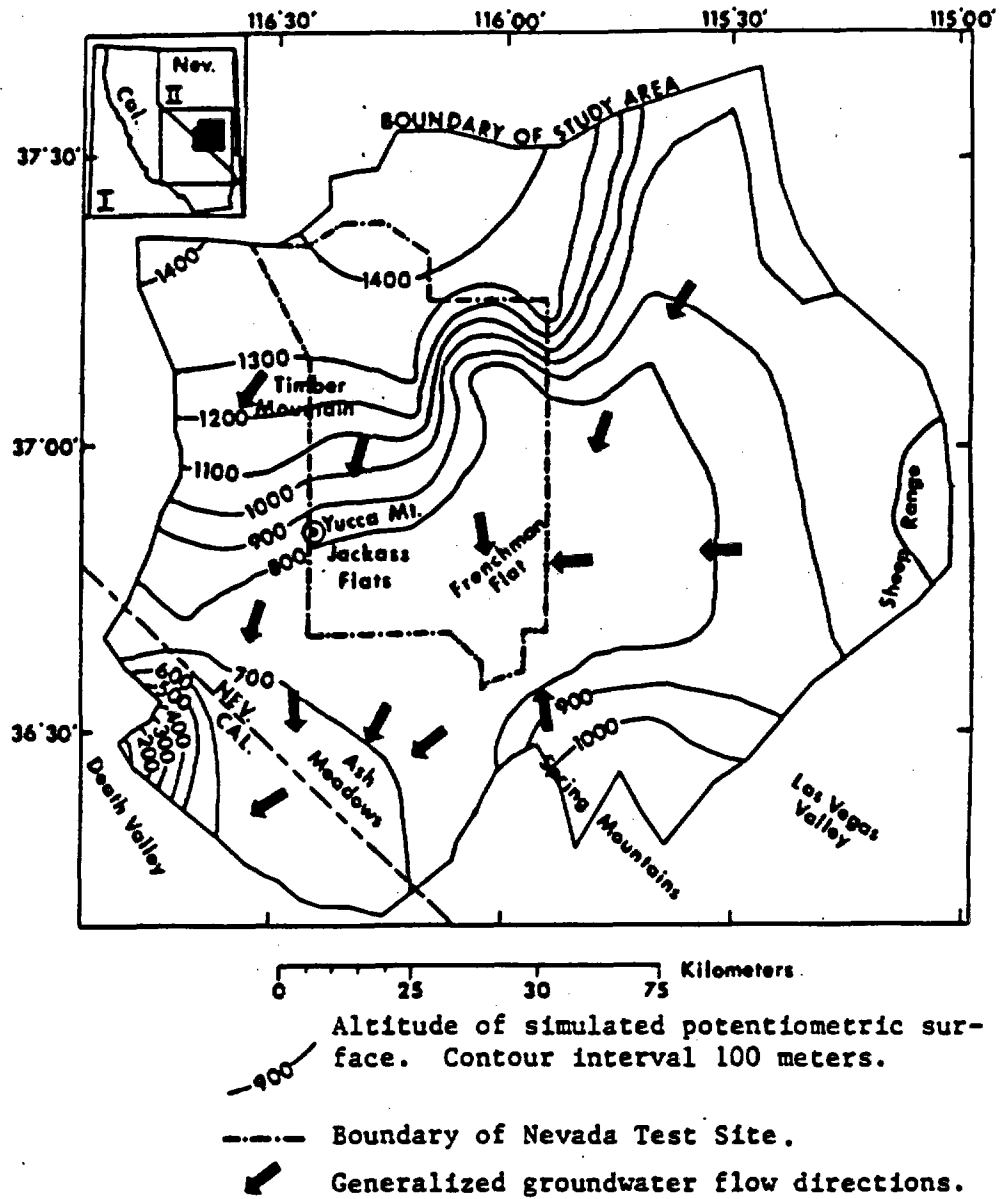


Figure 1. Area of interest in this study. Boundaries of the groundwater flow system, potentiometric surface contours and flow directions are from Waddell (1982, p. 33, fig. 3, and p. 3, fig. 1). This is termed the level III area. The level I and II areas are shown on the inset.

effect produces rainshadows downwind from major topographic obstacles. Precipitation is also limited by the amount of precipitable water and, because the dominant winds come from the Pacific Ocean, this is ultimately affected by patterns of sea surface temperatures. It is the sea-surface temperature pattern which controls the rate of evaporation of water from the ocean that will be carried inland as available moisture. Thus a large number of factors enter into the system of climatic variability within the area of concern.

Through the use of statistical procedures, we create a set of equations that describe the relation between these controlling factors and the climate that results. These equations are constructed using least squares procedures coupled with a stepwise regression iterative solution. A total of 37 independent variables are defined for use in the regressions. Ultimately, we derive equations for precipitation and temperature in each month of the year.

To allow application of these equations to create a grid of predicted values for use in the finite difference flow models, we must be able to specify values of the independent (or predictor) variables at each of these points. This is achieved by means of computer code. Computations make use of a grid of elevation data and reported values of sea surface temperature and dominant wind directions.

A site such as the proposed repository at Yucca Mountain must be stable for an extended period of time (over 10,000 years) because of the long-lived radioactive material to be contained within it. Thus we must concern ourselves with the possibility of changes in the hydrogeologic system that could have impact upon the repository. For clues about the changes that may be anticipated we must make use of the geologic record.

This record clearly shows that climate has not remained stable within the area of concern. Although the ultimate discharge point of groundwater passing beneath Yucca Mountain (Death Valley) is now arid and inhospitable, it was (over 25,000 years ago) the site of a major lake (Manly) nearly 200m deep (Figure 2). If conditions once again return to this state, will the repository remain stable? To answer this question we must once again rely upon the hydrogeologic models. Again estimates of the climatic conditions must be made available.

The equations previously described were developed using predictor variables that can be quite precisely specified in such climatic extremes. Only three variables need be determined: sea surface temperature, sea level and dominant wind directions. Exhaustive geologic research has in recent years made available estimates of sea surface temperatures and the amount of sea level lowering at the

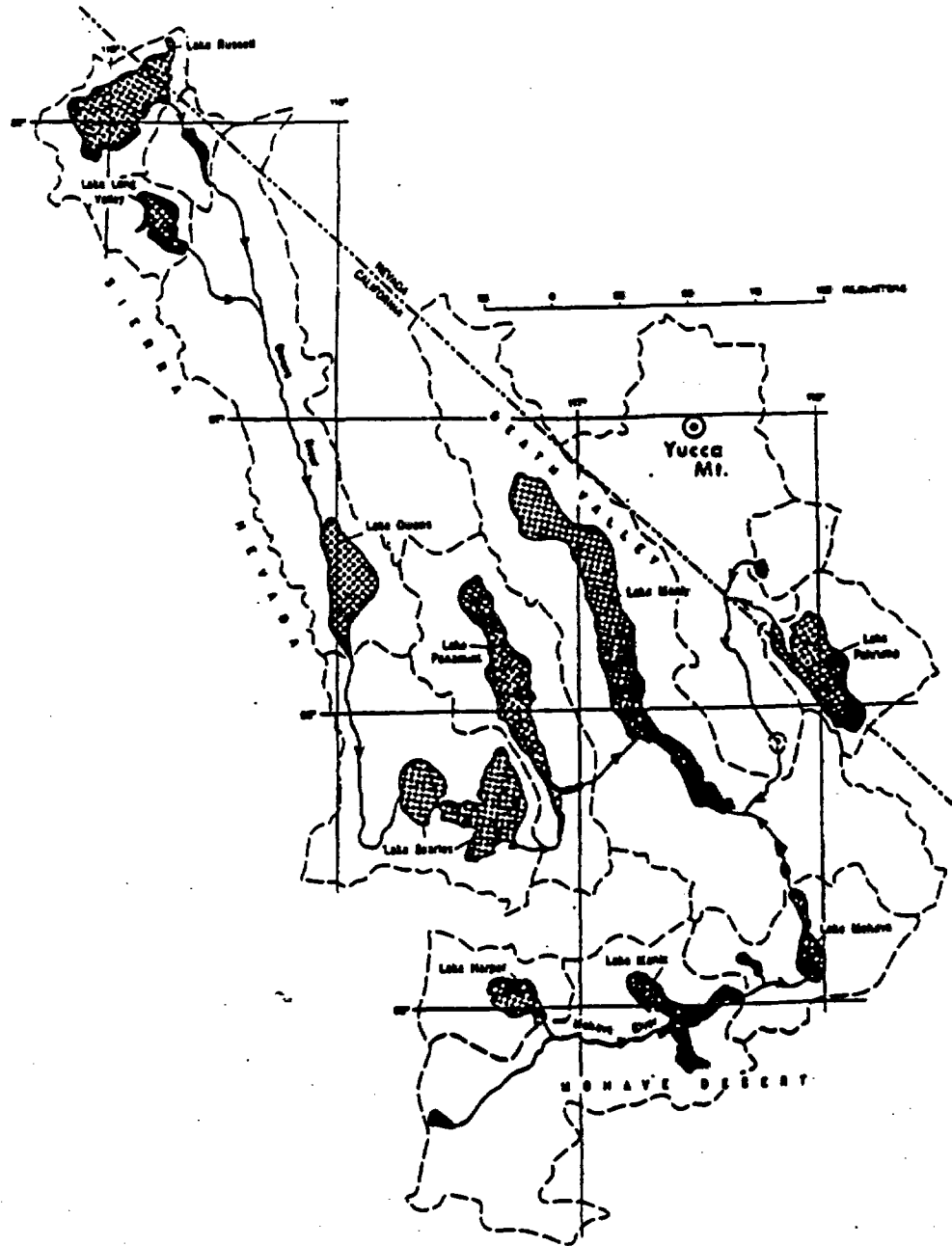


Figure 2. Configuration of lakes in the Death Valley drainage system at their last maximum stand in the Late Pleistocene. This (unspecified) date is informally referred to in the text as the Last Pluvial Maximum. Figure adopted from Morrison (1965, p. 278, figure 5).

time of this climatic extreme (the last glacial maximum). Concurrent research by meteorologists and paleoclimatologists has allowed estimation of dominant wind directions for the same period. With these, and the equations developed for modern climate, we can predict the past climate in the detail needed to allow the hydrogeologic model to be solved.

However, it is not just the change of climate alone that may impact upon the groundwater system. Because Death Valley is the discharge point for this system, such major changes of the water table as would be created by the presence of a lake could also affect groundwater flow. Thus, not only must we specify climate, we must also specify the size of the lake that can be anticipated. For this we have developed a separate computer code.

Thus there are three major elements to this report. We first describe the development of the equations of climate. Next, these equations are adapted to allow specification of the climate at the last glacial maximum. Finally, the lake system that can be anticipated under such climate extremes is determined. We conclude this discussion with a section describing how these predictions can be improved and extended.

THE METHOD OF CLIMATE PREDICTIONS

Development of the desired equations has relied on the capability of solving for a set of variables that represent the orographic influences upon climate within the area. For this we have used a digital elevation model at a spacing of 2½' latitude and longitude coupled with available bathymetric data and information concerning sea surface temperatures and dominant wind directions for the months of August and February.

We have developed a set of equations capable of predicting the historical conditions at the 124 climate stations of record in the level I area (Figure 3). These equations rely upon a set of variables that allow generalization of the climatic predictions to the entire region. Furthermore the variables included in the analysis are such that climatic changes accompanying glaciation can be reflected in the predictor variables and thus in the predictions.

Variables available within this modelling effort included the following: sea surface temperature in each of two months (August and February) at each point along the California coastline, distance from the coast to any point of concern along the wind vectors assumed to dominate the circulation pattern during the months of February and August, latitude and longitude of the point of interest, elevation of the point of interest, elevation and distance of the highest

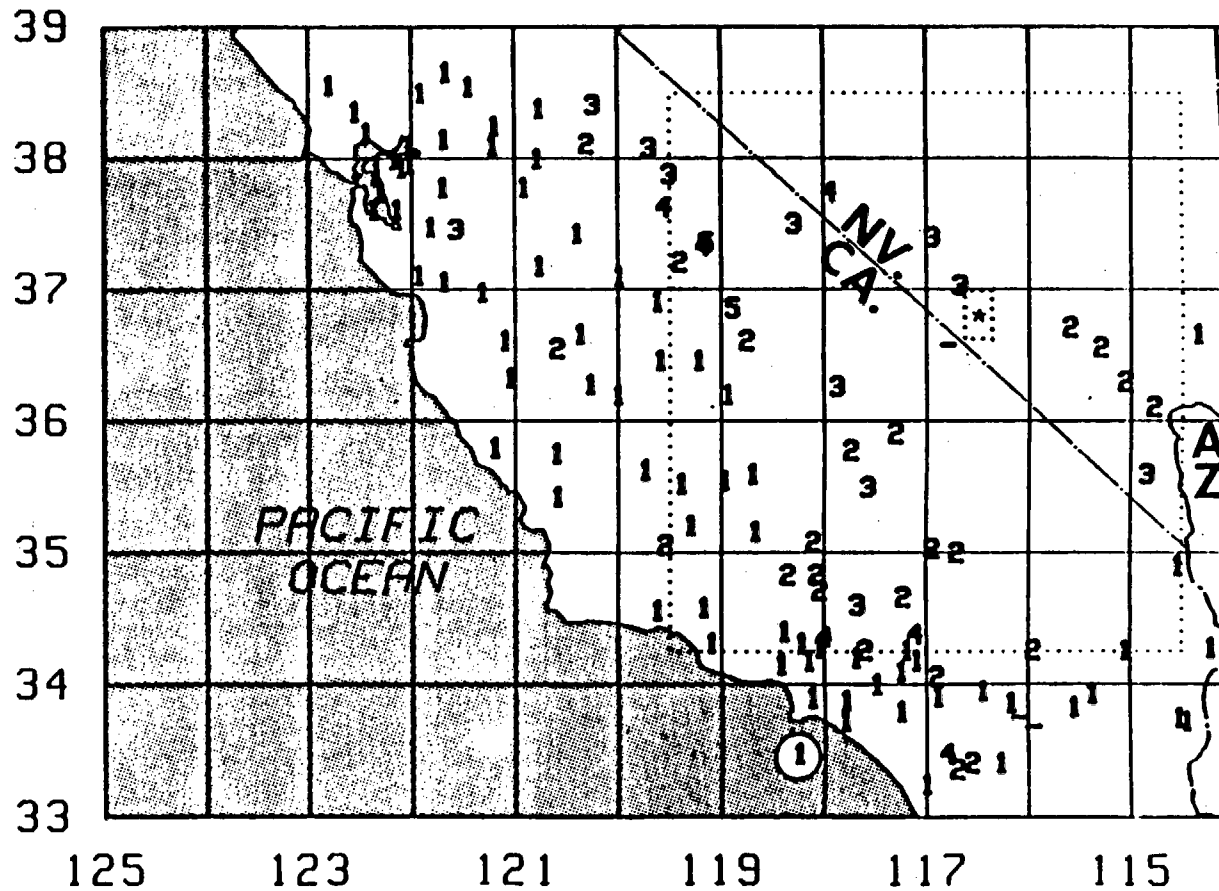


Figure 3. Locations of the 124 climate stations for which data were available. Elevations are given in units of 500 meters. The level II and level III areas are shown with dotted lines. An asterisk marks the location of Yucca Mtn. Stations below sea level are denoted by a "-".

point that would be crossed as winds travel from the coast to the point of interest, elevation and distance of the lowest point that would occur (between that highest point and the point of interest) along the assumed wind vector, and the slope in the westerly and southerly directions at the point of interest. Computation of the variables of concern was made under the assumption that the present dominant wind directions in February and August are 241° and 282° respectively. These variables are illustrated schematically in Figure 4.

From these variables a set of additional variables were computed and transformations of some of those variables were used. These additional variables are as follows: the natural logarithm of the distance from the coast, the natural logarithm of the distance from the highest upwind point, the natural logarithm of the distance from the lowest upwind point, the ratio of sea surface temperature to the natural logarithm of distance to the point from the coast, the ratio of the highest elevation to the natural logarithm of distance from that elevation to the point of concern, the ratio of the lowest elevation to the natural logarithm of distance to the point of concern, the difference in elevation between the highest upwind point and the point of concern, the difference in elevation between that of the lowest upwind point and the point of concern. Ratios of the drop and of the gain in elevation to the logarithm of their distances

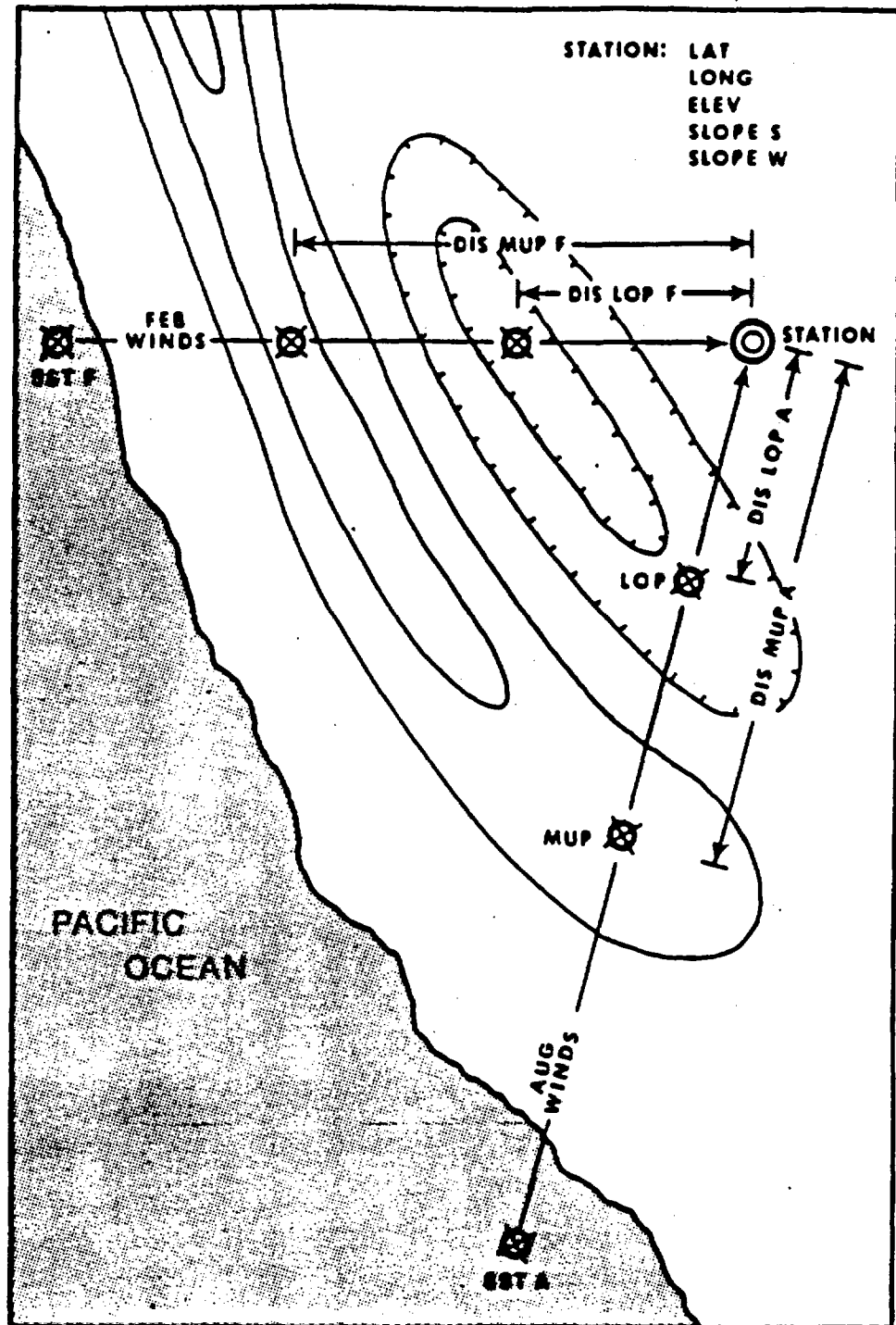


Figure 4. Schematic illustration of the predictor variables defined for use in the climate equations. Two wind vectors are shown. Each illustrates the assumed dominant wind direction in one of the months used.

were also used. All of these variables were then available for construction of predictive equations of temperature and precipitation. They are summarized in Table 1.

From these we have solved for the dependent variables in each month. These variables were the mean monthly temperature and the mean monthly precipitation in each of the twelve months. We also made a predictive equation of total precipitation and mean temperature over the year. The climate stations used in this analysis have been described in our previous report (Craig, 1983). The precipitation data were transformed using the cube root transformation also described in the earlier report. In Table 2 we report the order of entry for the variables that enter each of the equations for monthly temperature. In Table 3 we report the same information for the values of monthly precipitation. In Table 4 are reported the values of percent variance explained, adjusted for degrees of freedom for each of the twelve months for these two variables. As can be seen, our predictive equations are quite successful in estimating the values of temperature and precipitation in each of these months. All of the predictive equations are statistically significant and to the best of our knowledge these equations represent the most successful yet developed in making such predictions. Analysis of the residuals from these predictive equations has shown no systematic tendency for deviations.

Table 1. Listing of all independent variables defined in the study of climate and available for stepwise regression predictions of precipitation and temperature. Each variable in the second group is computed for both February and August. Thus, for example, there is ELMUPF and ELMUPA. In group three all months may be available. Thus there is a TJAN, TFEB --- and CUPJAN, CUPFEB, etc.

	<u>Name</u>	<u>Variable</u>
1.	LAT	Latitude of Point
	LONG	Longitude of Point
	ELEV	Elevation of Point
	SLOPES	Slope to South from Point to Next Adjacent Point of Grid
	SLOPEW	Slope to West from Point to Next Adjacent Point of Grid
	2.	ELMUP
DISMUP		Distance to Maximum Upwind Point
ELLOP		Elevation of Lowest Point Between
DISLOP		Distance to Lowest Point Between
ELEDROP		Elevation Drop (Maximum Upwind - Point Elevation)
ELEGAIN		Elevation Gain (Lowest Point Between - Point Elevation)
LNDIMUP		LN (Distance to Maximum Upwind Point + e)
LNDILOP		LN (Distance to Lowest Point Between + e)
DECADRP		Elevation Drop/LN (Dist. to Max. Upwind Point + e)
DECAGAN		Elevation Gain/LN (Dist. to Lowest Point Between + e)
DECAMAX		Elevation of Maximum Upwind Point/LN (Dist. to Max. Upwind Point + e)
DECAMIN		Elevation of Lowest Point Between/LN (Dist. to Lowest Point Between + e)
SST		Sea-Surface Temperature
DISCOS		Distance to the Coast (Along Wind Vector)
LNDICOS		LN (Distance to the Coast + e)
DECSST		Sea-Surface Temperature/LN (Distance to the Coast + e)
3.		T
	CUP	Cube Root of Monthly Mean Precipitation (if previously predicted)

Table 2. Results of stepwise regressions to predict monthly mean temperatures. Final coefficients of the regression equation are provided in the Appendix. Variables that enter but are later removed are not listed.

<u>Variable</u>		<u>Order of Entry</u>												<u>No. times used</u>
<u>No.</u>	<u>Name</u>	<u>J</u>	<u>F</u>	<u>M</u>	<u>A</u>	<u>M</u>	<u>J</u>	<u>J</u>	<u>A</u>	<u>S</u>	<u>O</u>	<u>N</u>	<u>D</u>	
1	LAT	-	3	-	-	-	-	-	-	-	-	-	-	1
2	LONG	-	-	-	-	-	-	2	-	-	-	-	-	1
3	ELE	3	1	-	2	3	-	-	-	-	5	-	2	6
4	EL MUP F	-	-	-	5	-	-	-	-	-	-	-	-	1
6	EL LOP F	-	-	-	-	-	-	-	3	-	-	-	-	1
10	DIS COS F	4	-	-	-	-	-	-	-	-	-	-	-	1
11	SST F	-	-	-	-	-	2	-	-	-	-	-	-	1
15	EL MUP A	4	-	-	-	-	-	-	-	-	-	-	-	1
17	EL LOP A	-	-	-	-	-	-	5	-	-	-	-	-	1
20	SLOPE S	-	-	-	-	-	-	-	-	-	3	-	-	1
21	DIS COS A	-	-	-	-	-	-	-	5	5	-	-	-	2
22	SST A	-	2	-	-	-	-	-	-	-	4	-	-	2
26	T JAN	-	-	-	-	-	-	-	-	-	-	1	1	2
28	T FEB	1	-	1	4	-	4	4	1	3	1	-	-	8
30	T MAR	2	-	-	-	-	-	-	-	-	-	-	3	2
32	T APR	-	-	2	-	2	-	-	-	6	-	3	-	4
36	T JUN	-	-	-	3	1	-	-	-	-	-	-	-	2
38	T JUL	-	-	-	-	-	-	-	-	-	-	-	6	1
40	T AUG	-	-	7	-	-	1	1	-	1	2	-	-	5
42	T SEP	-	-	3	-	-	-	-	-	-	-	-	-	1
44	T OCT	-	-	-	-	4	-	-	-	2	-	2	4	4
52	EL DROP A	-	-	5	-	-	-	-	-	-	-	-	-	1
54	EL DROP F	-	-	-	-	-	-	-	7	-	-	-	-	1
55	EL GAIN F	-	-	-	-	-	-	7	-	-	-	-	-	1
57	CUP FEB	-	-	4	1	-	3	3	-	-	-	-	7	5
63	CUP AUG	-	-	-	-	-	-	8	-	4	-	-	-	2
69	LN DI COS A	-	-	-	-	-	-	-	2	-	-	-	-	1
72	LN DI LOP A	-	-	-	6	-	-	-	-	-	-	-	-	1
73	LN DI MUP F	-	5	-	-	-	-	-	-	-	-	-	-	1
74	LN DI LOP F	-	-	-	7	-	-	-	-	-	-	-	-	1
75	DECA SST A	5	-	-	-	-	-	-	6	-	-	-	5	3
77	DECA MAX F	-	-	-	8	-	-	-	-	-	-	-	-	1
78	DECA MAX A	-	-	-	-	-	-	6	-	-	-	-	-	1
80	DECA MIN F	-	-	6	-	-	-	-	4	-	-	-	-	2
83	DECA DRP A	-	-	-	-	-	-	-	-	7	-	4	-	2
No. vars. in eqn.		5	5	7	8	4	4	8	7	7	5	4	7	

Table 3. Results of stepwise regressions to predict monthly mean precipitation. Final coefficients of the regression equations are listed in the Appendix. Variables that enter but are later removed are not listed.

Variable No.	Name	Order of Entry												No. times used
		J	F	M	A	M	J	J	A	S	O	N	D	
1	LAT	-	-	4	-	-	-	-	-	-	-	2	-	2
2	LONG	-	-	7	-	-	-	-	1	-	-	-	-	2
3	ELEV	-	-	-	-	-	-	-	-	-	-	6	-	1
4	EL MUP F	-	-	-	-	-	-	-	-	-	6	-	-	1
7	DIS LOP F	-	-	-	-	-	-	3	-	-	-	-	-	1
10	DIS COS F	-	-	-	-	6	-	-	-	-	3	-	-	2
11	SSTF	-	7	-	-	2	-	-	-	-	-	-	-	2
15	EL MUP A	-	-	-	-	-	-	2	-	-	-	-	-	1
16	DISMUP A	-	11	-	-	-	-	-	-	-	-	-	-	1
18	DIS LOP A	-	-	-	-	-	-	-	-	3	-	-	-	1
20	SLOPE S	-	5	-	10	-	-	-	-	-	5	-	-	3
21	DIS COS A	4	-	-	-	-	2	4	4	-	-	-	-	3
22	SSTA	-	-	-	-	-	-	4	2	-	-	-	-	2
28	T FEB	-	-	-	11	-	-	-	-	-	-	-	-	1
30	T MAR	-	-	-	5	-	-	-	-	-	-	-	-	1
38	T JUL	-	-	-	-	-	-	-	-	-	-	7	-	1
40	T AUG	-	2	-	-	-	-	-	-	-	-	-	-	1
42	T SEP	-	-	-	-	-	-	-	-	-	7	-	-	1
46	T NOV	-	-	-	-	-	-	-	-	-	-	-	3	1
52	EL DROP A	-	1	-	-	-	-	-	-	-	-	-	5	2
54	EL DROP F	5	6	8	-	-	-	-	-	-	-	-	-	3
56	CUP JAN	-	-	3	4	-	-	-	-	-	-	-	-	2
57	CUP FEB	2	-	1	2	-	-	-	-	-	-	1	1	5
58	CUP MAR	-	-	-	-	5	-	-	-	-	-	-	-	1
59	CUP APR	-	-	2	-	1	-	-	-	-	-	-	-	2
60	CUP MAY	-	-	-	-	-	1	-	-	-	-	-	-	1
62	CUP JUL	7	-	-	-	-	-	-	-	1	-	-	-	2
63	CUP AUG	-	-	-	-	-	-	1	-	-	2	5	-	3
64	CUP SEP	-	-	-	8	-	3	-	-	-	-	-	-	2
65	CUP OCT	-	-	-	-	3	-	-	-	2	-	-	-	2
66	CUP NOV	3	-	-	1	8	-	-	-	-	1	-	2	5
67	CUP DEC	1	-	-	3	4	-	-	-	-	4	-	-	4
69	LN DI COS A	-	-	6	7	-	-	-	-	-	-	-	-	2
70	LN DI COS F	-	-	-	-	-	4	-	-	-	-	-	-	1
71	LN DI MUP A	-	10	-	-	-	-	-	-	-	-	-	-	1
73	LN DI MUP F	6	4	-	-	-	-	-	3	-	-	-	-	3
74	LN DI LOP F	-	-	-	-	-	-	-	-	-	-	-	4	1
75	DECA SST A	-	-	-	9	-	-	-	-	-	-	-	6	2
76	DECA SST F	-	3	-	-	-	-	-	-	-	-	-	-	1
78	DECA MAX A	-	-	-	-	-	-	-	-	-	-	3	-	1
82	DECA GAN F	-	9	-	-	-	-	-	-	-	-	-	-	1
84	DECA DRP F	-	8	5	6	7	-	-	-	-	-	4	-	5
No. vars. in eqn.		7	11	8	11	8	4	4	4	3	7	7	6	

Table 4. Values of percent explained (adjusted R^2) and the standard error for each of the regression equations. Also reported for comparison are the R^2 values reported by Houghton (1979) for his precipitation equations.

Month	Temperature		Precipitation		
	R^2	st. er.	R^2	st. er.	Houghton
January	98.5	.358	95.7	.056	51.9
February	93.7	.384	84.5	.194	51.6
March	99.7	.160	98.6	.056	54.0
April	99.4	.264	97.4	.063	58.3
May	99.7	.202	95.3	.070	71.2
June	99.2	.417	80.7	.099	72.9
July	99.8	.208	81.9	.138	62.2
August	91.9	1.387	73.4	.176	55.6
September	99.6	.241	65.0	.095	70.8
October	98.4	.380	94.1	.064	52.3
November	96.9	.494	95.0	.086	58.8
December	99.3	.229	93.3	.062	55.5

Values of R^2 are computed when the observed values of other months are known. This represents the theoretical accuracy of the predictions. The actual precision will be roughly 90% of the theoretical. The best measure of the quality of the prediction is obtained by examination of the predictions themselves (Figures 18-30).

Using these equations, and a program to solve for the independent variables at each point within our level II grid area, we have made predictions of the temperature and precipitation in each of the twelve months of the year. Results of these predictions are described in the next section.



PREDICTIONS OF MODERN CLIMATE

Temperature

Using the equations for temperature described above, we have solved for monthly temperature and for mean annual temperature. These computations allow an estimated value at each grid point of the Level II grid. Values are arrayed at a spacing of $2\frac{1}{2}^\circ$ of latitude and longitude. Comparison of these predictions to the available climatic data shows an excellent agreement. In Table 5 we have listed those locations for which the observed value deviates from the predicted value by greater than two standard errors of the prediction. The standard errors of the estimate are also reported, for each equation, in Table 4. Analysis of residuals suggests no systematic deviations from normality (Table 6). As can be seen by inspection of these tables, the predictions are very close. Table 4 provides the value of adjusted R^2 , the percent variance explained, for each equation.

Solutions of the equations are illustrated as the top map in Figures 5-17. It should be noted in examining those figures that the coding scheme used to represent temperatures is the same in both figures for the same month. The bottom figure represents predictions for the last glacial maximum to be described later. This facilitates comparisons between present and past (LGM) climates; changes are more readily noted.

Table 5. Number of months for which the observed value at a station exceeds the predicted value by two standard errors (>2) and by three standard errors (>3) of the regression equation.

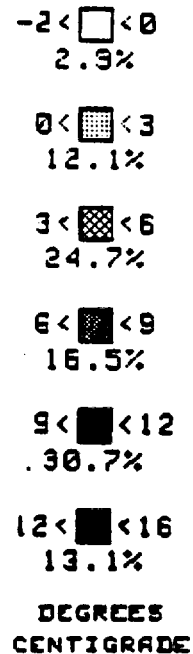
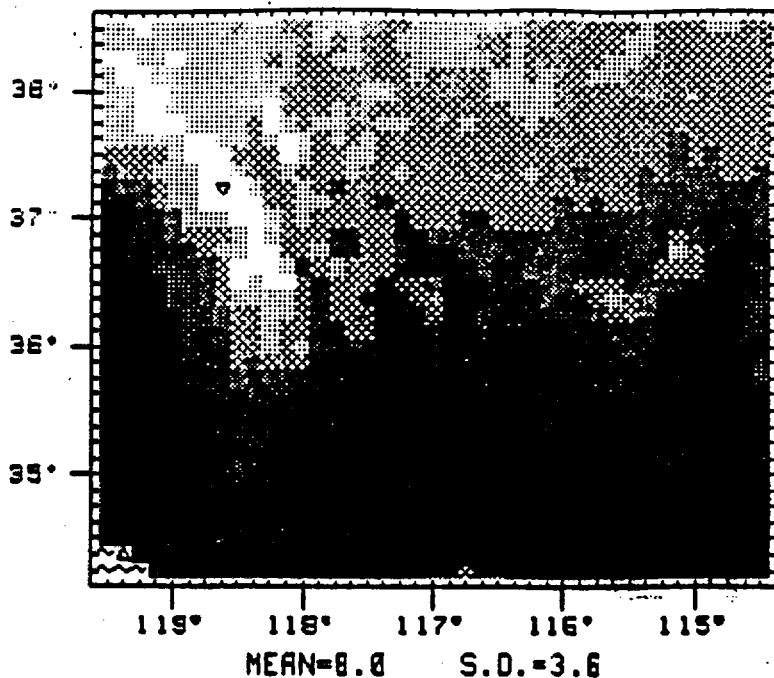
Sta. No.	>2	>3									
1.	2	0	27.	1	0	52.	0	0	77.	2	0
2.	2	0	28.	0	0	53.	0	0	78.	1	0
3.	0	0	29.	0	0	54.	2	0	79.	0	0
4.	1	0	30.	0	0	55.	0	0	80.	2	1
5.	1	0	31.	0	0	56.	2	0	81.	0	0
6.	1	0	32.	0	0	57.	0	0	82.	0	0
8.	0	0	33.	0	0	58.	0	0	83.	0	0
9.	1	0	34.	0	0	59.	0	0	84.	1	0
10.	0	0	35.	0	0	60.	0	0	86.	0	0
11.	4	0	36.	0	0	61.	0	0	87.	0	0
12.	0	0	37.	0	0	62.	2	0	88.	0	0
13.	0	0	38.	1	0	63.	0	0	89.	1	0
14.	1	0	39.	1	0	64.	2	0	90.	0	0
15.	2	0	40.	0	0	65.	0	0	91.	0	0
16.	1	1	41.	0	0	66.	1	0	92.	1	0
17.	1	0	42.	0	0	67.	0	0	94.	1	0
18.	2	0	43.	0	0	68.	3	1	96.	1	0
19.	0	0	44.	1	0	69.	4	0	97.	0	0
20.	1	0	45.	5	0	70.	1	0	98.	2	0
21.	0	0	46.	0	0	71.	0	0	99.	1	0
22.	2	0	47.	0	0	72.	2	0	100.	1	0
23.	0	0	48.	3	1	73.	0	0	101.	1	0
24.	0	0	49.	0	0	74.	0	0	102.	0	0
25.	0	0	50.	2	0	75.	0	0	103.	1	0
26.	4	1	51.	1	0	76.	1	0	104.	0	0
									105.	0	0
									106.	1	0
									107.	2	0
									108.	0	0
									109.	0	0
									110.	1	0
									111.	2	1
									112.	1	0
									113.	2	0
									115.	2	0
									116.	0	0
									117.	1	0
									118.	1	0
									119.	1	0
									120.	0	0
									123.	1	1
									126.	1	0
									127.	0	0
									129.	0	0
									130.	2	1
									131.	0	0
									132.	1	0
									136.	2	0
									139.	2	0
									140.	0	0

Table 6. Measures of skewness (g_1) and kurtosis (g_2) of the residuals from the equations to predict temperature and precipitation. These values have been standardized so that the expected variance is one under an assumption of normality. Values exceeding ± 2.35 suggest rejection of the null hypothesis at the alpha = 5% level.

Month	Temperature		Precipitation	
	g_1	g_2	g_1	g_2
JAN	-0.83	1.71	-2.21	6.36*
FEB	0.95	-0.23	1.26	1.03
MAR	-0.07	0.11	-0.85	-1.11
APR	1.23	-0.49	-0.52	0.71
MAY	-1.83	-0.27	-2.51	-0.11
JUNE	0.24	1.16	-1.73	2.85
JULY	0.04	-0.98	-0.64	0.60
AUG	-0.96	-0.02	0.70	-0.33
SEP	1.85	2.83	-1.49	0.08
OCT	0.04	2.26	-0.82	-0.07
NOV	26.76*	119.59*	0.71	-0.18
DEC	-0.34	0.68	-1.17	-1.21

* These significant values are due to a single observation. Examination of the data for this station has shown that values for this month are probably inaccurately reported. More representative data become available estimates will be recomputed and are expected to be considerably improved.

MODERN JANUARY TEMPERATURE



L.G.M. JANUARY TEMPERATURE

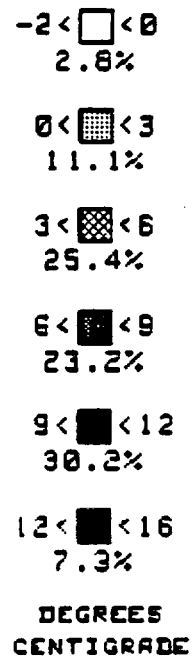
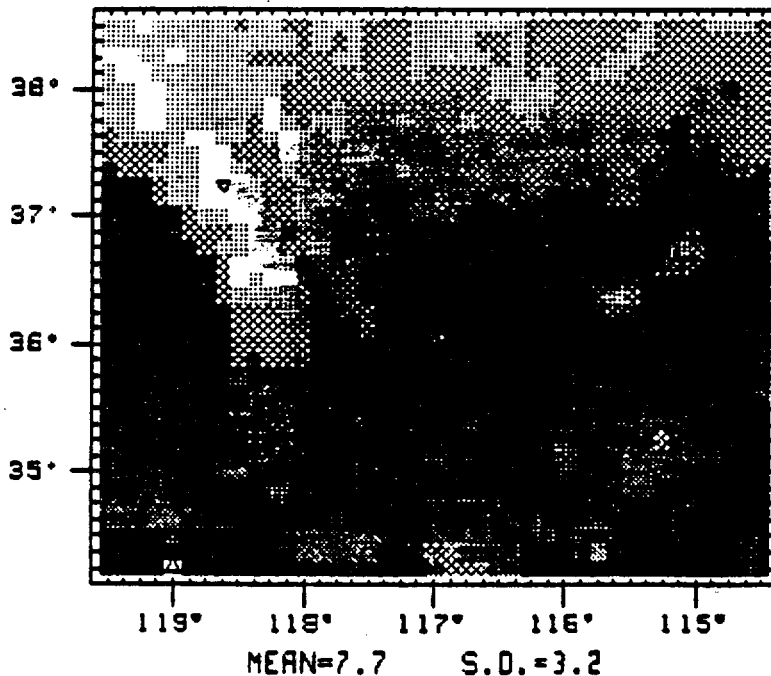
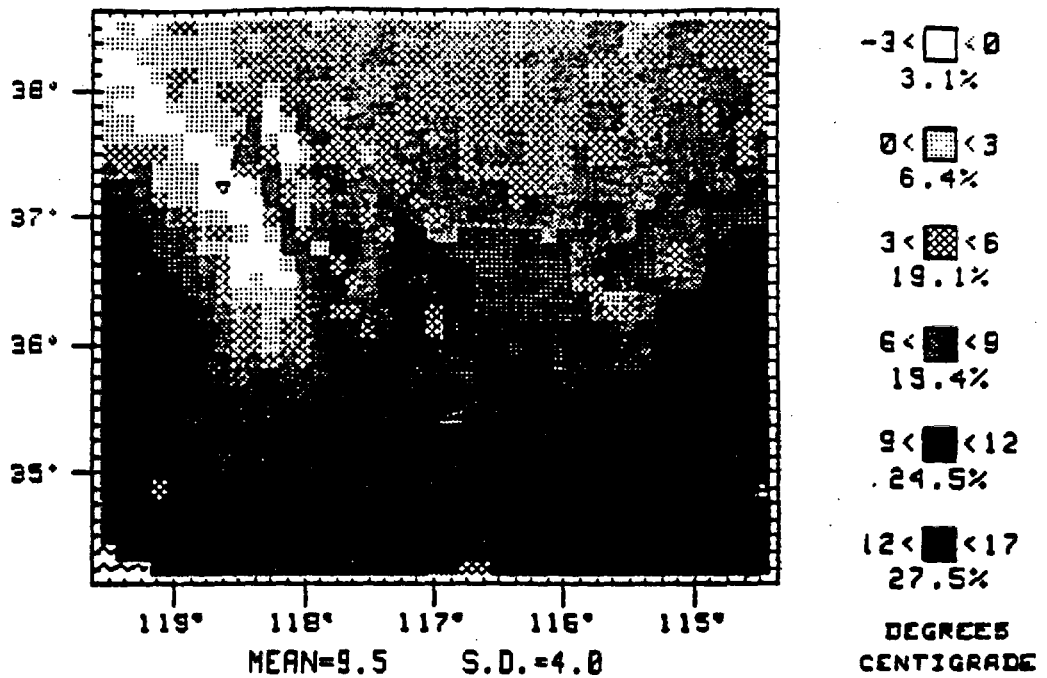


Figure 5. January modern (top) and last glacial maximum (bottom) temperatures.

MODERN FEBRUARY TEMPERATURE



L.G.M. FEBRUARY TEMPERATURE

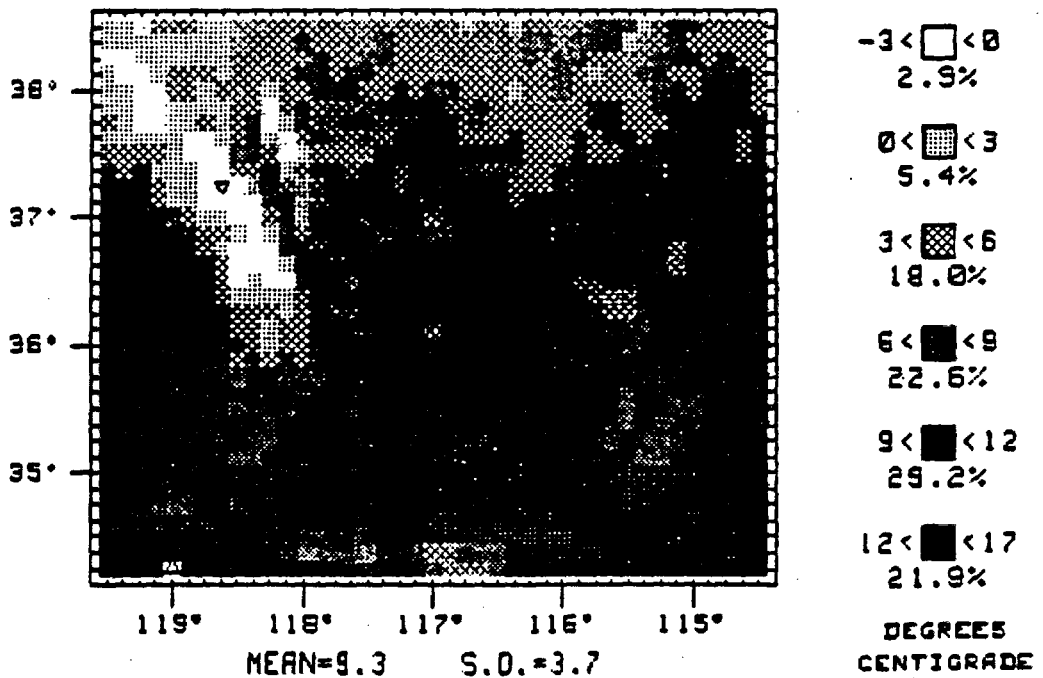


Figure 6. February modern (top) and last glacial maximum (bottom) temperatures.

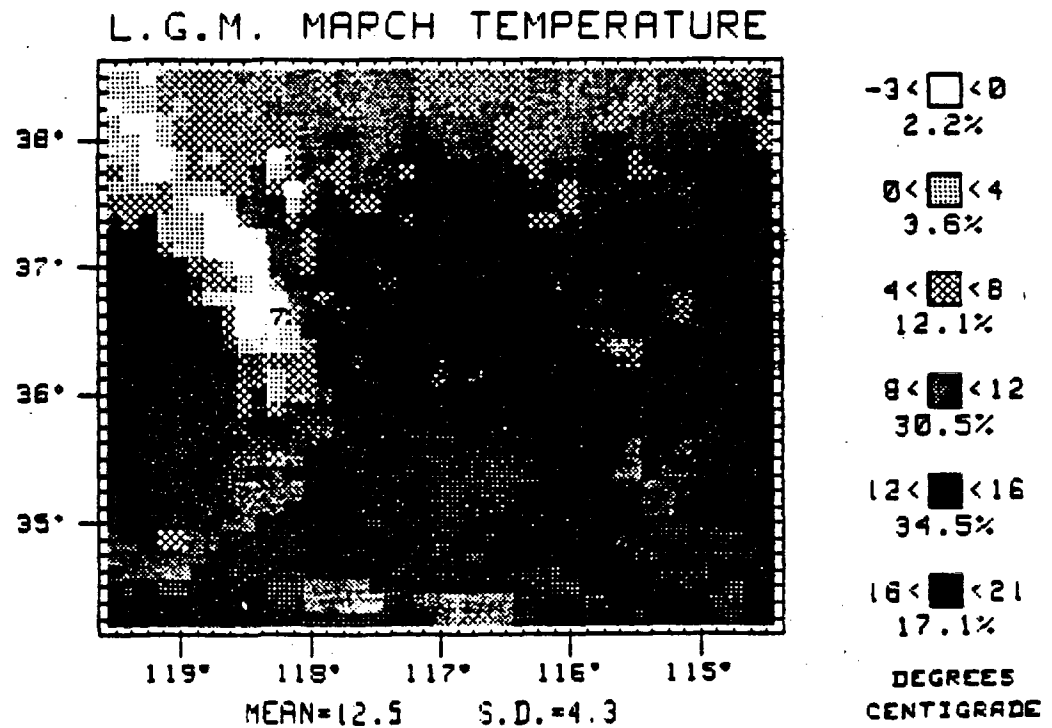
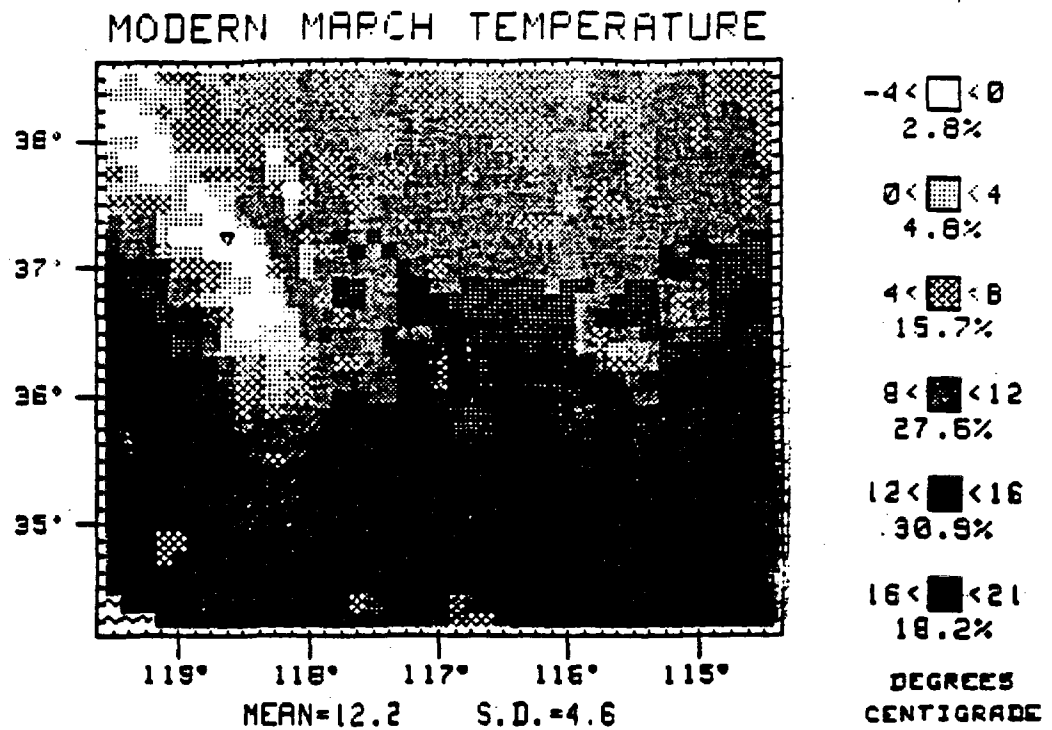


Figure 7. March modern (top) and last glacial maximum (bottom) temperatures.

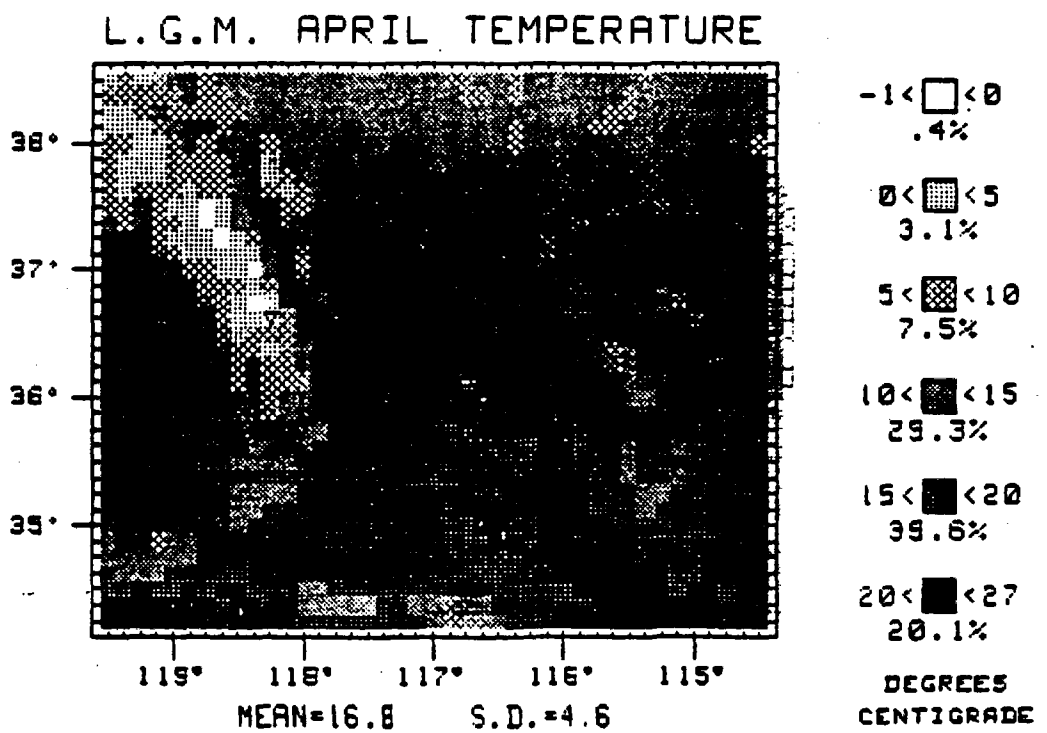
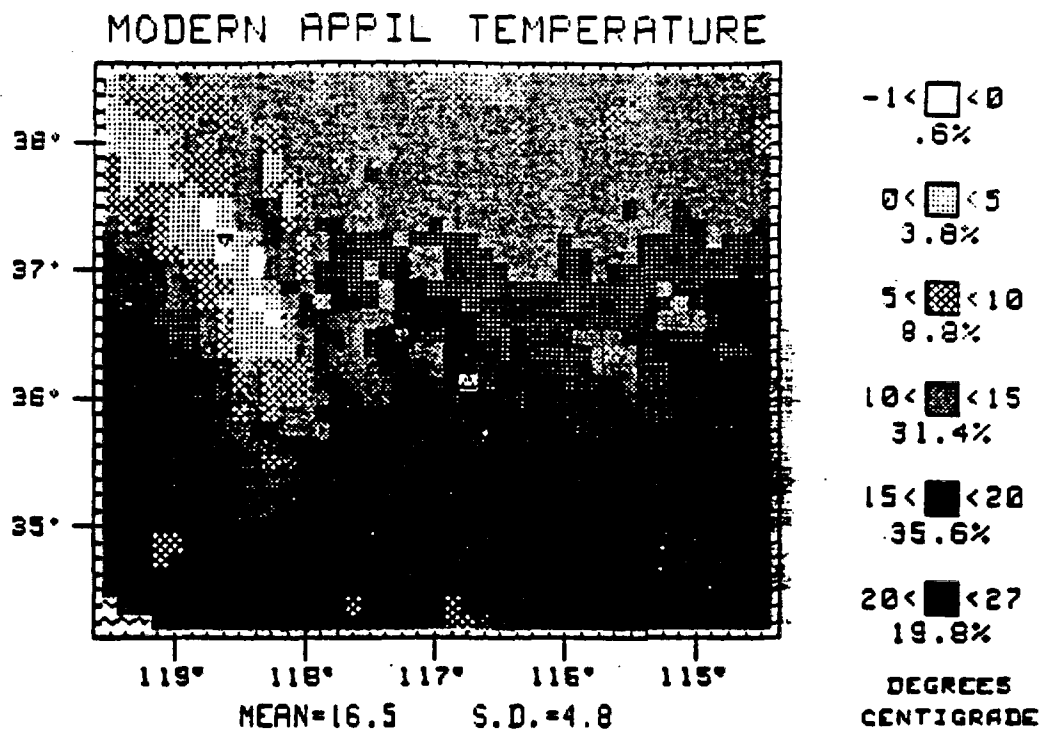
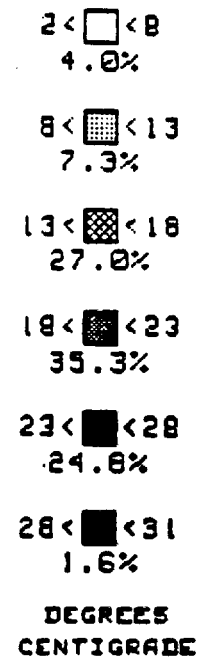
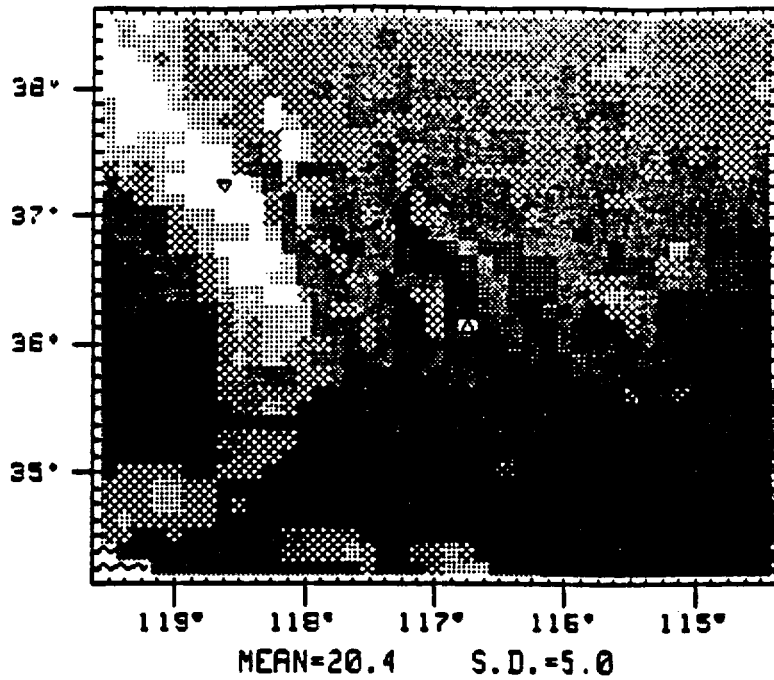


Figure 8. April modern (top) and last glacial maximum (bottom) temperatures.

MODERN MAY TEMPERATURE



L.G.M. MAY TEMPERATURE

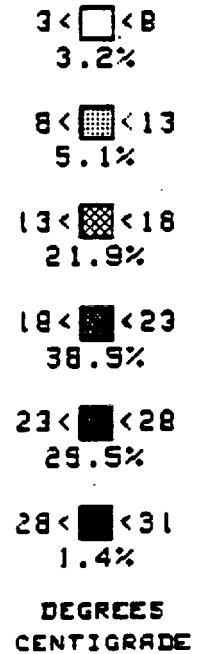
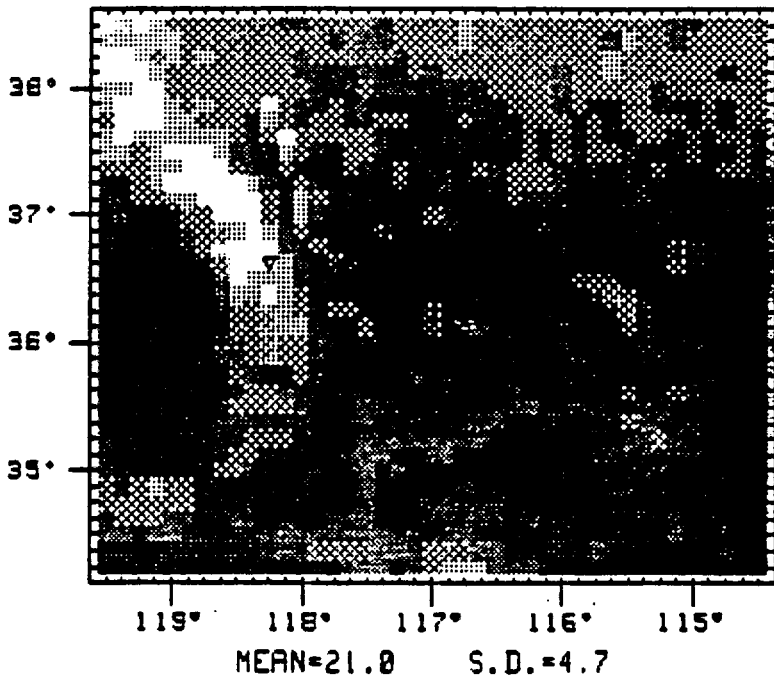
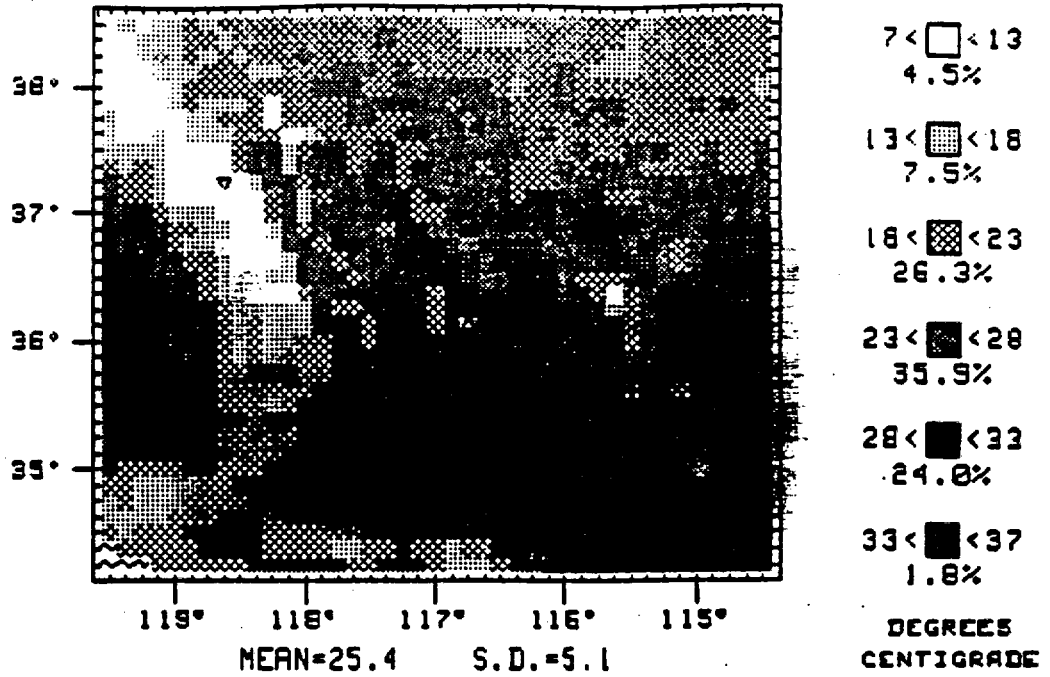


Figure 9. May modern (top) and last glacial maximum (bottom) temperatures.

MODERN JUNE TEMPERATURE



L.G.M. JUNE TEMPERATURE

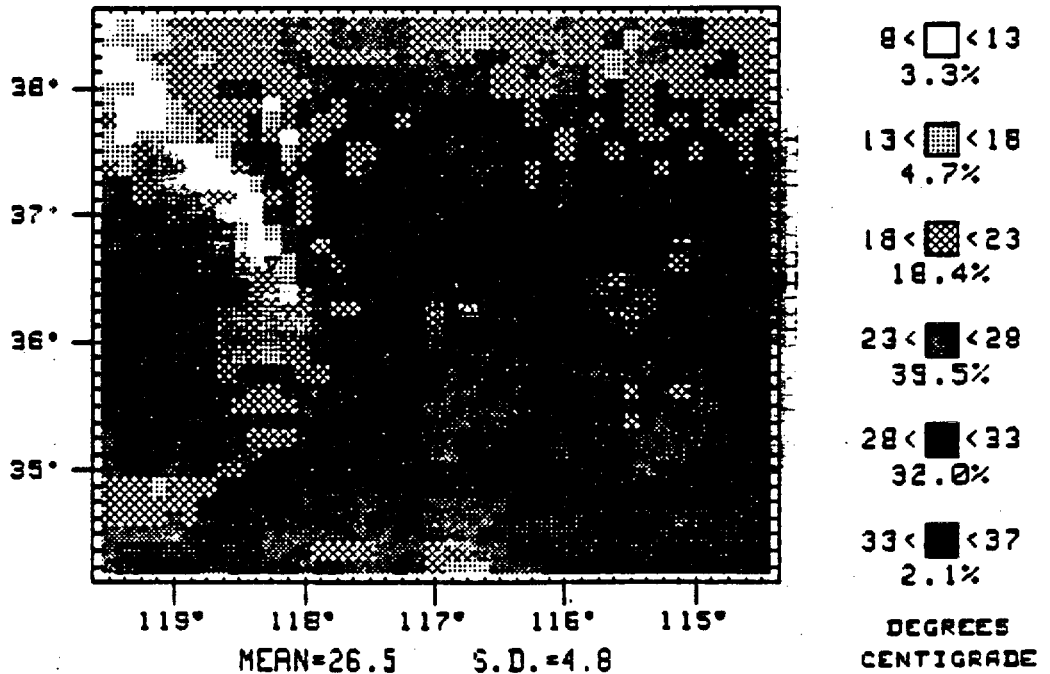


Figure 10. June modern (top) and last glacial maximum (bottom) temperatures.

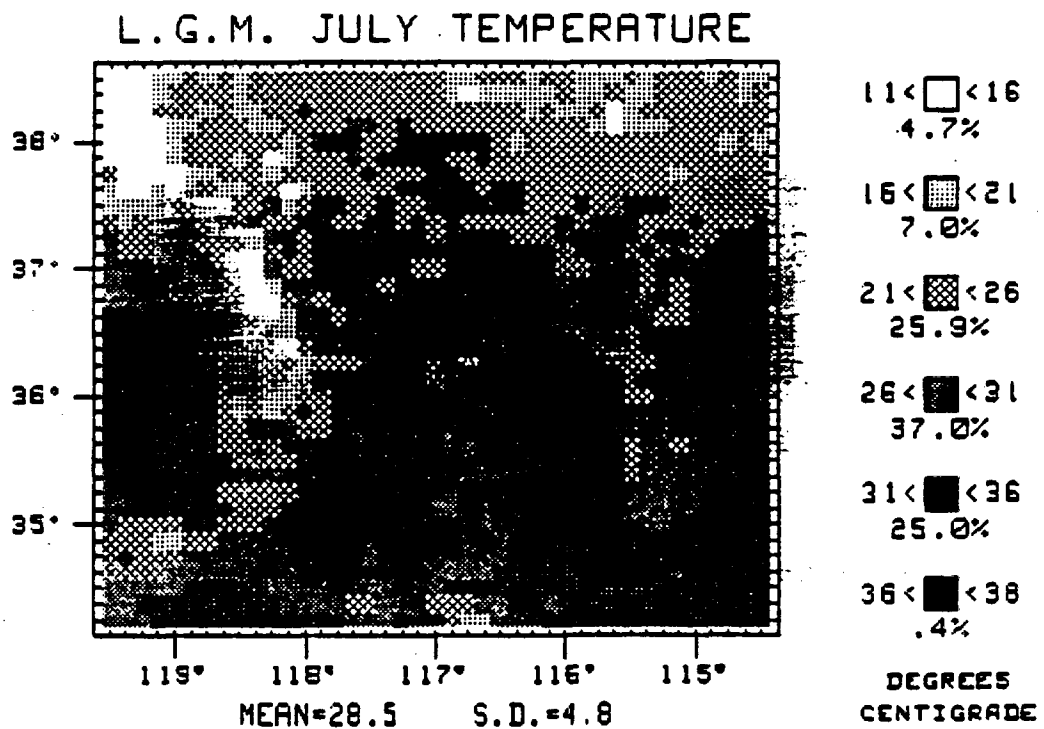
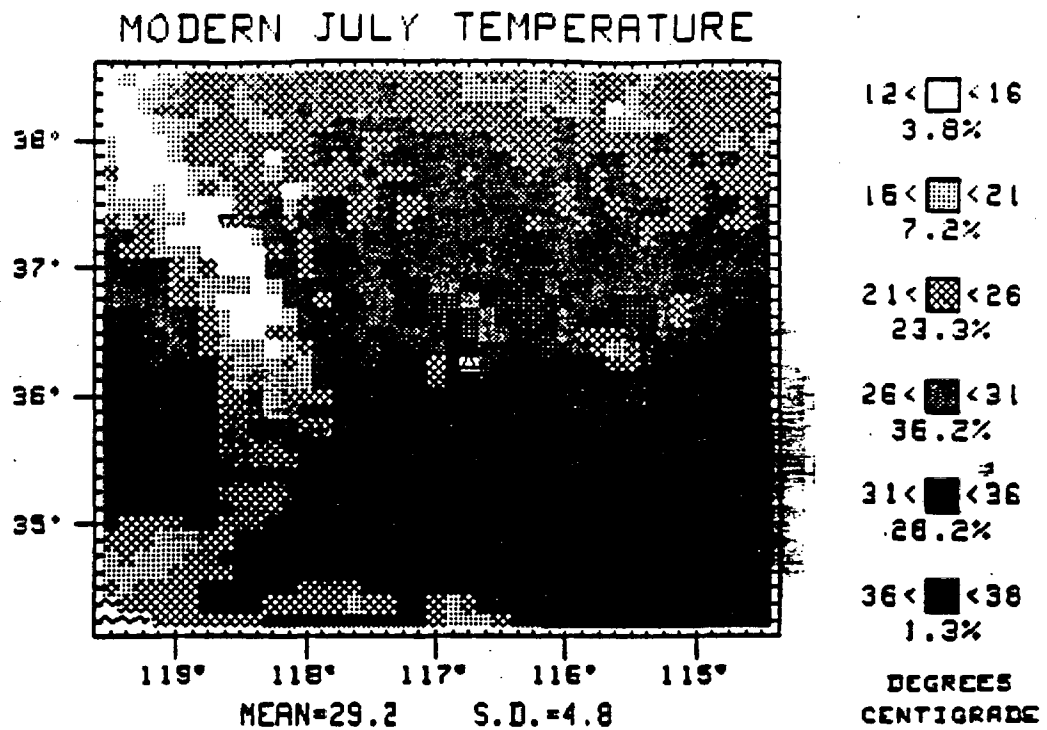
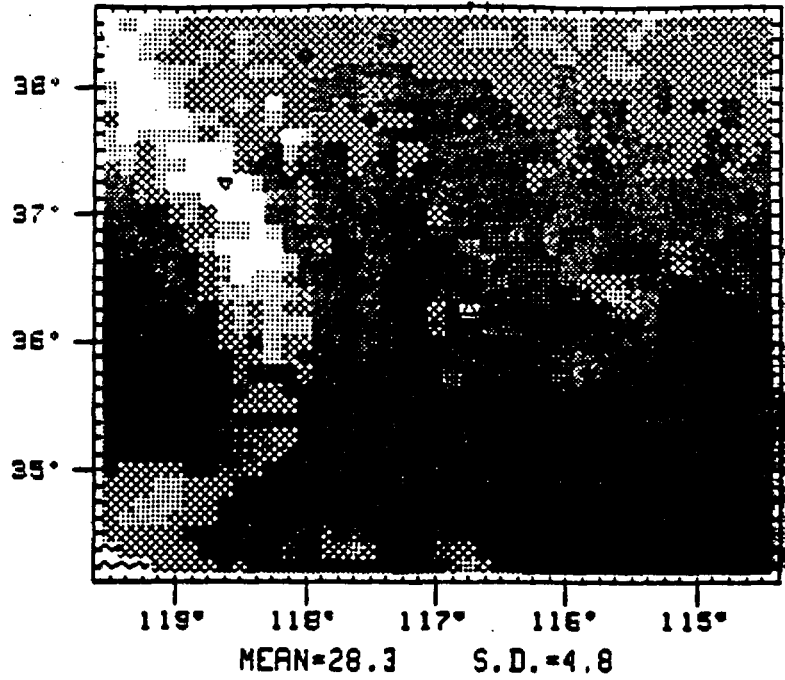


Figure 11. July modern (top) and last glacial maximum (bottom) temperatures.

MODERN AUGUST TEMPERATURE



L.G.M. AUGUST TEMPERATURE

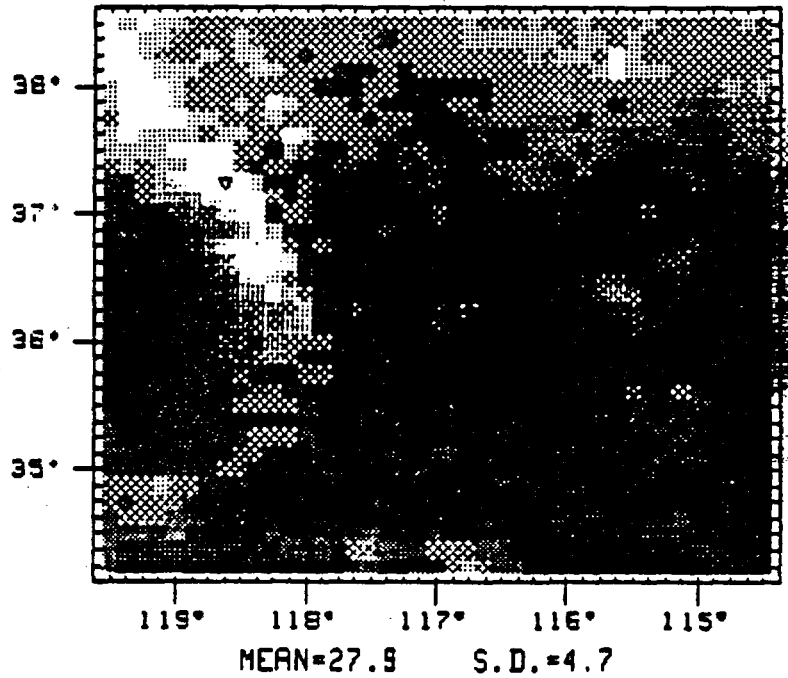
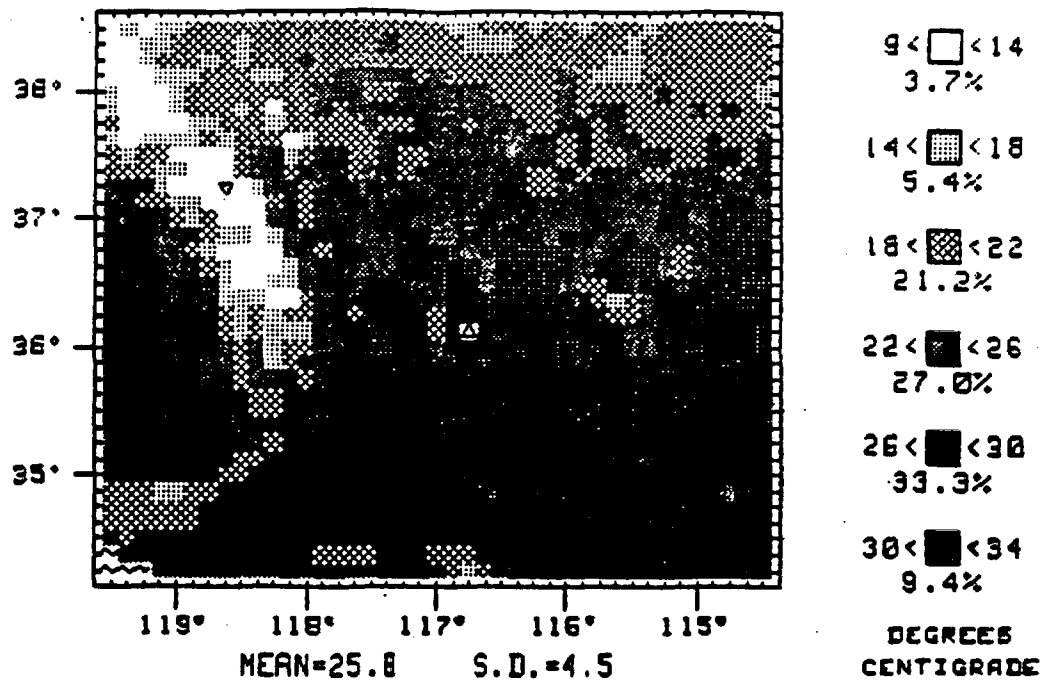


Figure 12. August modern (top) and last glacial maximum (bottom) temperatures.

MODERN SEPTEMBER TEMPERATURE



L.G.M. SEPTEMBER TEMPERATURE

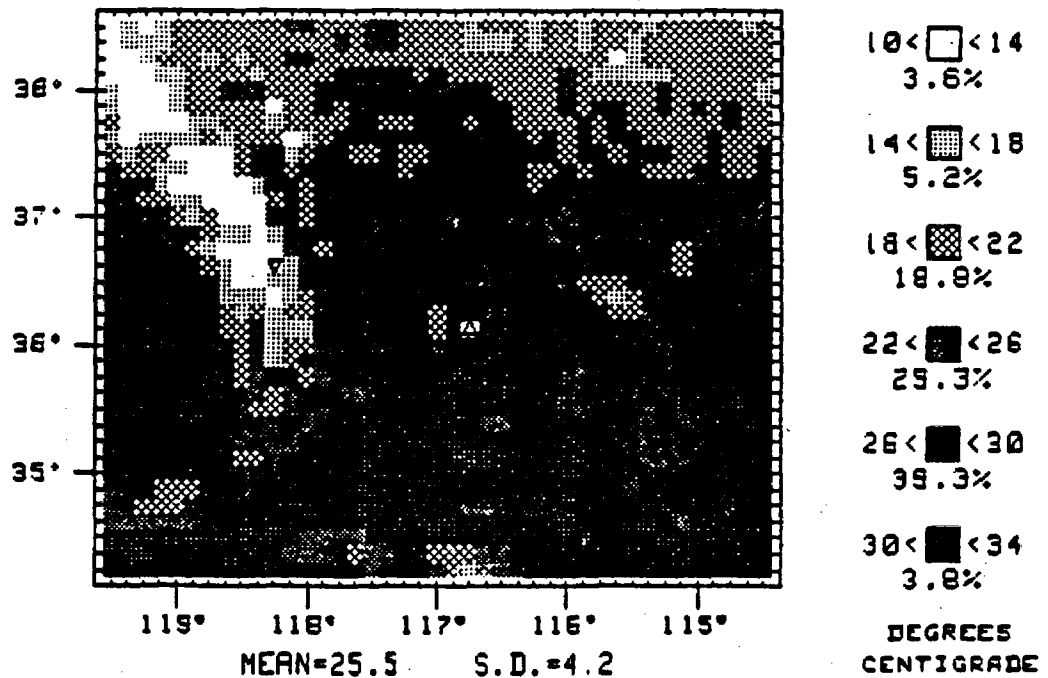
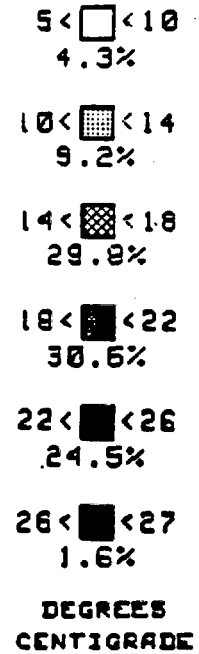
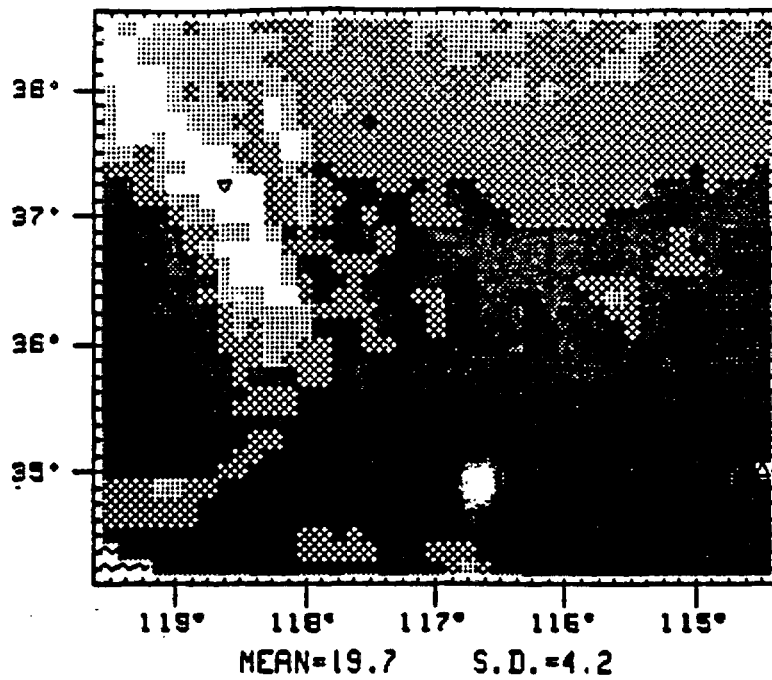


Figure 13. September modern (top) and last glacial maximum (bottom) temperatures.

MODERN OCTOBER TEMPERATURE



L.G.M. OCTOBER TEMPERATURE

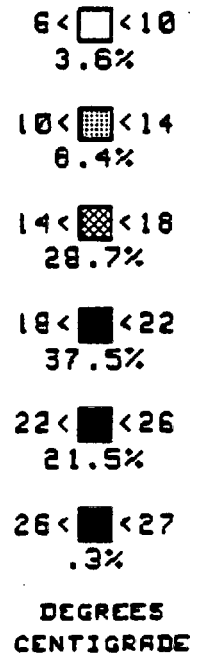
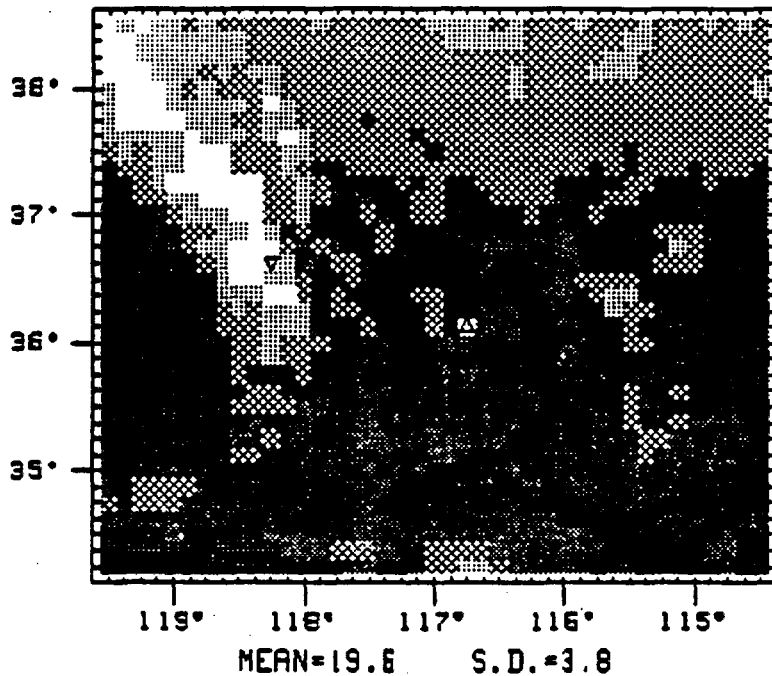
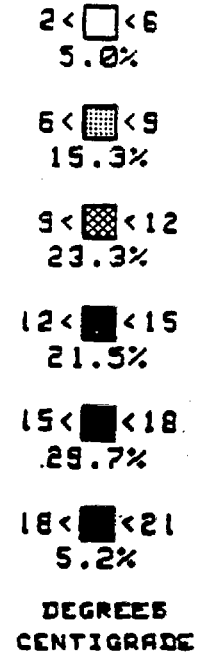
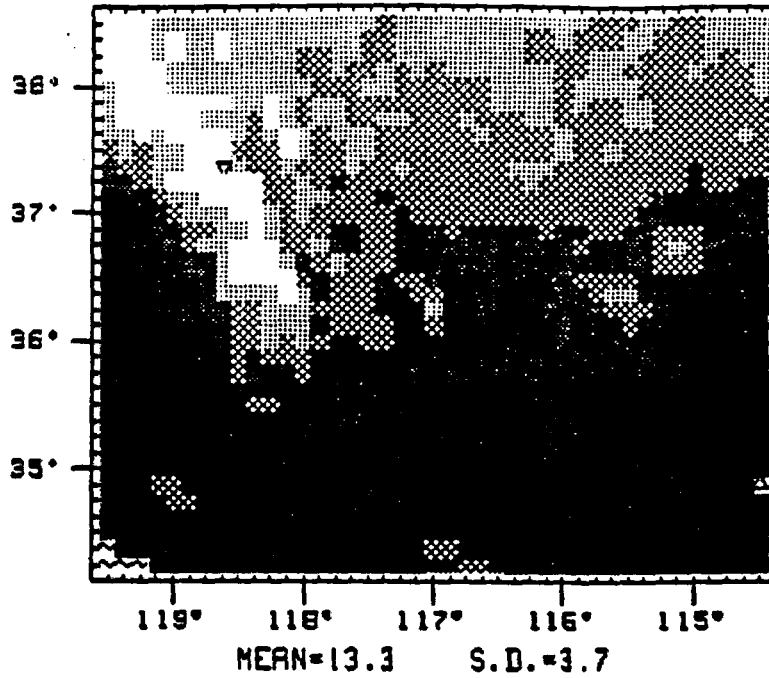


Figure 14. October modern (top) and last glacial maximum (bottom) temperatures.

MODERN NOVEMBER TEMPERATURE



L.G.M. NOVEMBER TEMPERATURE

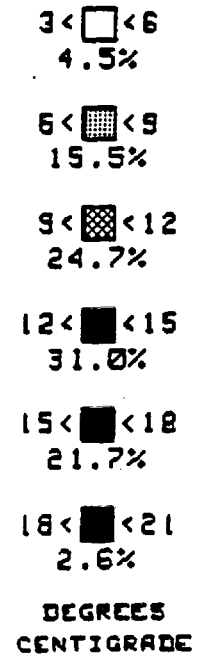
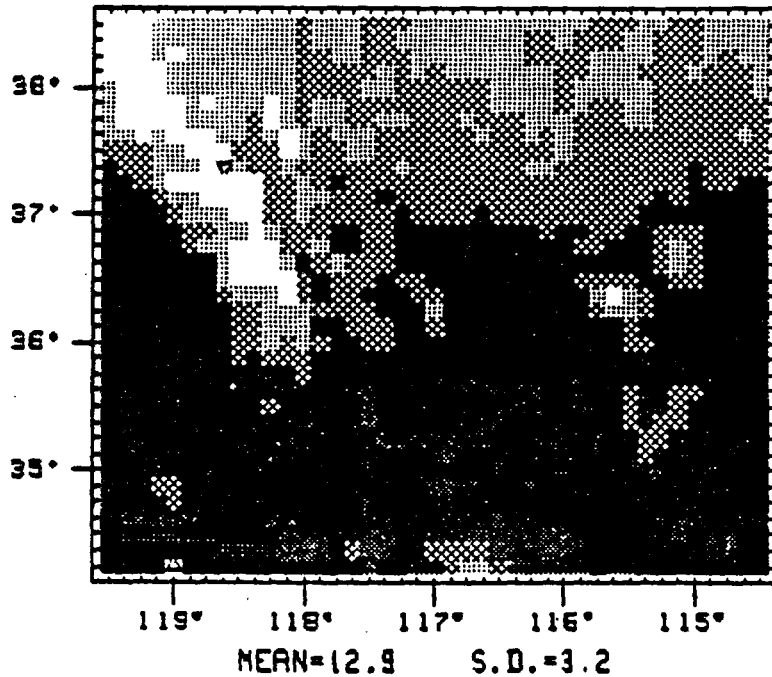
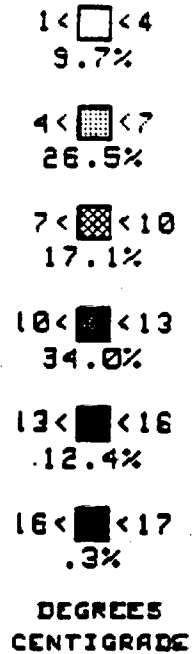
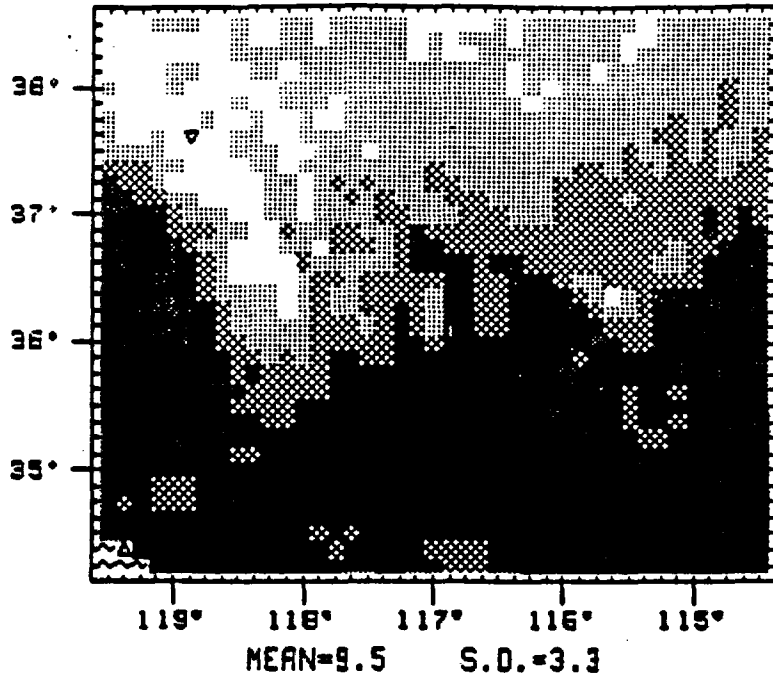


Figure 15. November modern (top) and last glacial maximum (bottom) temperatures.

MODERN DECEMBER TEMPERATURE



L.G.M. DECEMBER TEMPERATURE

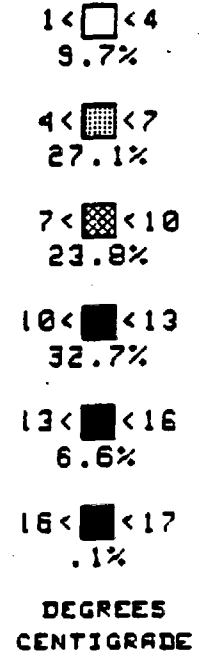
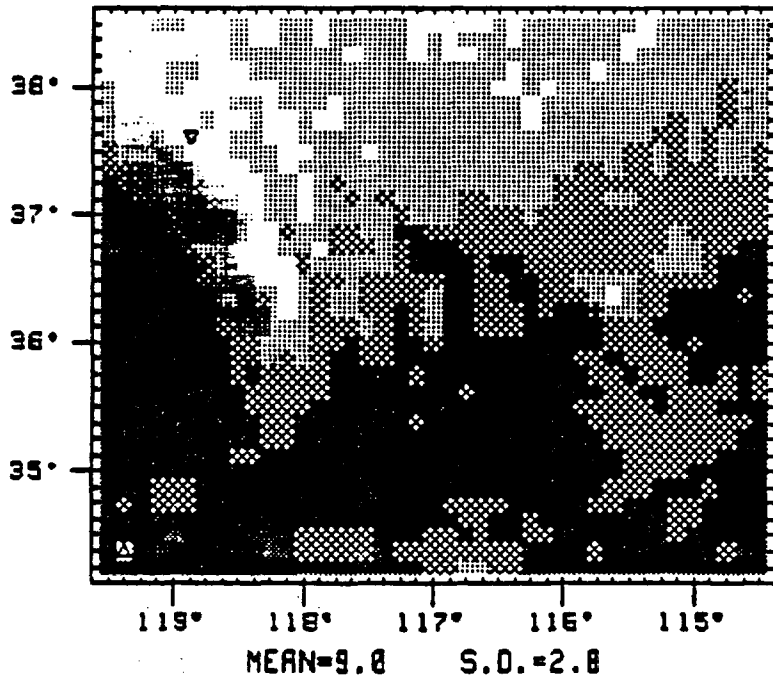


Figure 16. December modern (top) and last glacial maximum (bottom) temperatures.

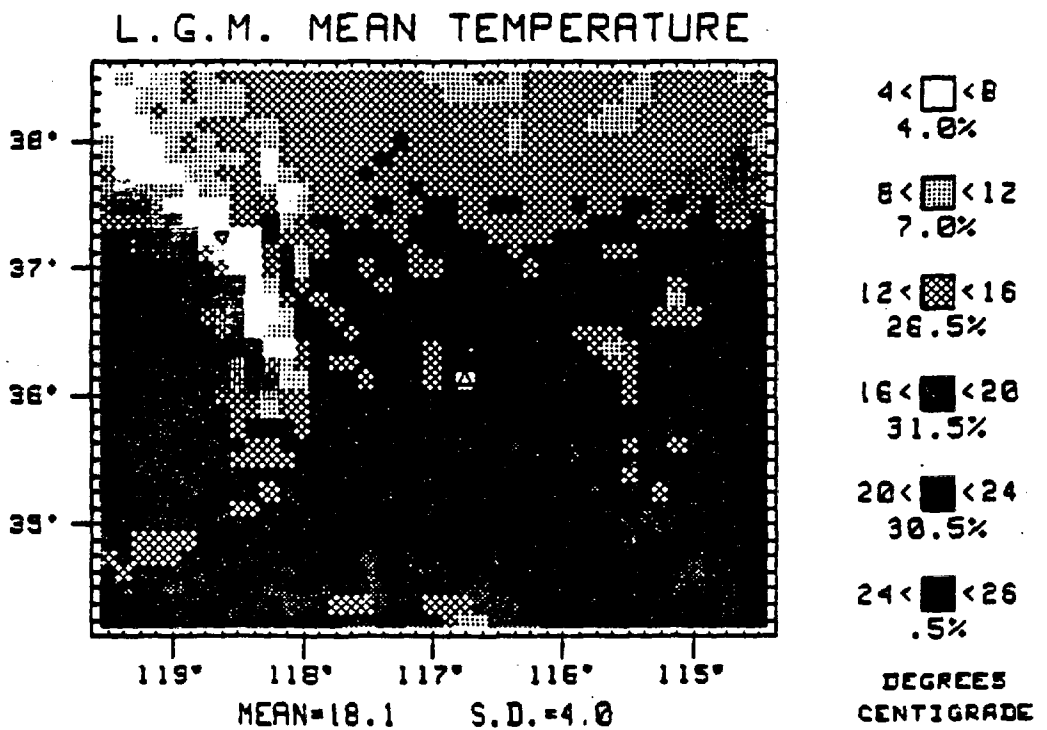
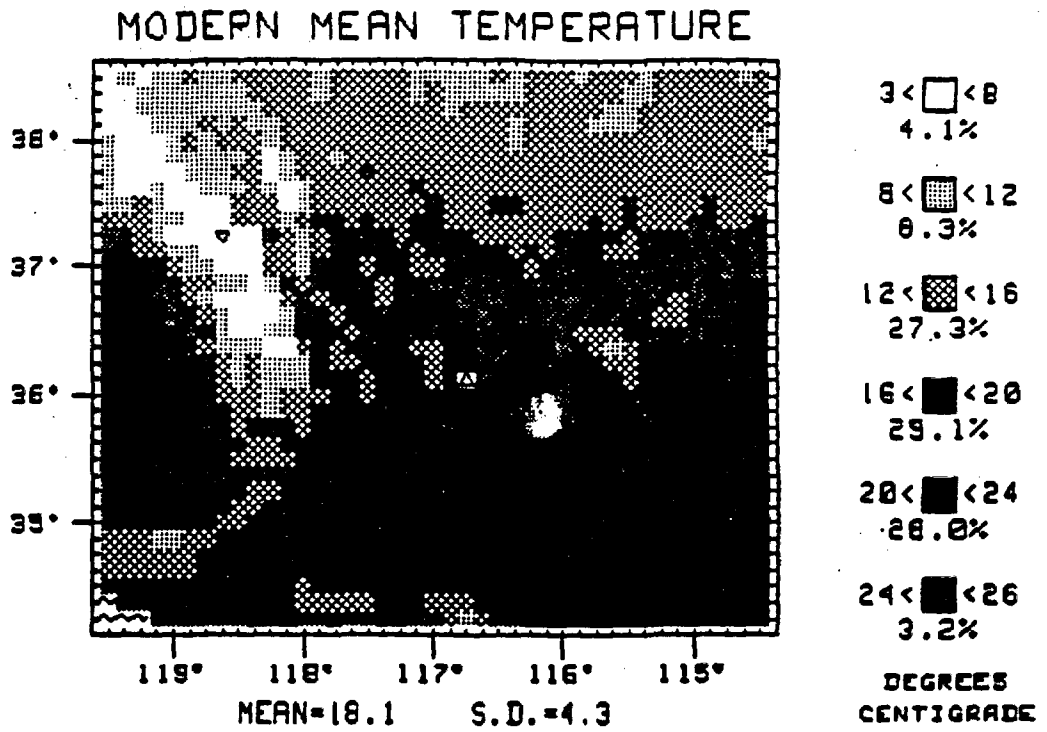


Figure 17. Mean annual modern (top) and last glacial maximum (bottom) temperatures.

The coding scheme represents the temperature using six different symbols. Except for adjusting the zero class limit, each symbol is applied over an equal range of values equal to one-sixth of the total range between absolute maximum and absolute minimum for that month. Of course, since the lowest temperature may occur at the LGM and the maximum in the present month, we determine the total range of values across both dates and then scale all values.

The six symbols were chosen to represent the highest temperature with the darkest character. Successively lighter characters represent cooler temperatures. This has the advantage of making the highest elevations white and of course snow is most common there. Discretizing the temperatures to six levels has the disadvantage of disguising much information. Many subtle differences are lost. Color displays are available and they are a great aid to show the subtler variations. Only careful examination of the figures will reveal the detail that is available. Of course, exact values for any point can be extracted from the equations.

In general, the resulting predictions show the very strong control elevation exerts upon temperature. The lowest temperatures consistently occur in the highest elevations. The converse is also true. Death Valley, the southeastern Mojave Desert and the lowest portions of the San Joaquin Valley are hot. During the summer months the San Joaquin Valley is not as hot as the Mojave Desert and Death Valley

(in each figure the hottest point is marked with a Δ , the coldest with a ∇). Subzero temperatures are found in the Sierra Nevada Mountains and the White Mountains during the winter months (January through April). Coastal regions (in the southwestern part of the area) show the Mediterranean climate, warmer in winter and cooler in summer than comparable elevations in the remainder of the region. Relatively warmer temperatures also characterize the low elevations bordering the Colorado River. These are the warmest points in early spring and fall. Even comparatively minor highlands such as the Panamint Mountains, Inyo Mountains, Spring Mountains and the Sheep Mountains are identified in the predictions as remaining relatively cool.

Overall, we conclude that the predictive equations correctly model the temperature patterns typical of this region. The statistical measures are reassuring. In examination of residuals we have seen no systematic pattern of deviation. There are relatively large deviations (comprising 4% of the samples exceeding two standard errors, 0.5% exceeding three standard errors, see Table 5) are near what would be expected from a normal distribution (4.55% and .27% respectively), there is no spatial pattern to those deviations that would suggest systematic bias, and finally the spatial patterns and temporal patterns of predictions correspond to the intuition of those familiar with the present regional climate there.

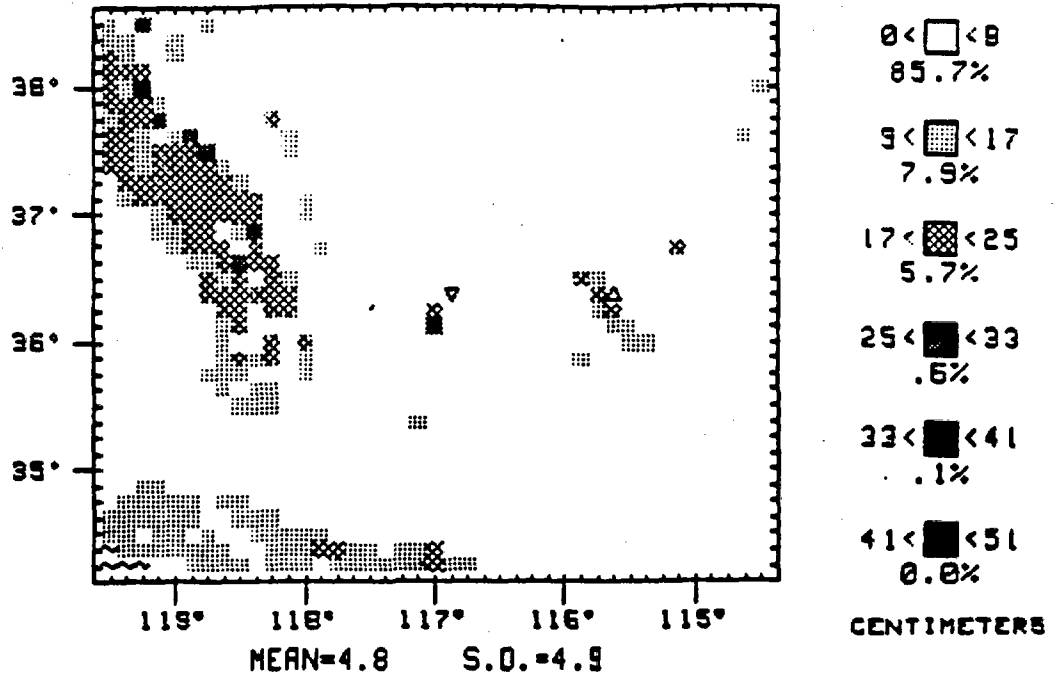
Precipitation

Again, we illustrate the estimates of modern precipitation throughout the entire level II area (Figures 18-30) for each month and for the annual total. For these displays we use a coding scheme similar to that of the temperatures. As with temperatures, we show the highest precipitations in the grids with the lightest symbol (a blank) and lowest precipitations with the darkest symbol. This has the effect of showing higher elevations in darker shades. Because of the great increase of precipitation at the last glacial maximum, the sixth class for the very highest values is usually only occupied at the LGM.

Examination of Figures 18-30 reveals the expected strong elevation control of precipitation. Areas of highest precipitation include: the Sierra Nevadas, the White and Inyo Mountains, the Spring Mountains and the highest parts of the Panamint Range. These higher elevations are sites of greatest precipitation only in the cooler months, however. During the summer season of convective storms the higher plateaus in eastern Nevada receive the most rainfall, as would be expected (note the locations of the highs in July, August and September). Indeed, the pattern of the Great Basin low shows quite clearly in August.

In general, the lowest elevations receive scanty rainfall and it is fairly evenly distributed throughout the

MODERN JANUARY PRECIPITATION



L.G.M. JANUARY PRECIPITATION

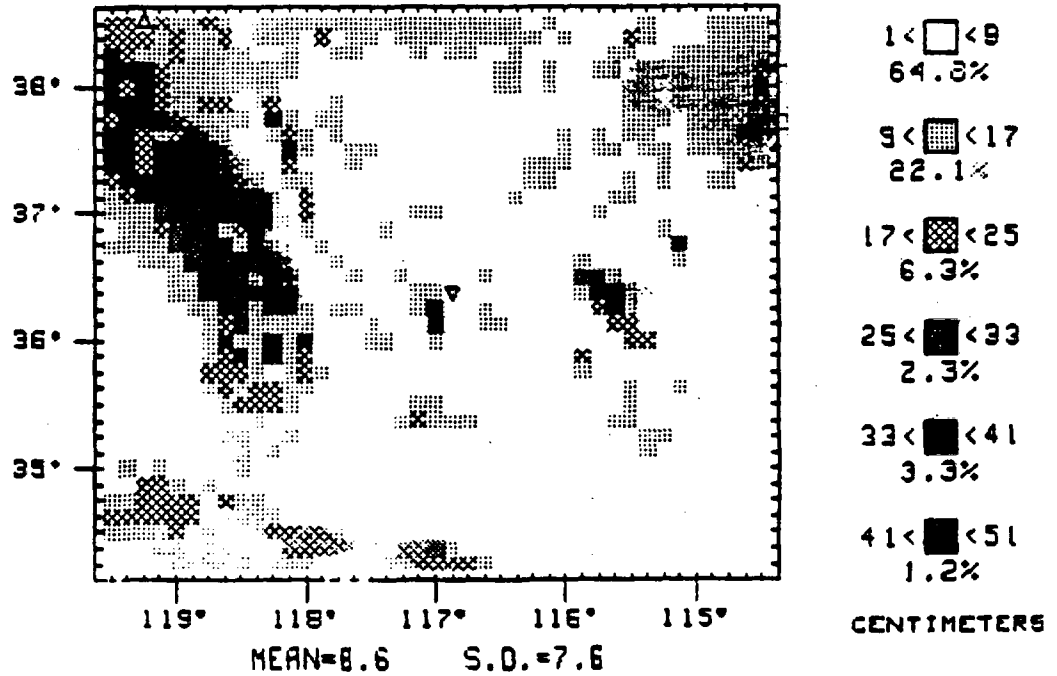
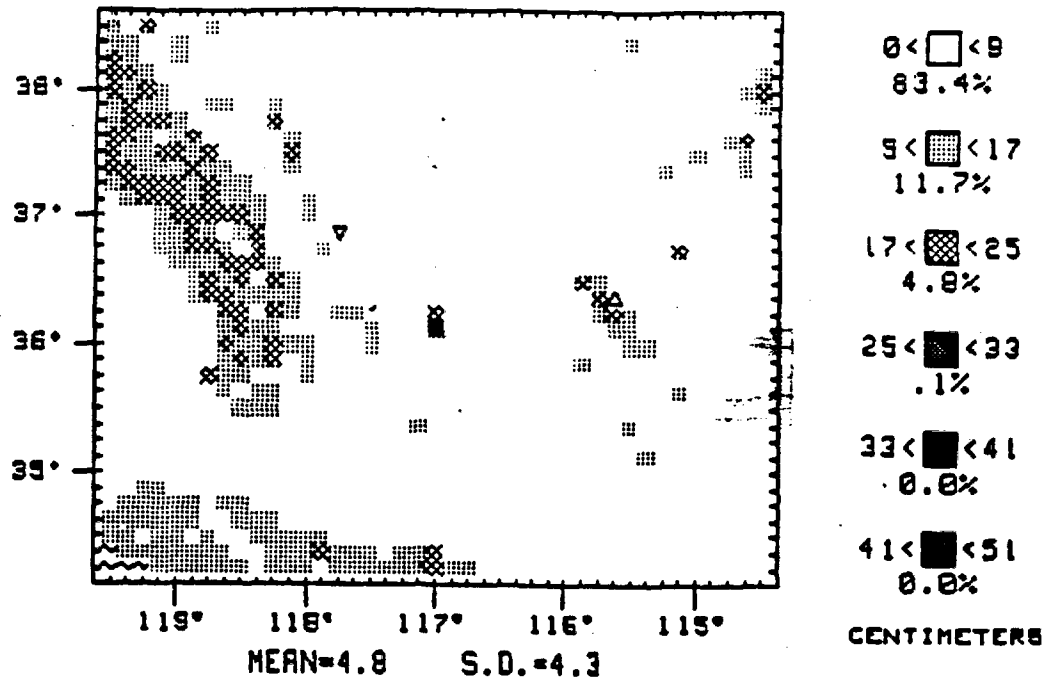


Figure 18. January modern (top) and last glacial maximum (bottom) precipitation.

MODERN FEBRUARY PRECIPITATION



L.G.M. FEBRUARY PRECIPITATION

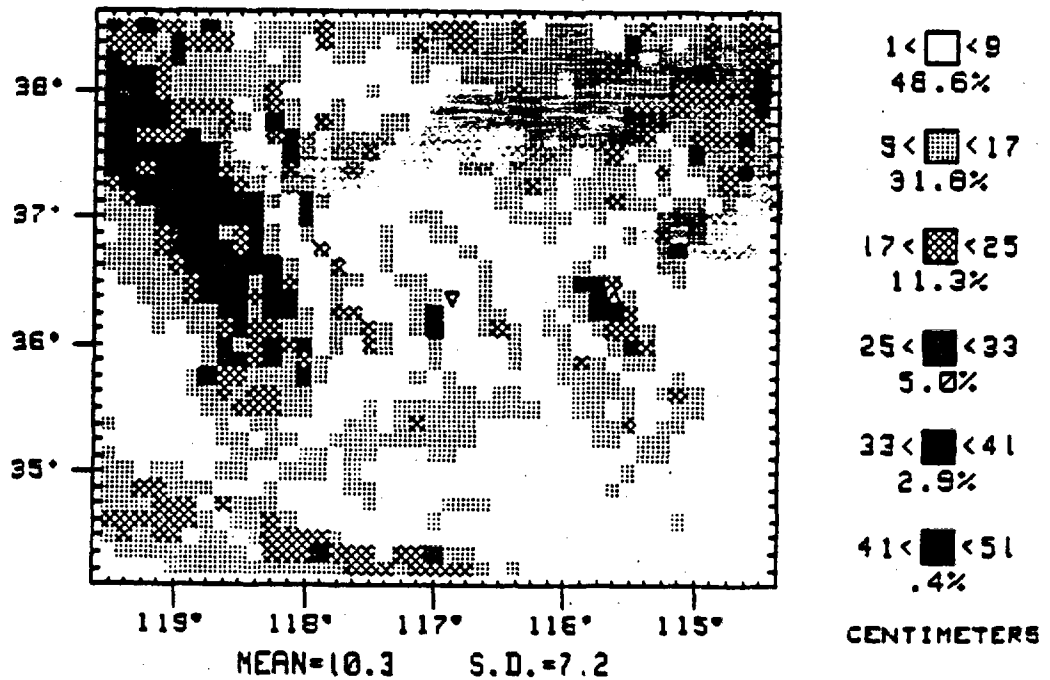
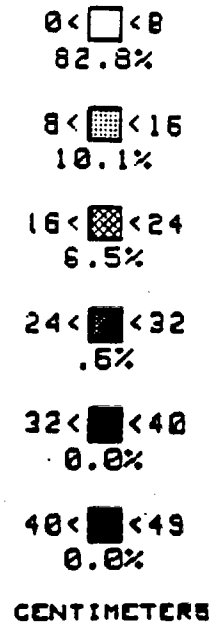
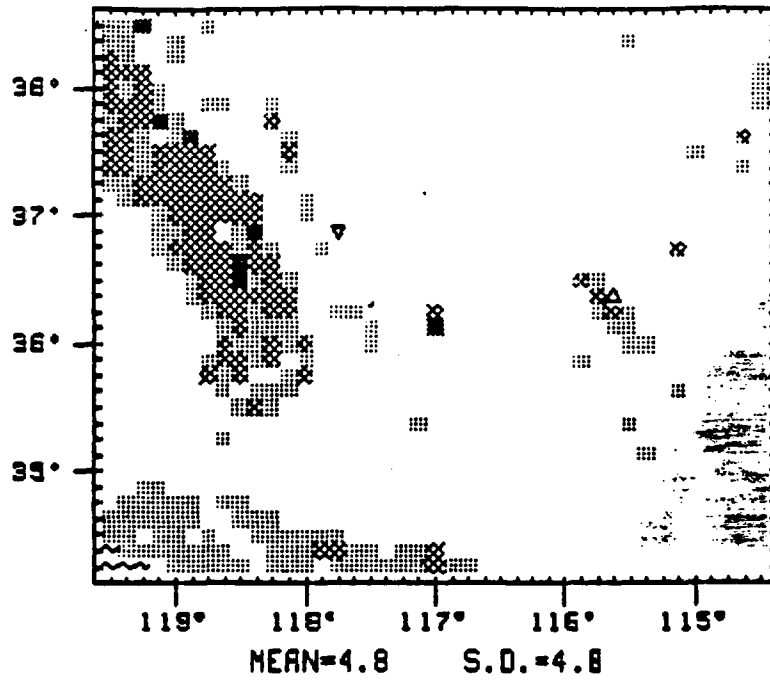


Figure 19. February modern (top) and last glacial maximum (bottom) precipitation.

MODERN MARCH PRECIPITATION



L.G.M. MARCH PRECIPITATION

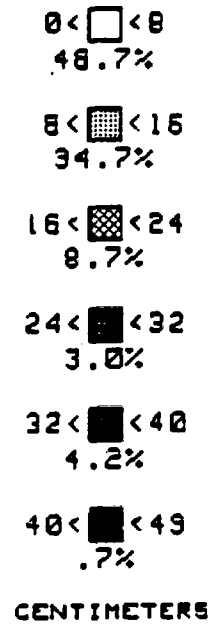
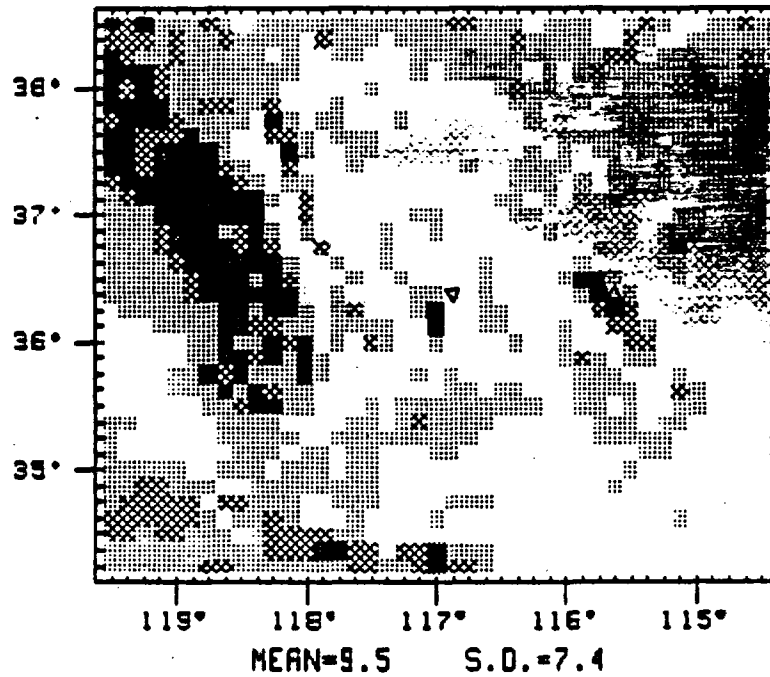
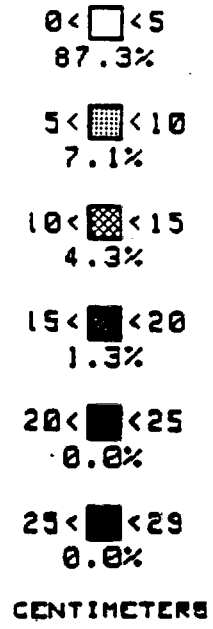
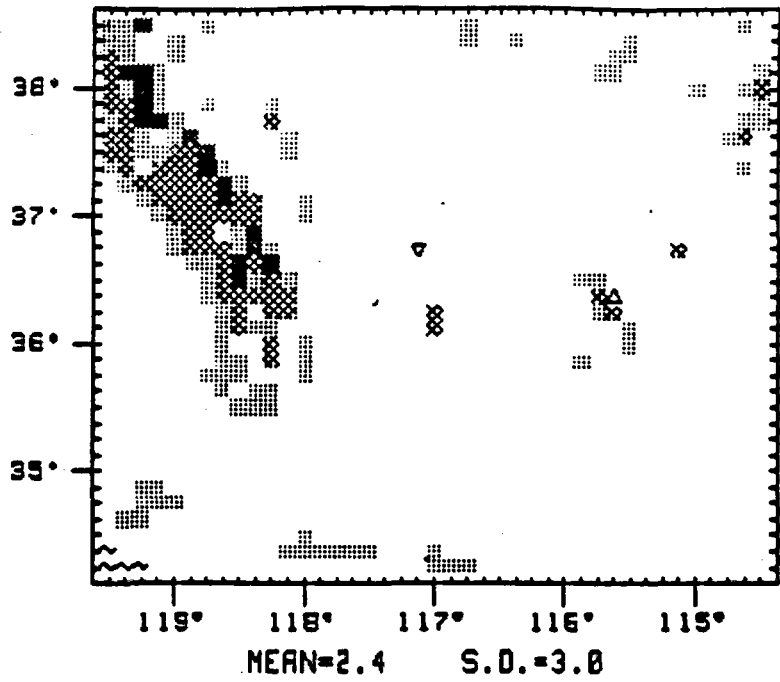


Figure 20. March modern (top) and last glacial maximum (bottom) precipitation.

MODERN APRIL PRECIPITATION



L.G.M. APRIL PRECIPITATION

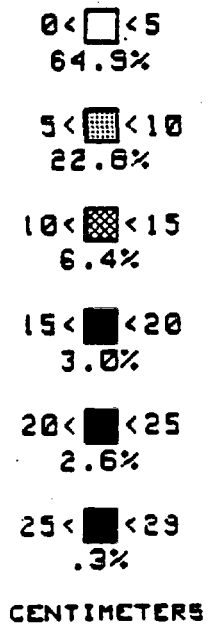
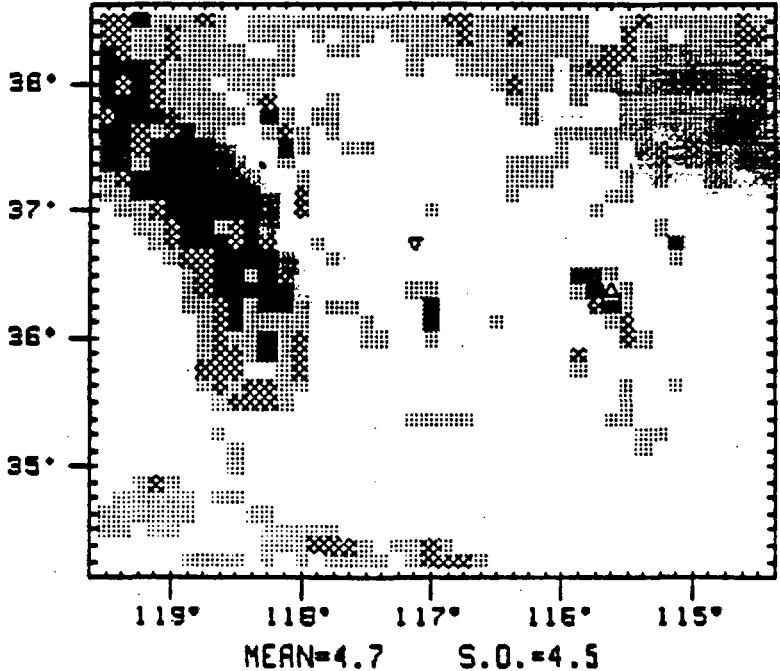


Figure 21. April modern (top) and last glacial maximum (bottom) precipitation.

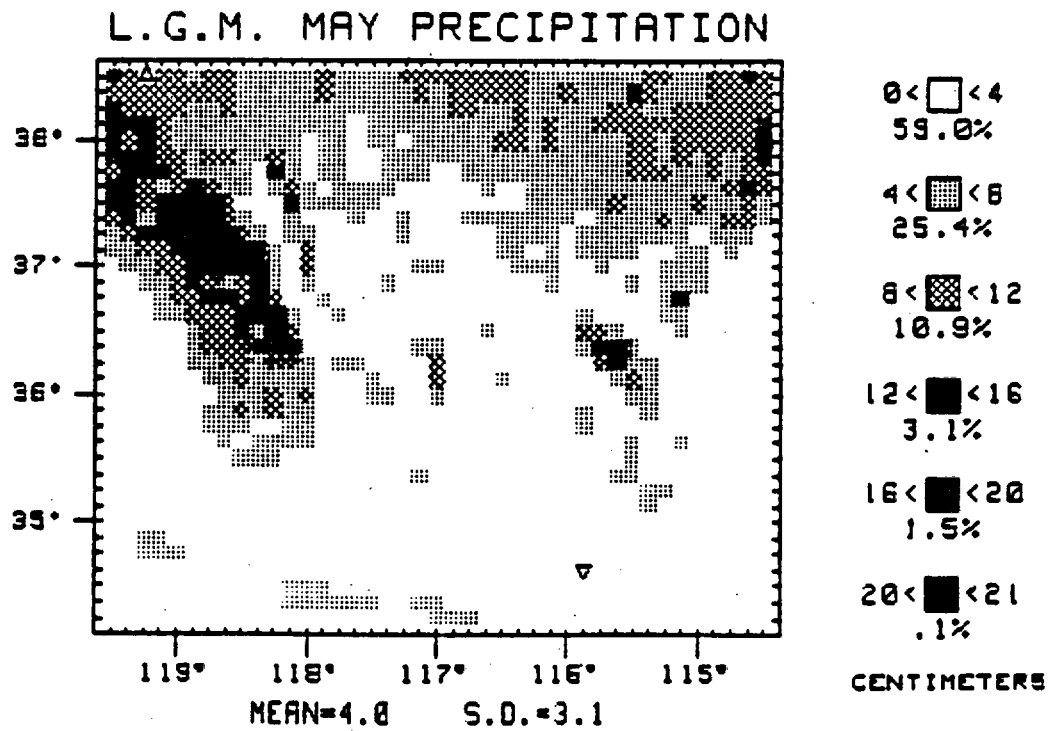
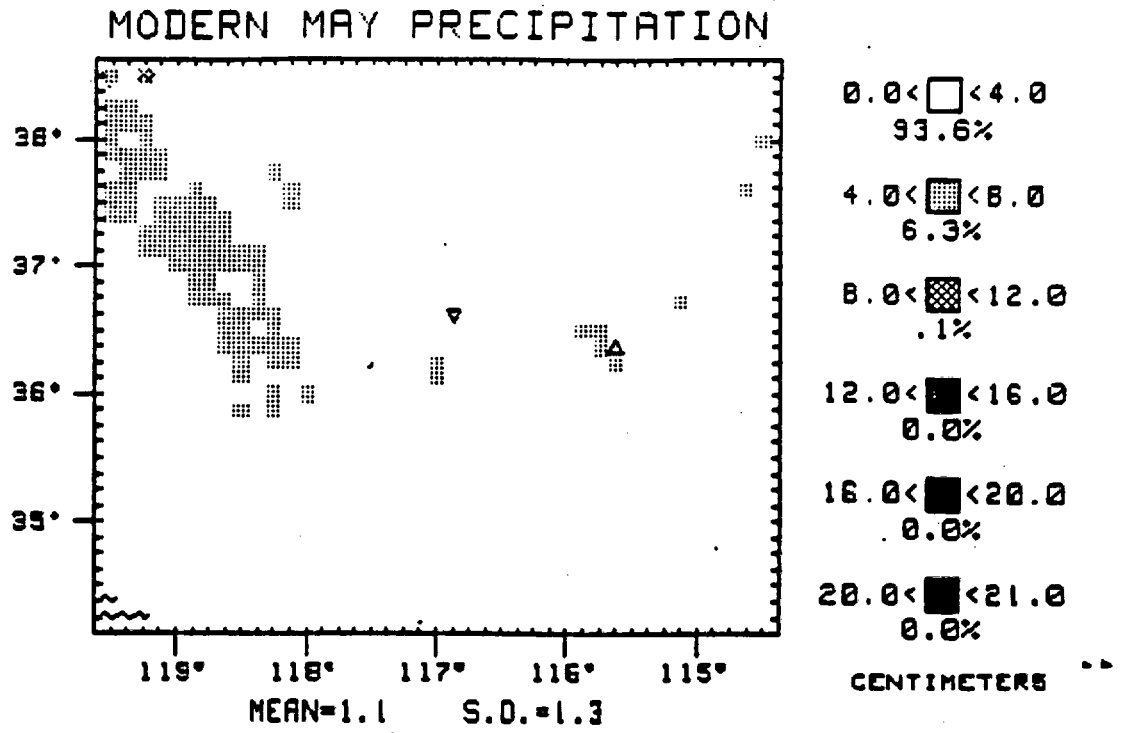


Figure 22. May modern (top) and last glacial maximum (bottom) precipitation.

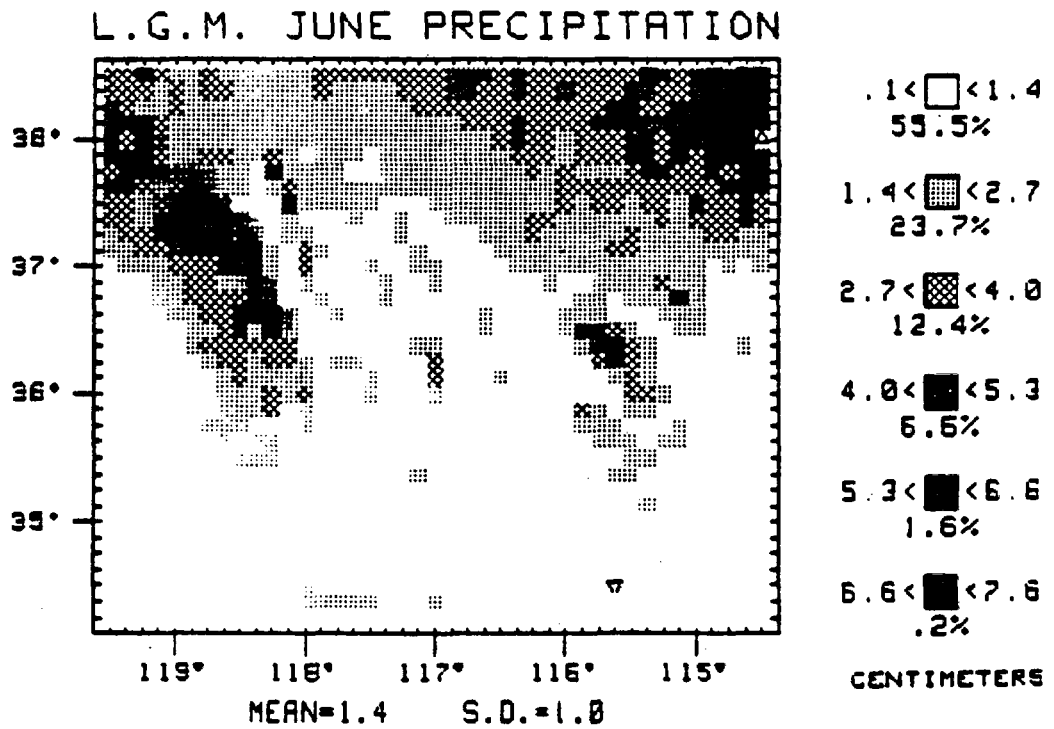
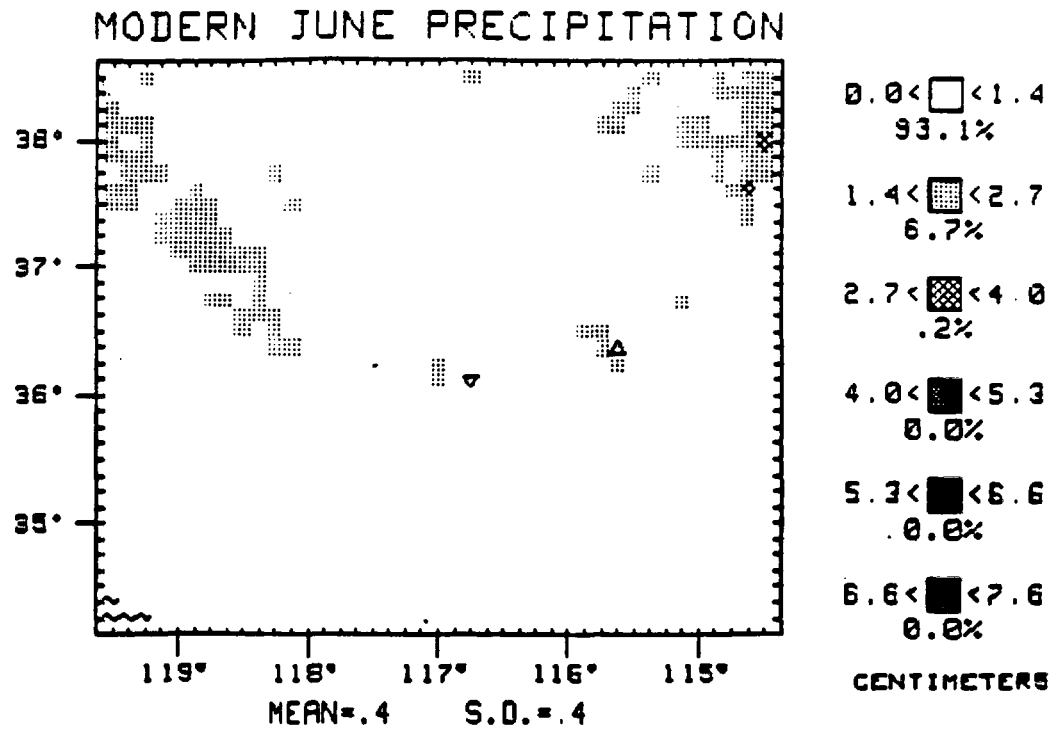
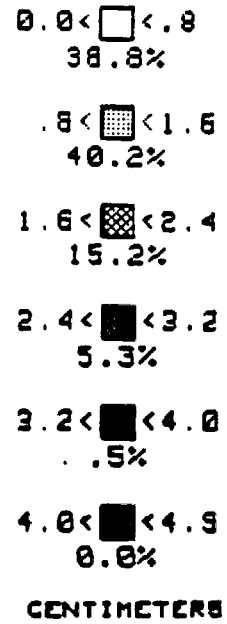
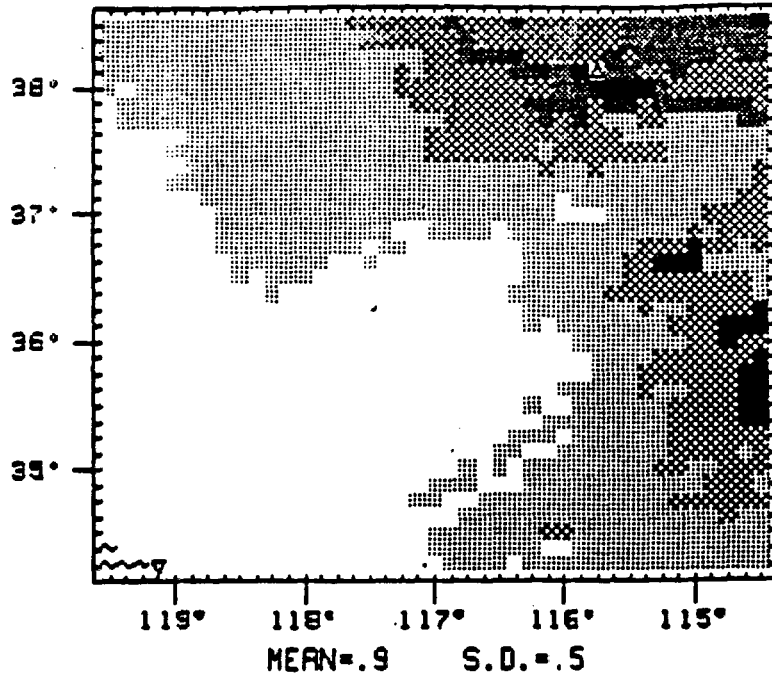


Figure 23. June modern (top) and last glacial maximum (bottom) precipitation.

MODERN JULY PRECIPITATION



L.G.M. JULY PRECIPITATION

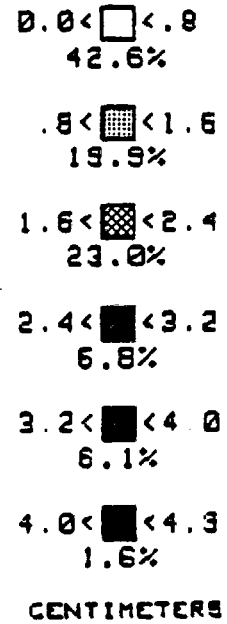
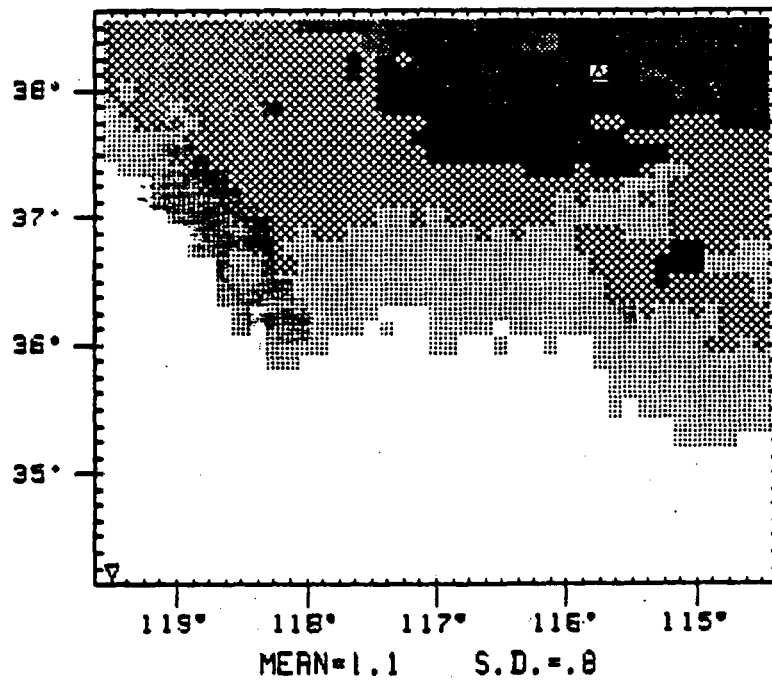
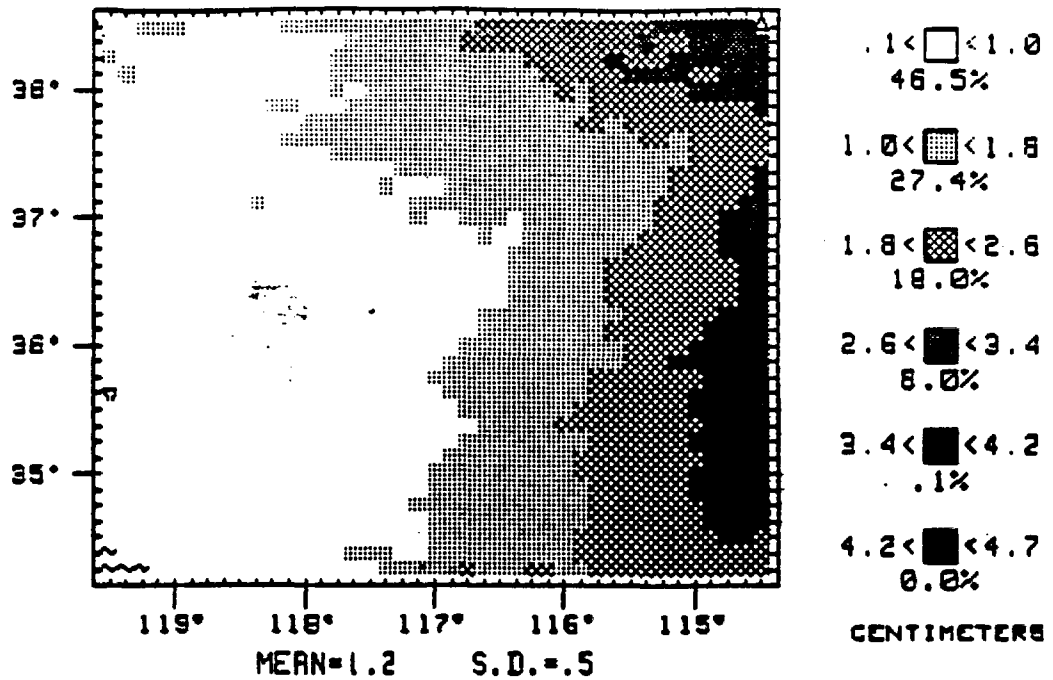


Figure 24. July modern (top) and last glacial maximum (bottom) precipitation.

MODERN AUGUST PRECIPITATION



L.G.M. AUGUST PRECIPITATION

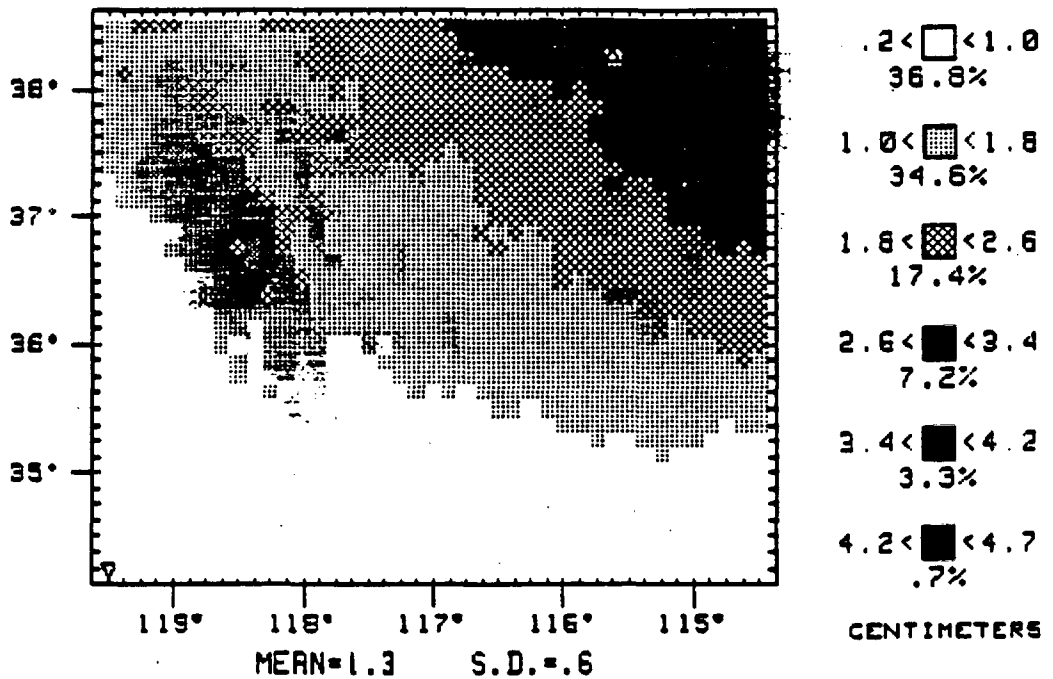
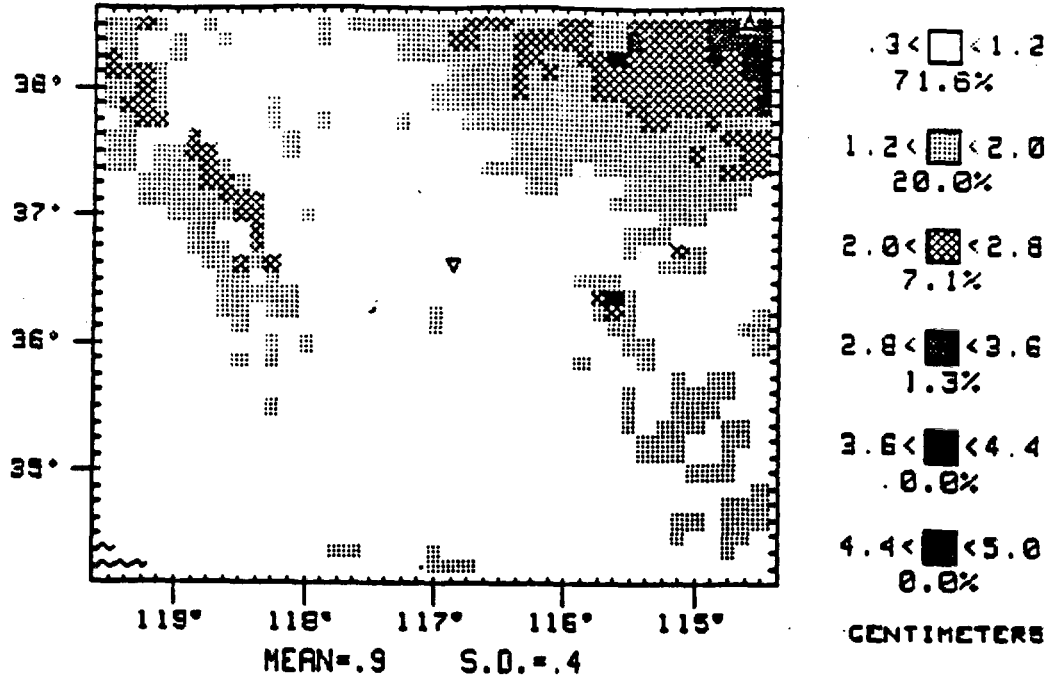


Figure 25. August modern (top) and last glacial maximum (bottom) precipitation.

MODERN SEPTEMBER PRECIPITATION



L.G.M. SEPTEMBER PRECIPITATION

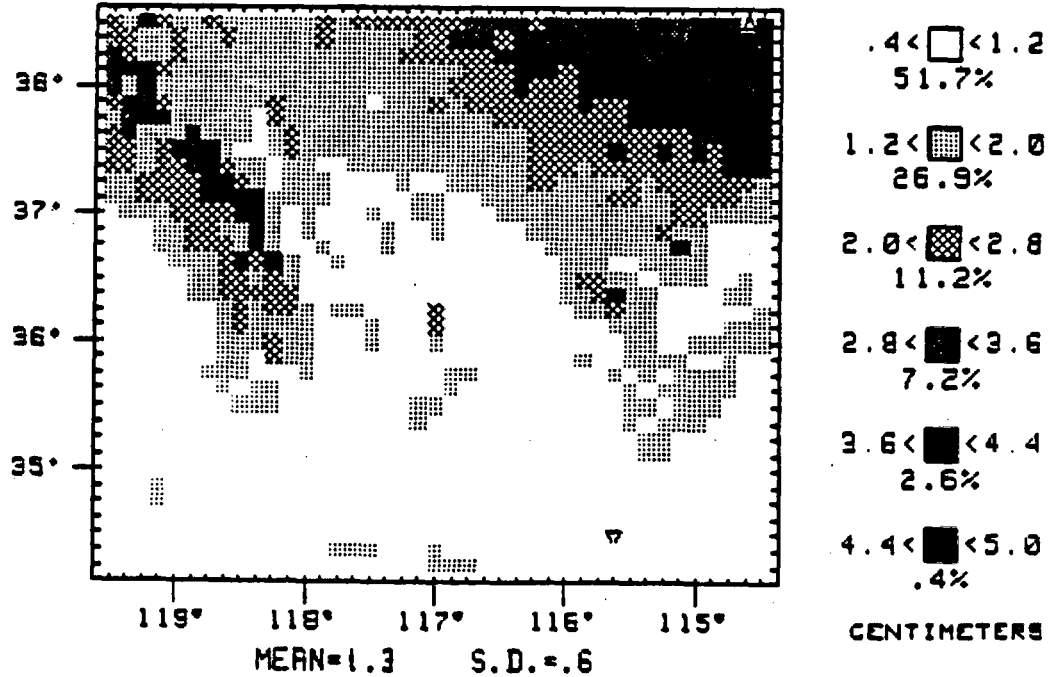
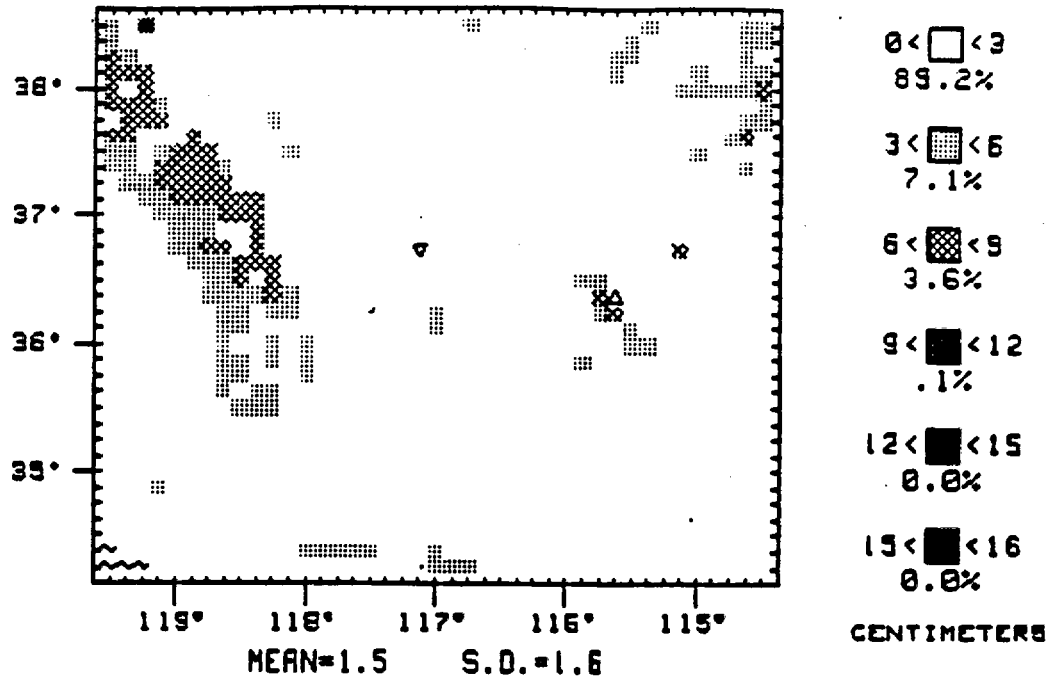


Figure 26. September modern (top) and last glacial maximum (bottom) precipitation.

MODERN OCTOBER PRECIPITATION



L.G.M. OCTOBER PRECIPITATION

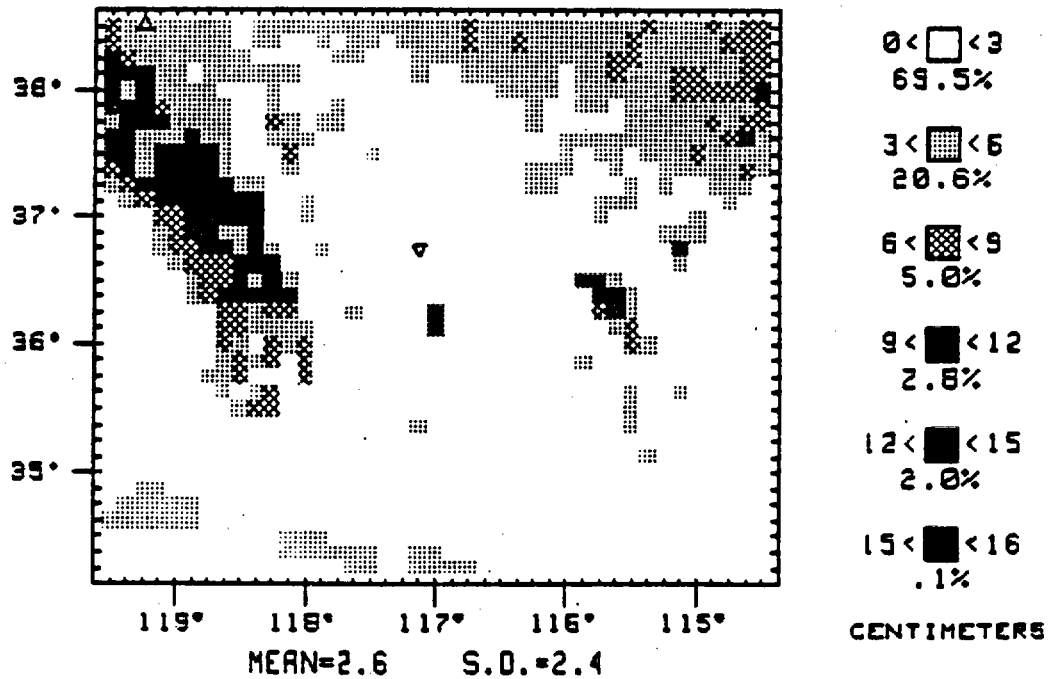
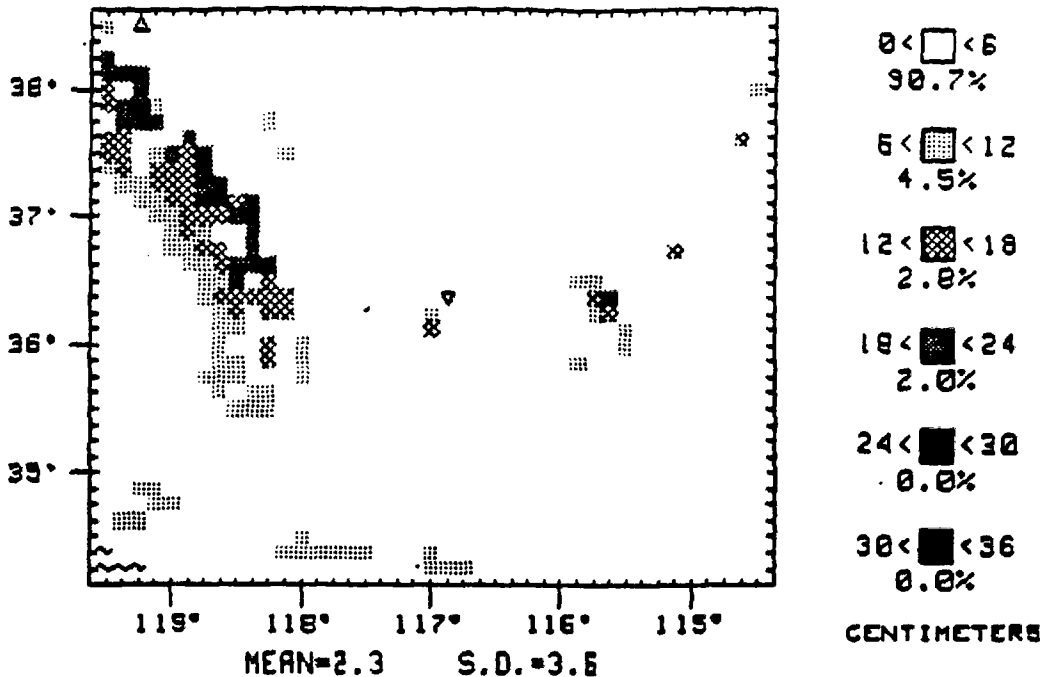


Figure 27. October modern (top) and last glacial maximum (bottom) precipitation.

MODERN NOVEMBER PRECIPITATION



L.G.M. NOVEMBER PRECIPITATION

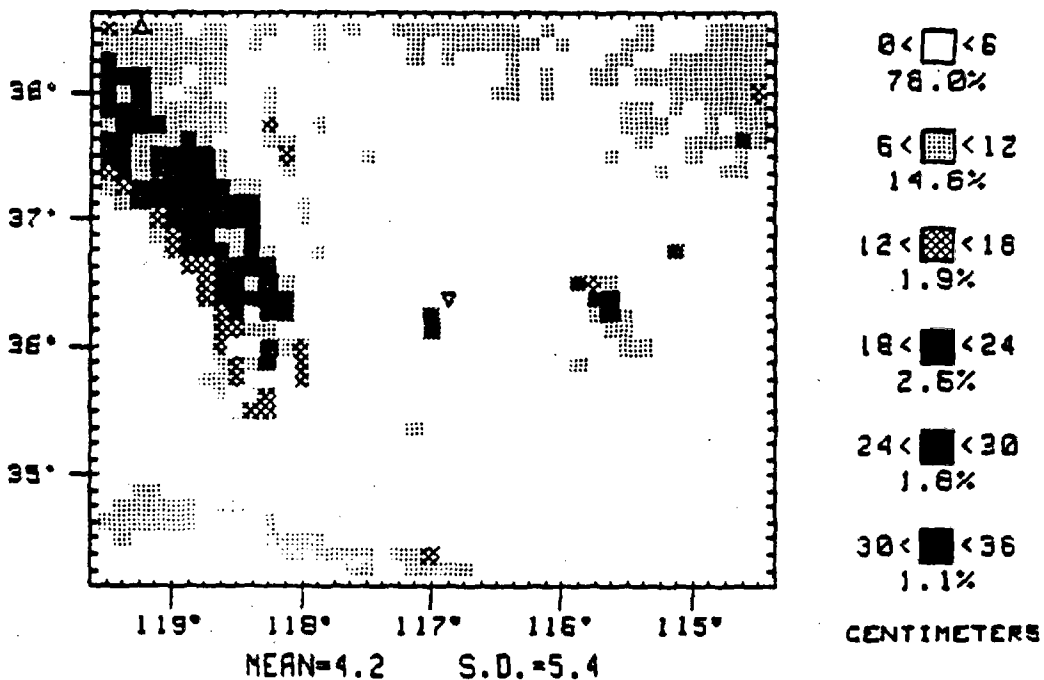
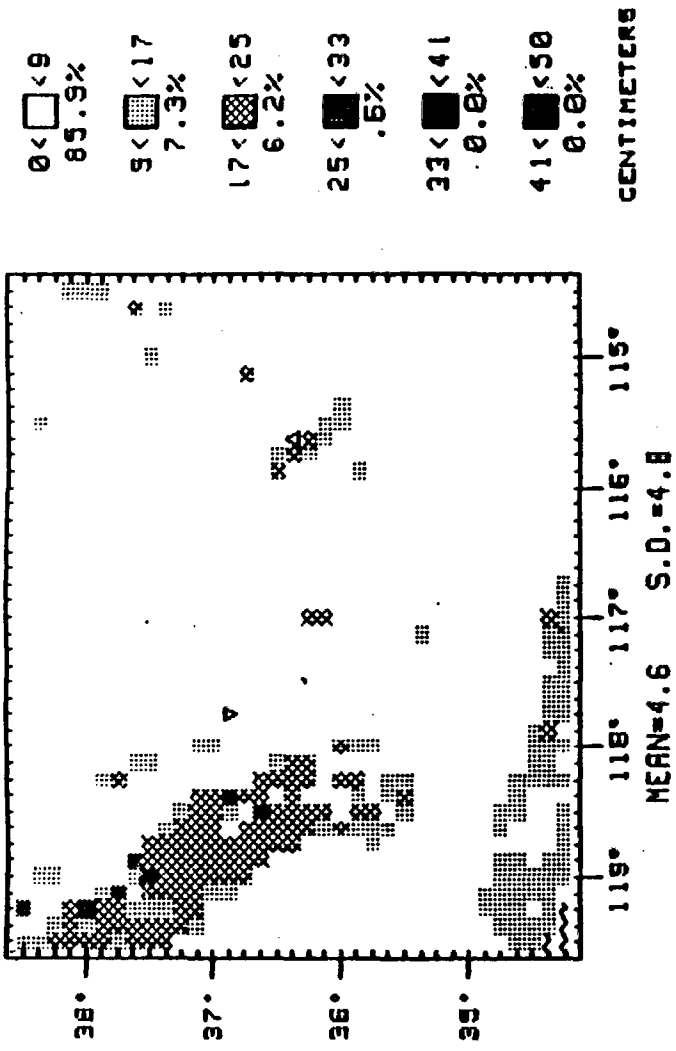


Figure 28. November modern (top) and last glacial maximum (bottom) precipitation.

MODERN DECEMBER PRECIPITATION



L.G.M. DECEMBER PRECIPITATION

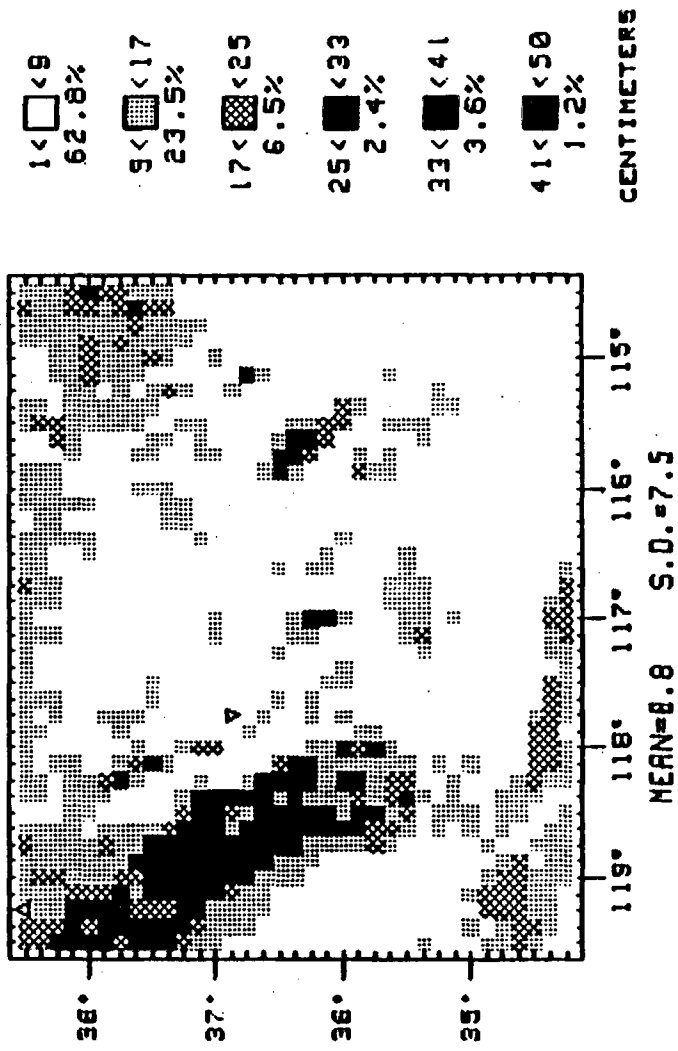
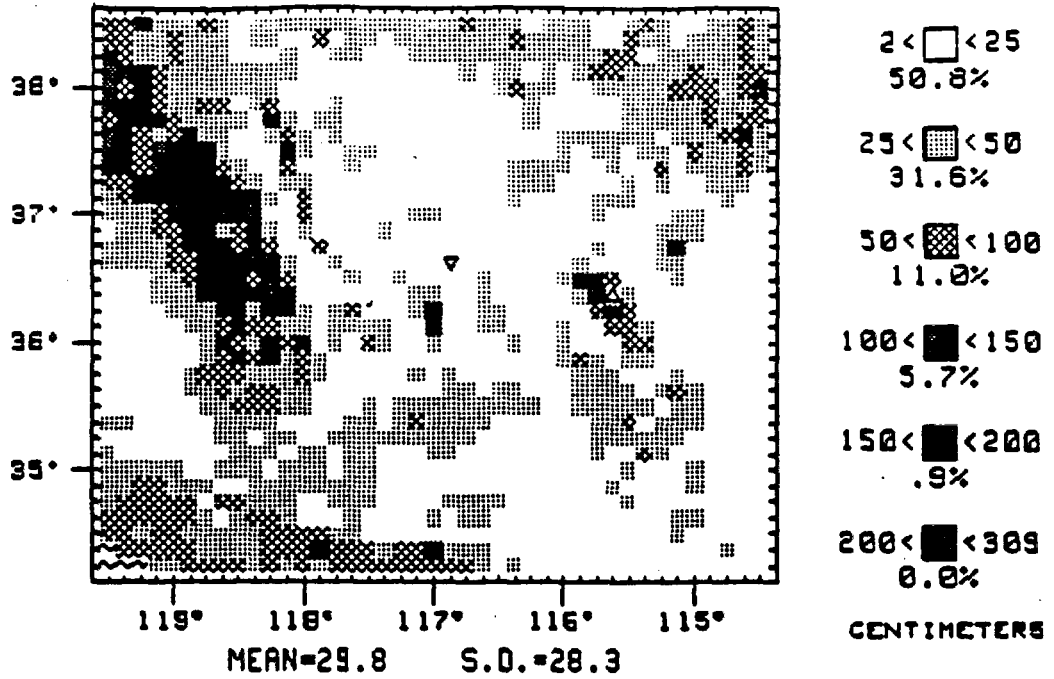


Figure 29. December modern (top) and last glacial maximum (bottom) precipitation.

MODERN TOTAL PRECIPITATION



L.G.M. TOTAL PRECIPITATION

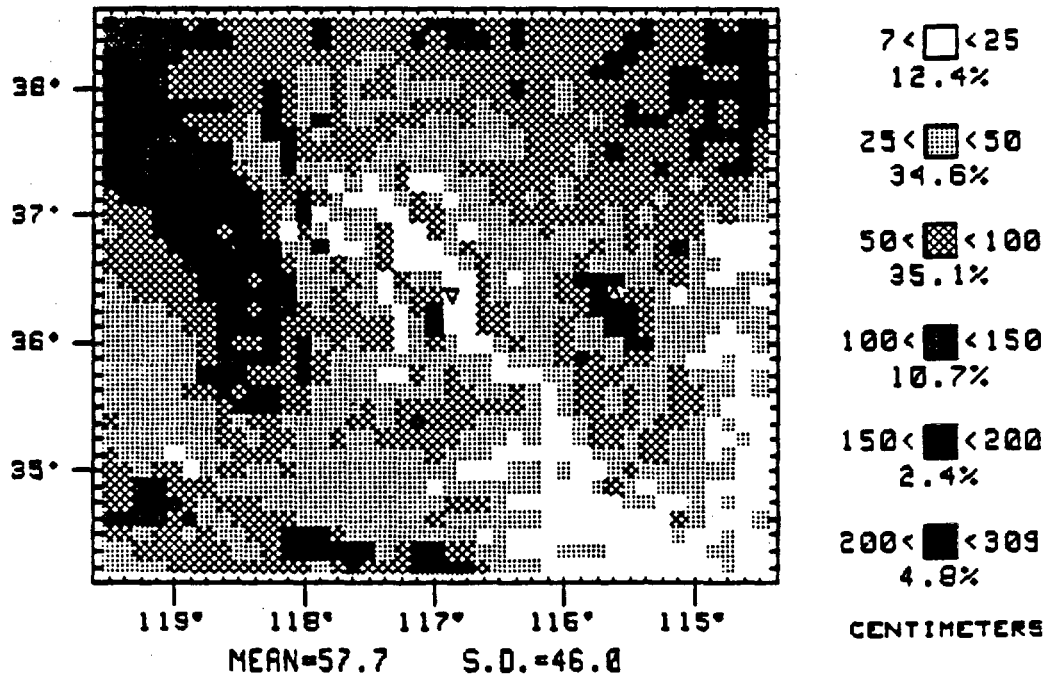


Figure 30. Total annual modern (top) and last glacial maximum (bottom) precipitation.

year. Thus the driest points in Death Valley only receive about 2cm rainfall. It should be noted that the standard deviation of this prediction is 1.05. Thus there is about a one-in-seventeen chance that no precipitation will be observed in Death Valley in a given year. This agrees reasonably well with meteorological observations there. For example, Hunt (1975, p. 19, fig. 8) reports two years - of 48 - which had no rainfall. He also reports an average of 4.22cm for the 48 yrs. Hunt's station is not, of course, the driest point.

Other arid regions (less than 25cm per year) include the Mojave Desert, the low-lying areas along the Colorado River, the San Joaquin Valley, Death Valley, Panamint Valley and Owens Valley. Semi-arid regions (25cm to 50cm per year) include: the higher elevations in Nevada, the western foothills of the Sierras, and much of coastal California. Thus the predicted patterns correspond quite closely to that observed.

More exact evaluation of these data result from examination of the precise values of the predictions rather than relative patterns. The most meaningful comparisons are to the actual weather records. Differences between observed and predicted precipitation were computed for each of the 124 stations where data could be obtained. In Table 5 were listed those stations where deviations exceed two standard

errors of the regression equation (from 0.06 to 0.19, depending on the month, see Table 4). About 4% of the stations show these relatively large residual errors. This is slightly fewer than the number expected (4.55%) but well within the acceptable limits for the hypothesis of normality.

There is no evidence to suggest that the residuals are not normally distributed. This was tested with Fisher's g_1 and g_2 (Table 6). Only single outliers appear in histograms of the residuals and these are due to different climate stations in each case. Furthermore, no spatial pattern of unusual residuals can be detected. It is concluded that the fit of the model is acceptable.

Consideration of the predictions for individual months reveals the expected seasonal variations within this highly diverse area. Precipitation is greatest (mean = 48cm) in January, February, and March; least (mean = .4cm) in June with gradual and consistent changes in between (see Figures 5-16). The Mediterranean climate of coastal California (extreme southwest) is evident. There precipitation reaches a separate maximum in March and is quite low at other times in the year. It reaches a minimum there in July. Since the highest elevations receive the greatest precipitation in winter months - months which are characterized by sub-zero temperatures - it is reasonable to assume that considerable snowpacks form there, especially in the Sierra Nevada.

Several glaciers do exist in the Sierras today. Finally, the very low precipitations coupled with the high temperatures at the lowest elevations will almost certainly result in a significant water deficit there in the summer months, and in places throughout the year. This is consonant with the known climatic conditions in these arid areas. Thus the seasonal patterns reflected in these predictions correspond well with common observations.

For comparison the values of R^2 reported by Houghton (1979) -- in the only comparable predictive model known to us -- are also reported in Table 4. As can be seen (Table 4) our equations represent a significant improvement upon Houghton's. This is especially important in that Houghton's predictions are simply *relative* precipitation at adjacent stations, one upland and one lowland. That is a simpler task since it assumes prior knowledge of the lowland values. Of course, our task requires prediction of both highland and lowland climates.

Because of their noted successes in describing the present climate of the area we are encouraged to extrapolate these predictions at the conditions of the last glacial maximum. As in the case of the temperature equations, these precipitation models are constructed of variables that do allow solution at other geologic times. Thus we have solved the

equations using the boundary conditions assumed to represent the last glacial maximum. Those solutions are depicted in the bottom illustrations of Figures 18-30 and are described in detail in the following section.

APPLICATION TO OTHER GEOLOGIC BOUNDARY CONDITIONS

A significant advantage of these equations is that they are based upon a set of variables representing the physical factors that control orographic climates. We have included variables that reflect: (1) adiabatic cooling in unsaturated and saturated conditions, (2) adiabatic heating (3) diffusion and mixing, (4) available precipitable water, (5) insolation and, (6) atmospheric pressure. Thus, the relative importance of each physical process is evaluated and represented. Furthermore, by including the values of temperature and precipitation already predicted, the known systematic intra-annual variability is preserved.

A further advantage of the equations we have used is that they were constructed using variables that do not require modern observational meteorological equipment to estimate. An example of such (undesirable) variables would be the atmospheric pressure, or the relative humidity. Although these variables are doubtlessly of importance, they are not readily predictable for times other than the present. The variables we have used are available within the geologic record. Thus, using these variables we can estimate climate for other periods.

The majority of variables we use are derived directly from the elevation grid. To apply this grid to other

times carries with it the implicit assumption that elevation has not changed from that time to today. To the extent that this assumption is not correct the estimates of climate will be in error. We have not yet studied this question in detail. Our effort to date has concentrated upon the climate during the last glacial maximum (~18K yr BP). For this relatively recent period we assume that change in topography has been minor. Sensitivity analysis of this point could be performed. Presumably the solutions will decrease in accuracy over longer time spans in an approximately monotonic fashion. This will hold whether we are predicting the past history or the future. For times at great distances (say approaching 100,000 years) additional phenomena will become increasingly important in defining the climate.

Besides the elevation grid, three additional variables must be known in order to predict climate using these equations. Sea-surface temperature, dominant wind patterns and sea-level each must be known. Both sea-surface temperature and dominant wind patterns must be estimated for two months - February and August. We have structured our equations to take advantage of the availability of estimates of sea-surface temperatures in both of these months because of recent advances made by members of the CLIMAP project

(McIntyre, et al., 1981). Using a statistical transfer function based upon the relative abundances of several nannoplankton species (Imbrie and Kipp, 1971) these workers have constructed estimates of modern sea-surface temperatures in these two months. From sediment cores in oceanic areas they have been able to apply the same equations to relative abundances of species preserved in the record. With this procedure, estimates for almost any date in the Quaternary could, in theory, be produced. A temporal limitation arises because of species evolution and extinction. Comprehensive maps of sea-surface temperature in August and February at the last glacial maximum have been produced. With these we can compute the sea-surface temperatures that are required in our equations.

It is more difficult to obtain estimates of dominant wind vectors for other times. Geologic evidence is available on a very irregular basis. The estimates we do have could easily reflect aberrant, rather than typical, conditions. An indirect approach that yields systematically available estimates is to use an atmospheric General Circulation Model (GCM) to solve for equilibrium circulation patterns under assumed boundary conditions. Such GCM solutions are regularly obtained for modern conditions. Because of the CLIMAP (1976; McIntyre, et al., 1981) project such boundary conditions have been estimated for the last glacial maximum.

We can use such GCM's to solve for the winds (meridional and zonal) at each of two atmospheric levels (400mb and 800mb) for both August and February (Gates, 1976). The meridional and zonal vectors are combined to yield a dominant wind vector direction. We use the values at the 400mb level since the higher altitude winds are closely descriptive of the regional circulation pattern that would pass over such a high range (>4000m) as the Sierra Nevada. It appears probable that circulation patterns shifted to the south during the last glacial maximum. The wind pattern has a direct impact on the value of every other variable (except elevation and slope at the site).

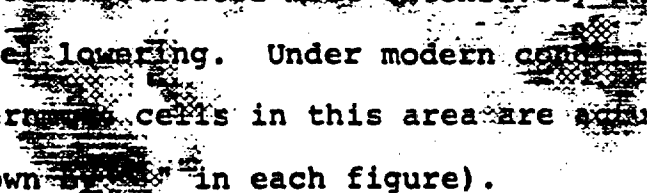
The last variable that must be known in order to solve the climate equations is the sea surface elevation. Sea level was lowered during the Quaternary; ice sheet growth ties up significant quantities of water. During melting the sea level rises again. We are interested in altitude of points above the current sea level. That altitude reflects the atmospheric pressure at that site and hence the degree of saturation. We assume that as sea level falls during a glaciation the column of air will fall in unison since the absolute mass of air remains constant. Any increase in sea surface temperature due to atmospheric derived heating during sea level lowering (Tinkler, 1983) is assumed to be reflected in the changed sea-surface temperatures as recorded by the CLIMAP group.

Since the equations have been constructed so as to allow estimates at other times we illustrate this capability by solving for the temperature and precipitation at the last glacial maximum. This is a convenient time for several reasons. As mentioned above, detailed and systematic reconstructions of the needed predictor variables are available (McIntyre, et al., 1981; Cayan, 1976), this is the best-documented paleoclimatic condition available. Furthermore, the area of interest (level III) contains geologic records that have been carefully studied for paleoclimate indicators. Thus we have the opportunity of testing our calculations against a number of independent lines of evidence. The most sensitive paleoclimatic indicator, paleo-lake levels, are well-documented in this period. We perform specific tests which are described in a later chapter.

PREDICTIONS OF LAST GLACIAL MAXIMUM CLIMATE

With these equations we have made estimates of the climatic conditions within the study area when the last global ice sheets were at a maximum areal extent. Accompanying this glacial maximum was a decrease in sea surface temperature off the California coast of several degrees centigrade and a drop in sea level of approximately 104 meters (mean of two values reported by Denton and Hughes, 1981, p. 272). To estimate the coastal configuration we have used bathymetric data obtained from the National Oceanic and Atmospheric Administration. For the more northerly portion of the study area bathymetric data were not available and we assume a gentle coastal gradient of approximately 2.1° . Although we believe that wind directions would become more southerly in each of the two months, February and August. For this analysis we do not assume a shift in dominant winds of these months. Under those assumed conditions we have solved for the same independent variables (Table I) at each grid point within the level II study area. Then, using those values we have made estimates of temperature and precipitation in each of the twelve months over this entire region. The results of these estimations are summarized below.

Temperature

Turning attention to the predictions of temperatures for the last glacial maximum it can be seen that the strong relation of temperature with elevation is preserved (Figures 5-17 bottom). The Sierras remain the relatively coolest portion of the area. Other high peaks, including the Spring Mountains and the Panamint Range become slightly cooler. Across the months the maritime influence in the southwestern portion of the area diminishes markedly. This is most apparent in comparing predicted temperatures for August and December. In August, temperatures in the southwest are much warmer, over 9°C warmer; although most of the Great Basin is cooler by up to 3°C. December temperatures in the southwest are slightly cooler, in places by up to 3.8°C. Such a change from a maritime climate there is not surprising, the ocean retreated most extensively in this area due to sea level lowering. Under modern conditions the four southwestern cells in this area are actually within the ocean (shown by  in each figure).

At the low elevations immediately surrounding Death Valley and extending southward into the Mojave Desert, the areal extent of zones of highest temperature shrink noticeably. Roughly one-twelfth as much of that area lies within the highest temperature zone. This in turn would imply that evapotranspiration from soil and vegetation will be lessened

around the margins of some basins. Furthermore, if lakes begin to grow, and as they rise to higher (cooler) elevations, evaporation from their surface will be lessened.

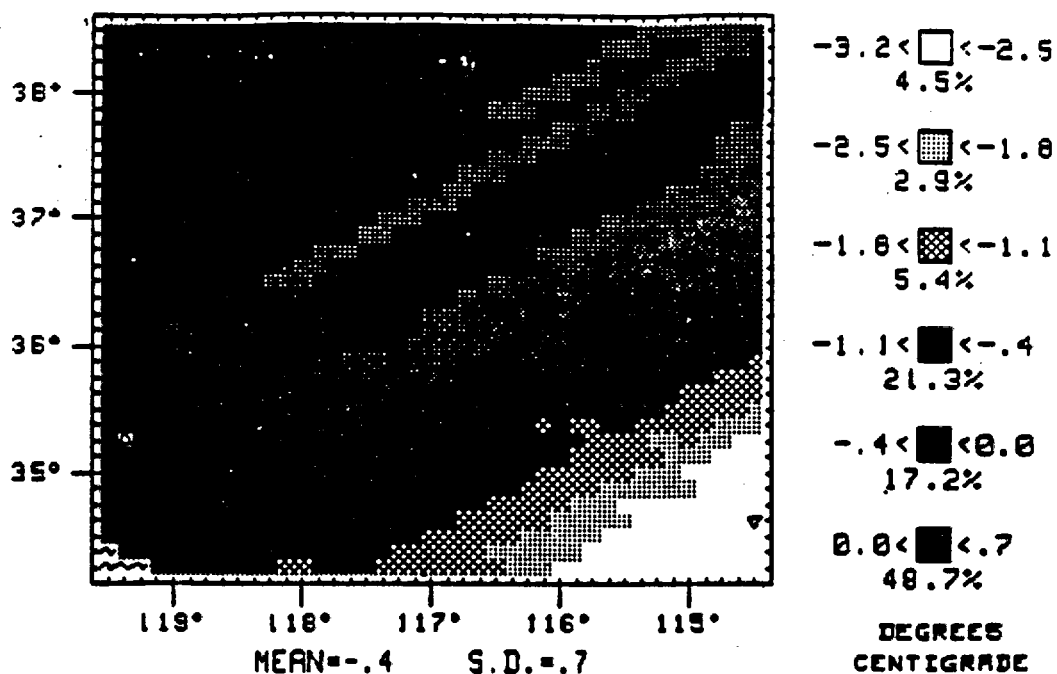
Remarkably, there is no consistent overall pattern of temperature change that typifies the entire area, even within any single month. Changes vary depending upon a bewildering variety of factors and are not subject to simplistic interpretation. For example, in every month temperatures decrease over large parts of the area. However, there are also significant portions of the area in which temperatures actually rise. In some spots, that rise is quite dramatic, as noted above as much as 9° in some parts of coastal California in August.

In order to more clearly illustrate these changes, we have calculated the differences in predicted values at each point, Δ_{ij} :

$$\Delta_{ij} = LGM_{ij} - P_{ij}$$

By subtracting the predicted values at present, P_{ij} , from the predicted values at the last glacial maximum, LGM_{ij} the difference is positive where temperatures rose in the last glacial maximum, negative where temperatures fell.

LGM MINUS MOD JANUARY TEMPERATURE



LGM MINUS MOD JANUARY PRECIPITATION

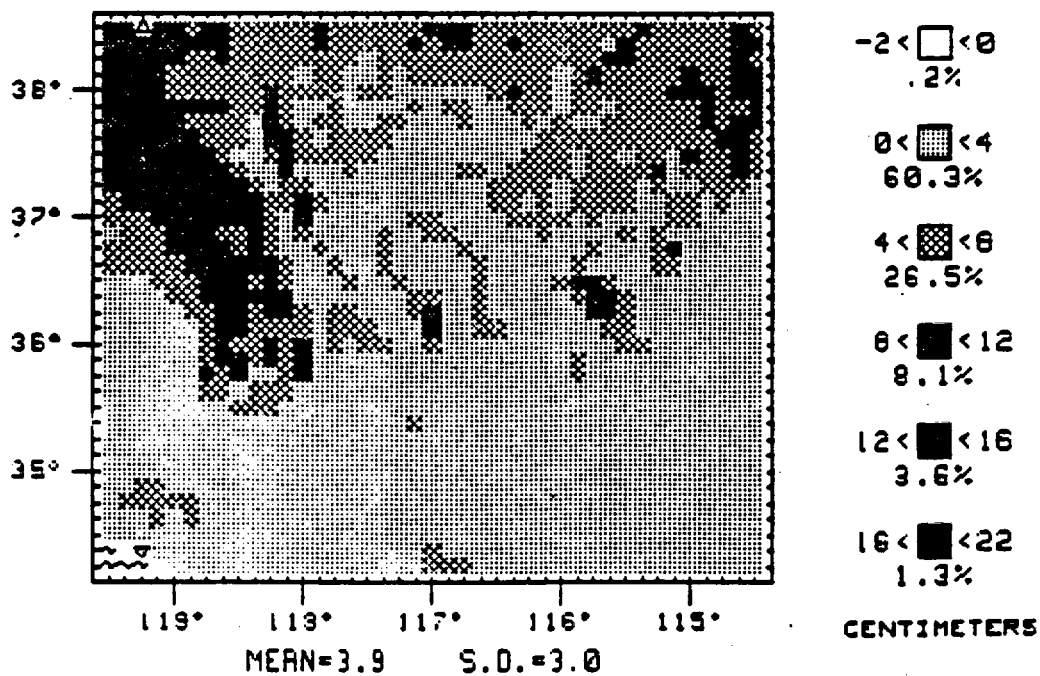
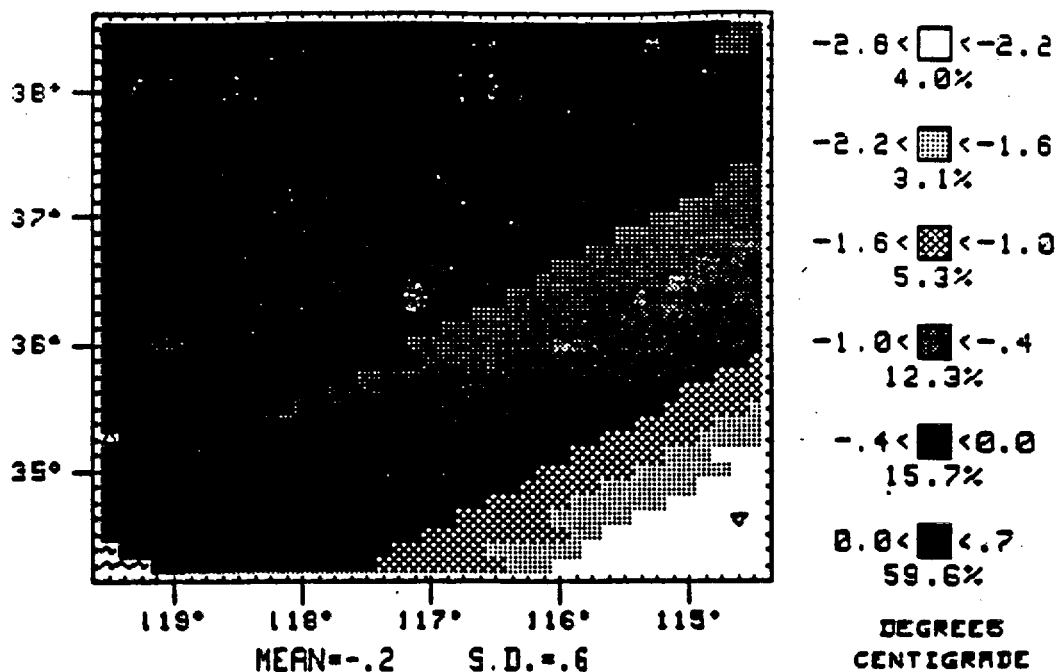


Figure 31. January temperature change (top) and precipitation change (bottom).

LGM MINUS MOD FEBRUARY TEMPERATURE



LGM MINUS MOD FEBRUARY PRECIPITATION

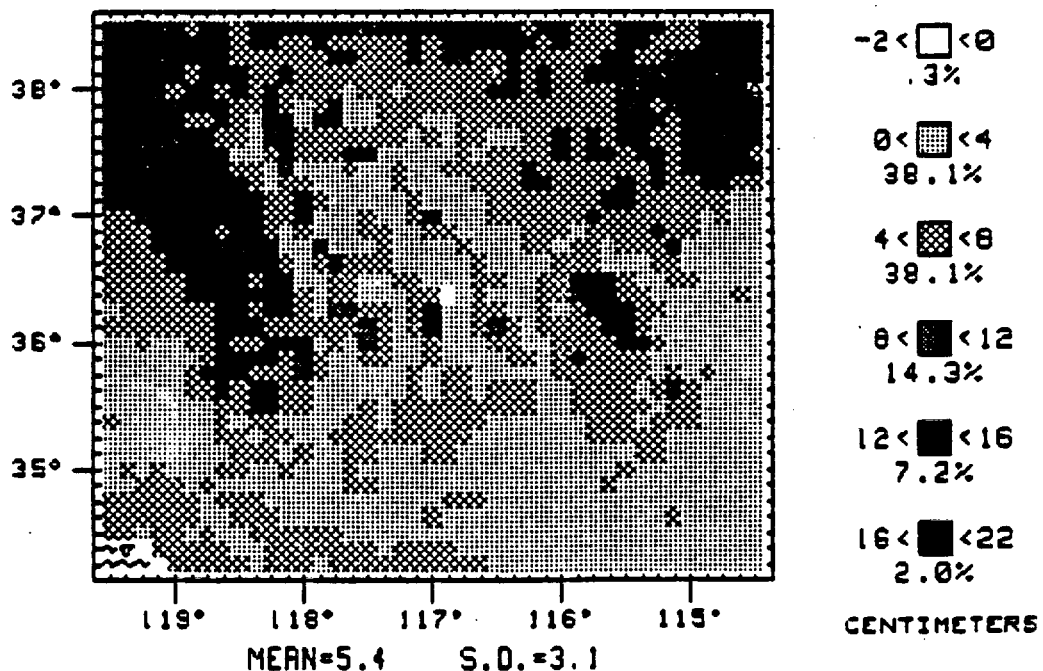
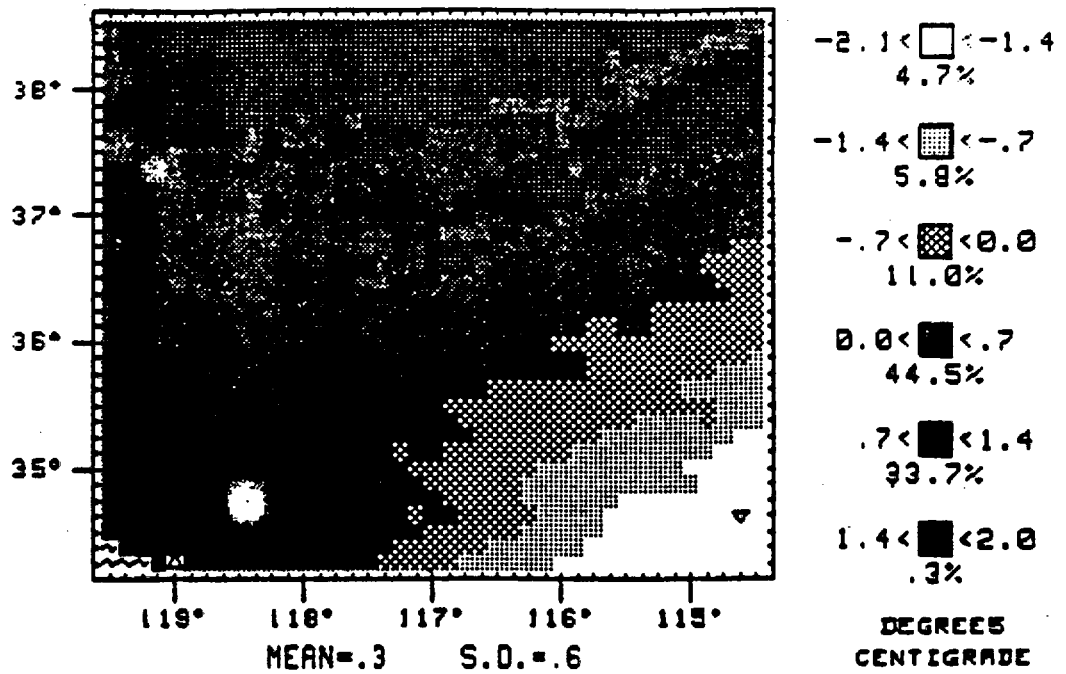


Figure 32. February temperature change (top) and precipitation change (bottom).

LGM MINUS MOD MARCH TEMPERATURE



LGM MINUS MOD MARCH PRECIPITATION

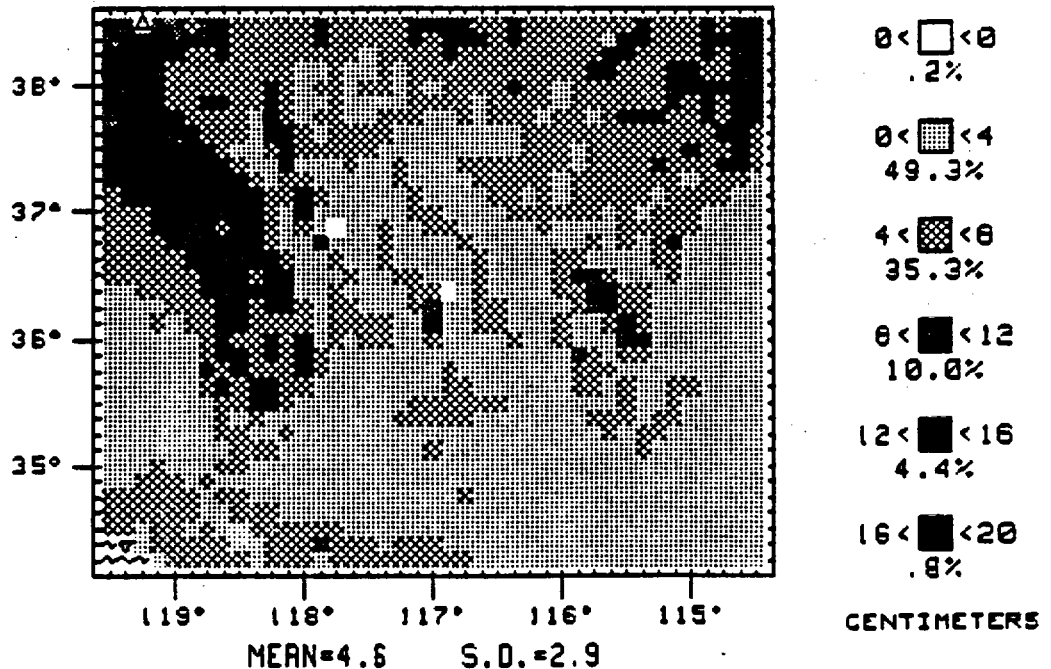
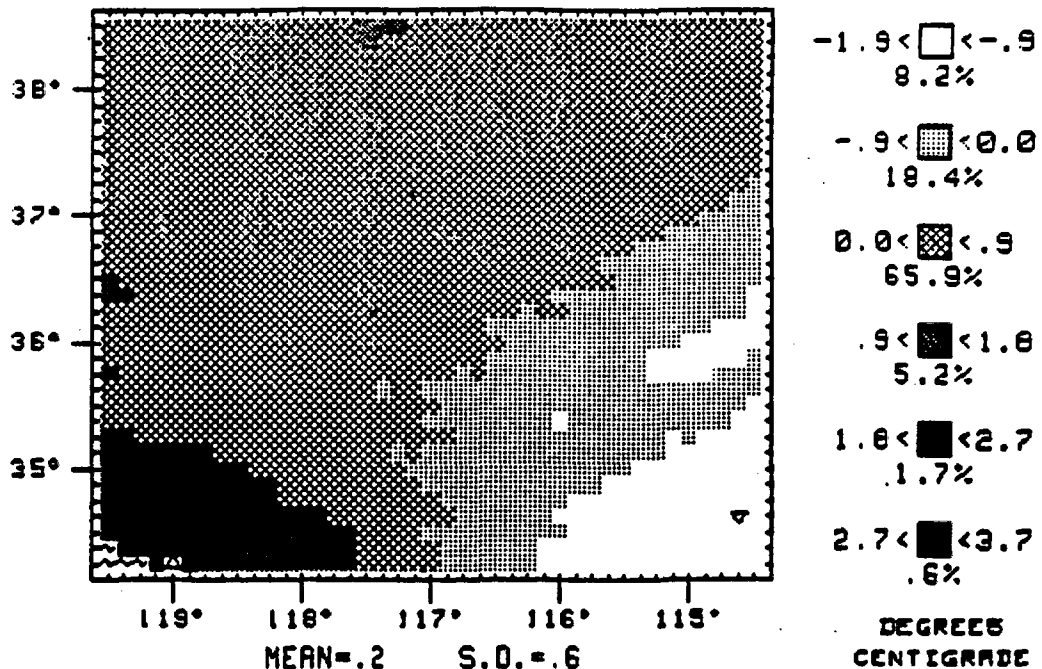


Figure 33. March temperature change (top) and precipitation change (bottom).

LGM MINUS MOD APRIL TEMPERATURE



LGM MINUS MOD APRIL PRECIPITATION

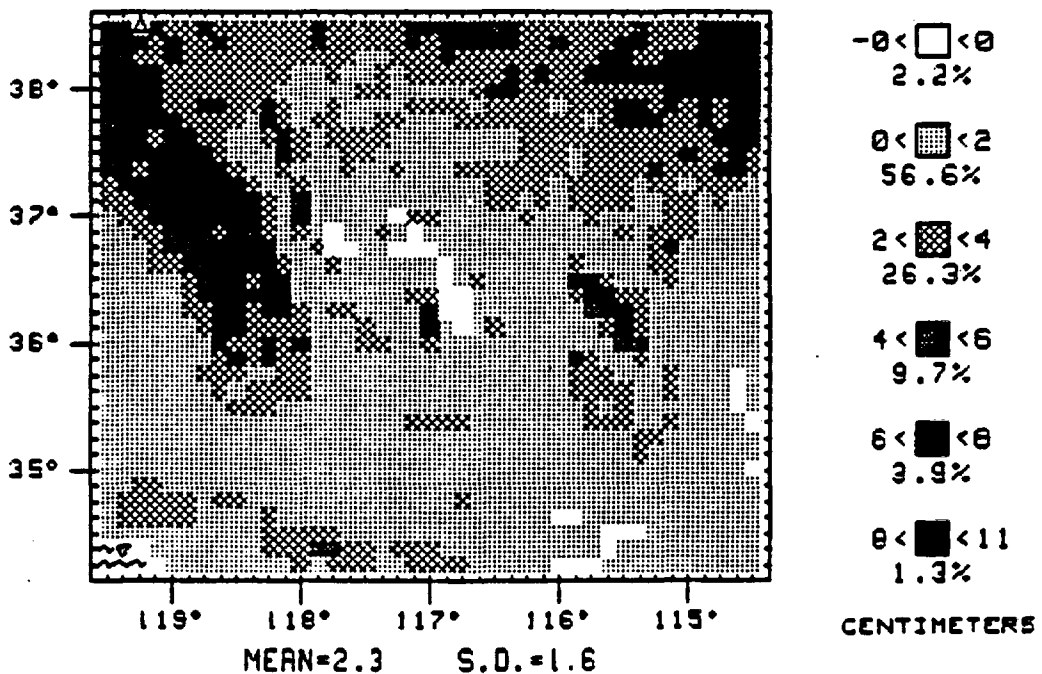
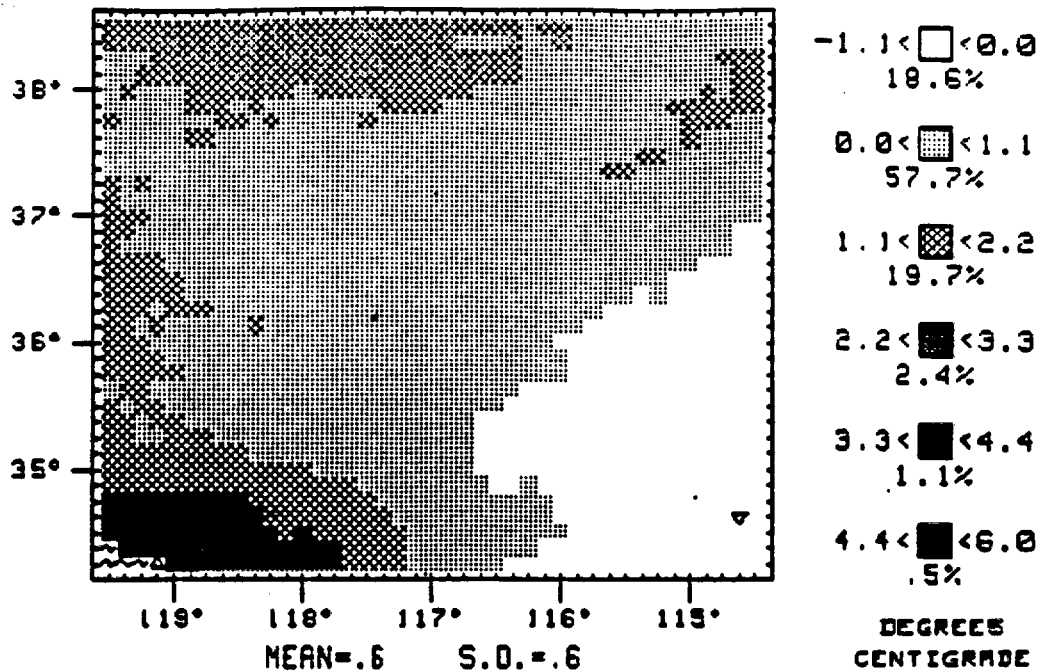


Figure 34. April temperature change (top) and precipitation change (bottom).

LGM MINUS MOD MAY TEMPERATURE



LGM MINUS MOD MAY PRECIPITATION

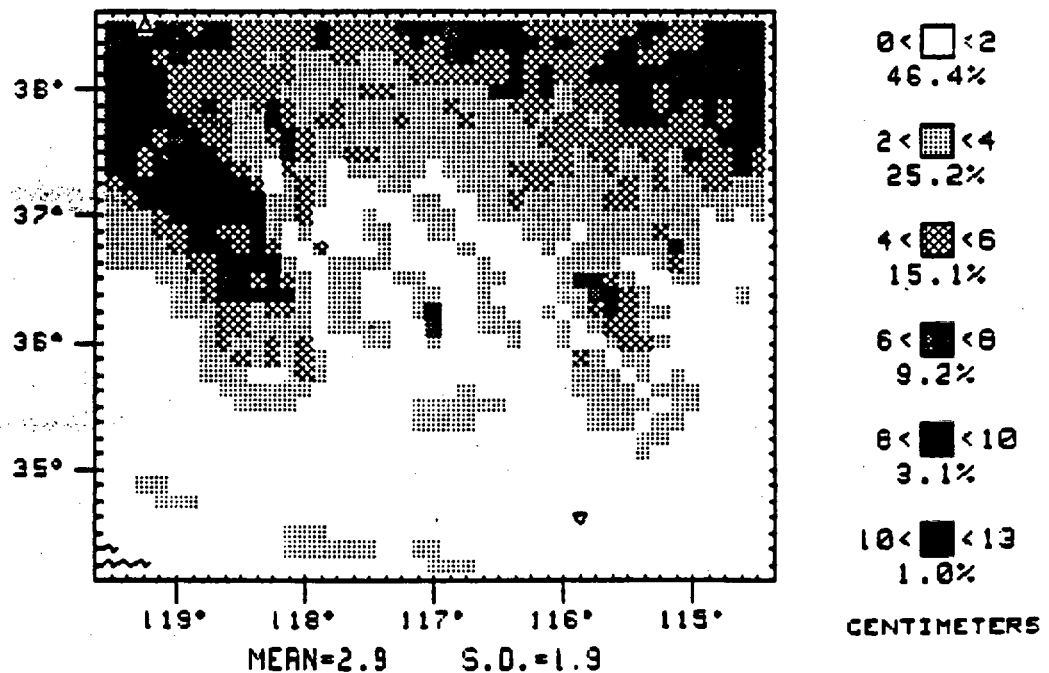
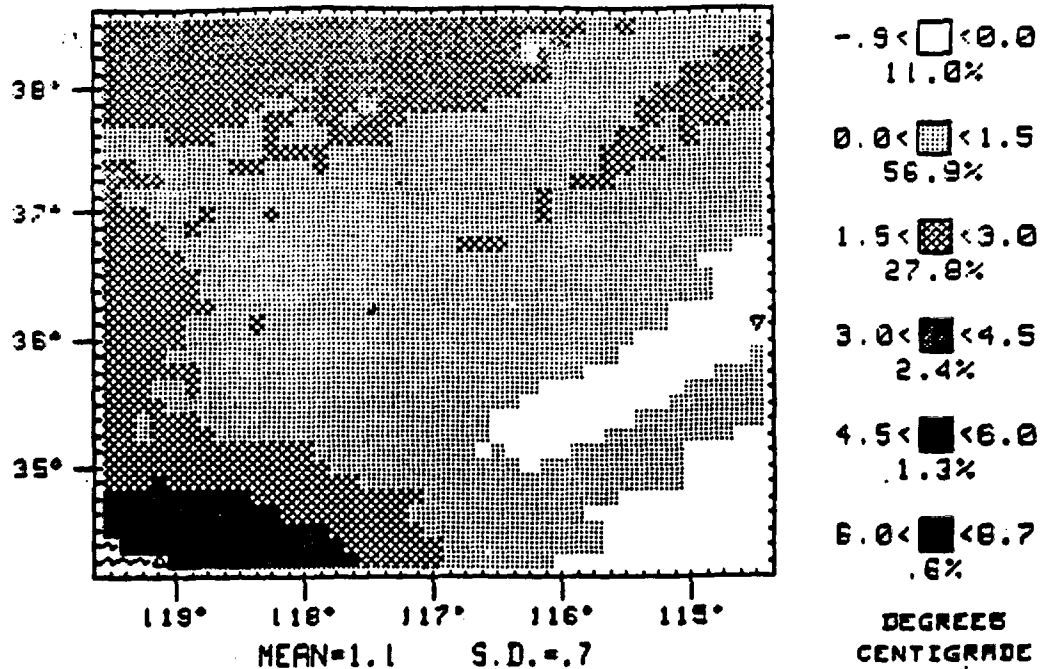


Figure 35. May temperature change (top) and precipitation change (bottom).

LGM MINUS MOD JUNE TEMPERATURE



LGM MINUS MOD JUNE PRECIPITATION

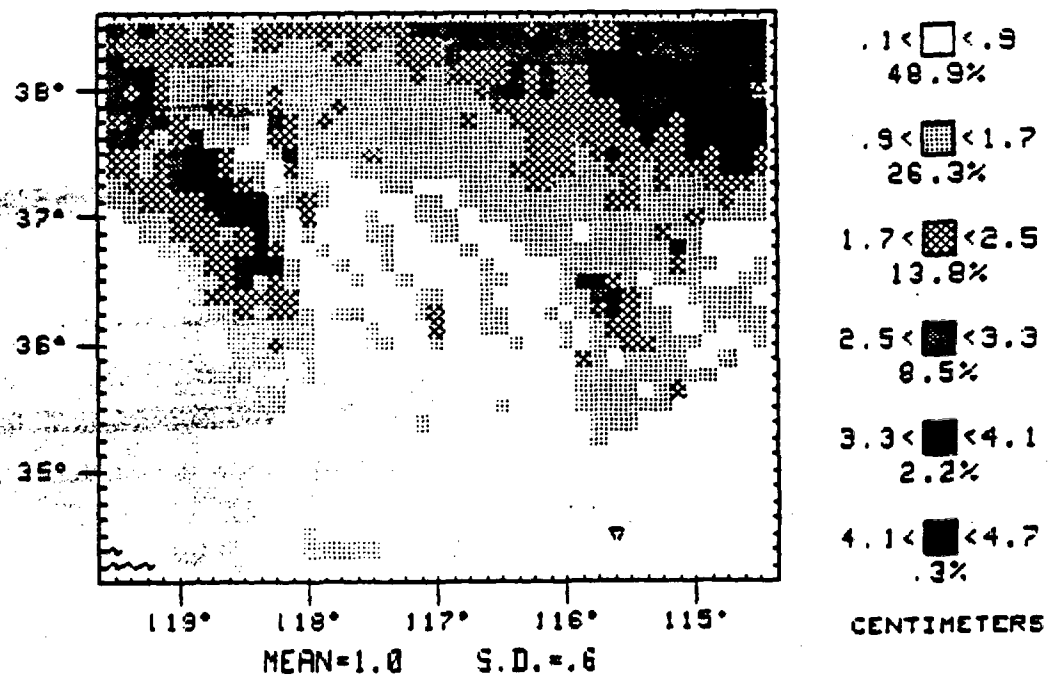
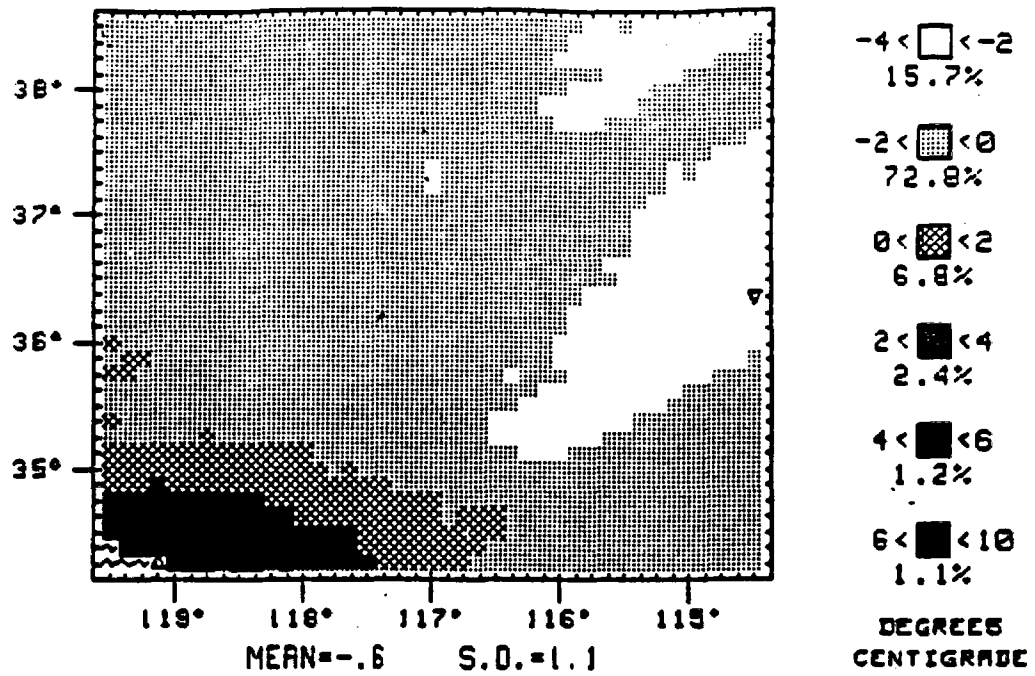


Figure 36. June temperature change (top) and precipitation change (bottom).

LGM MINUS MOD JULY TEMPERATURE



LGM MINUS MOD JULY PRECIPITATION

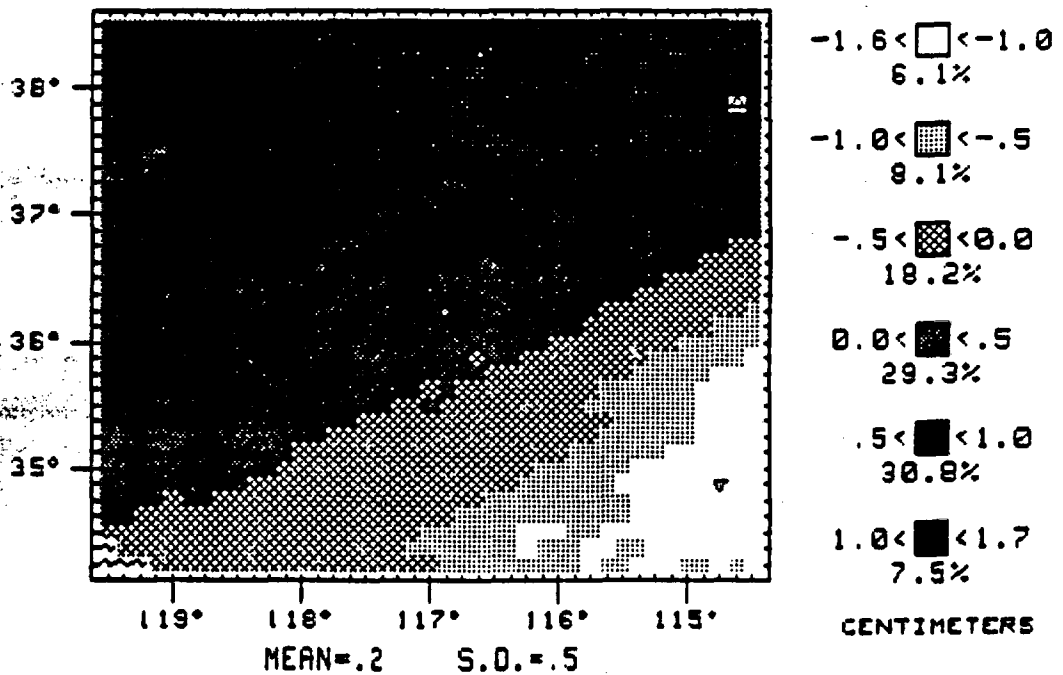
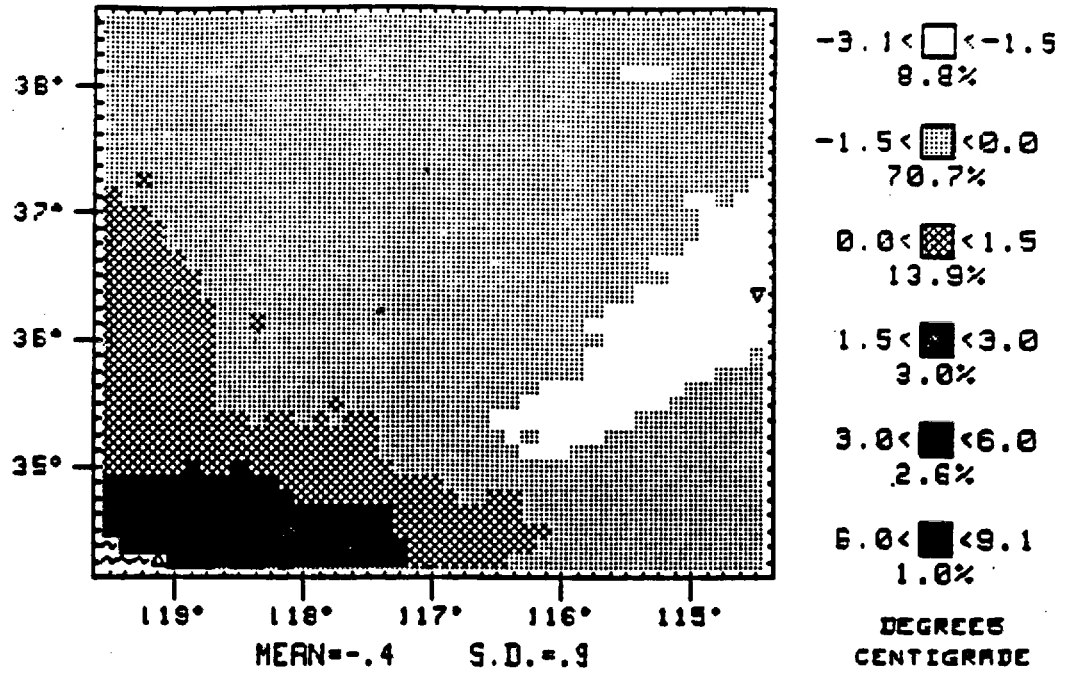


Figure 37. July temperature change (top) and precipitation change (bottom).

LGM MINUS MOD AUGUST TEMPERATURE



LGM MINUS MOD AUGUST PRECIPITATION

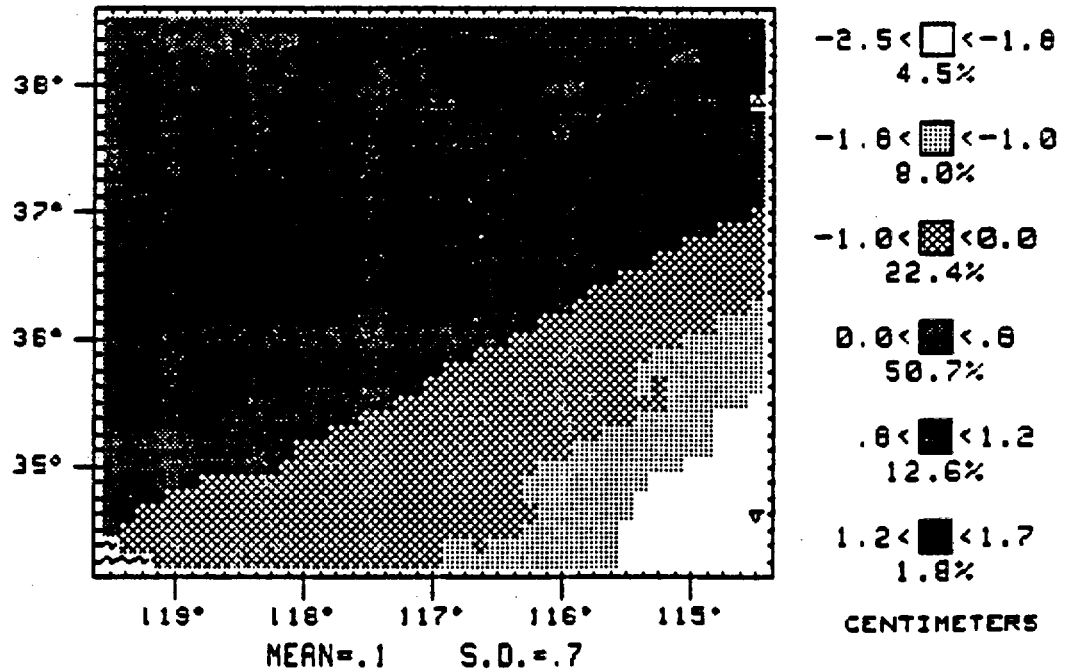
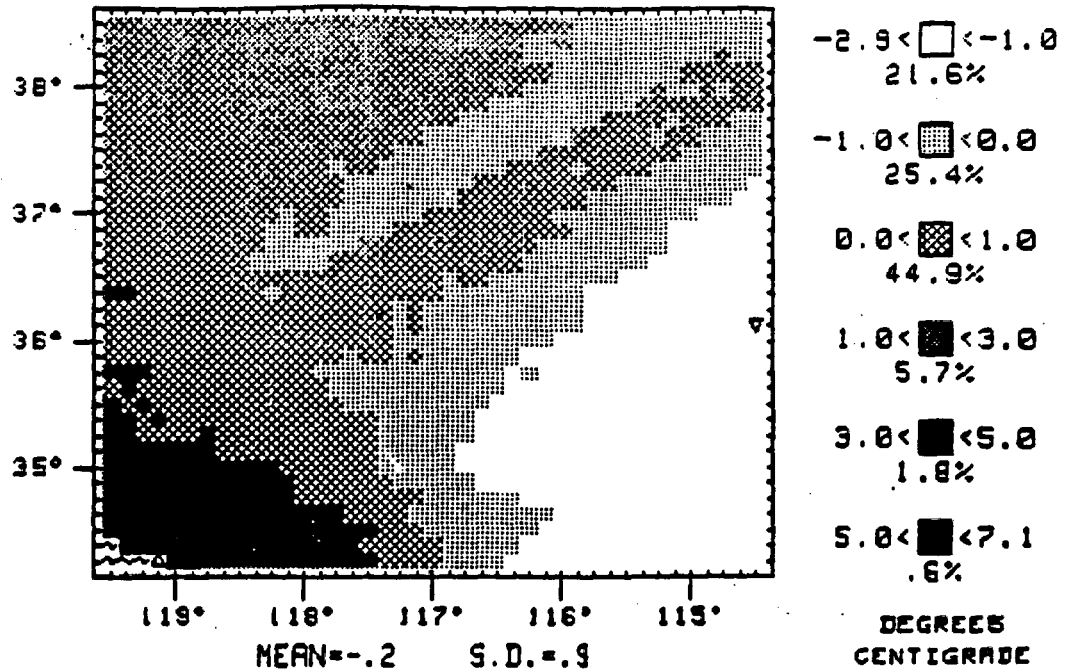


Figure 38. August temperature change (top) and precipitation change (bottom).

LGM MINUS MOD SEPTEMBER TEMPERATURE



LGM MINUS MOD SEPTEMBER PRECIPITATION

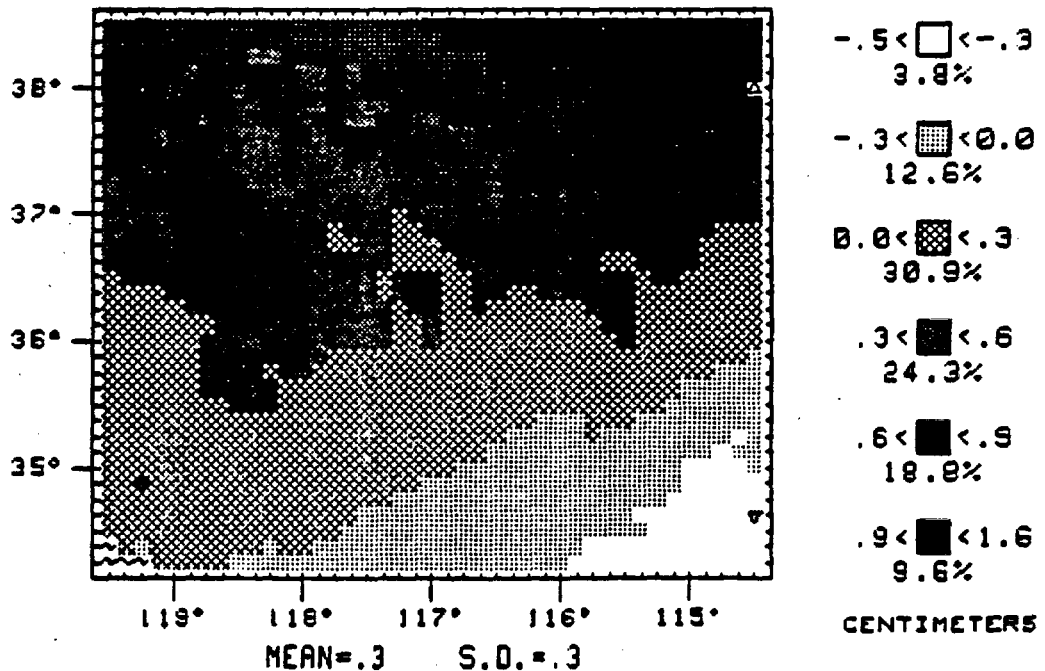
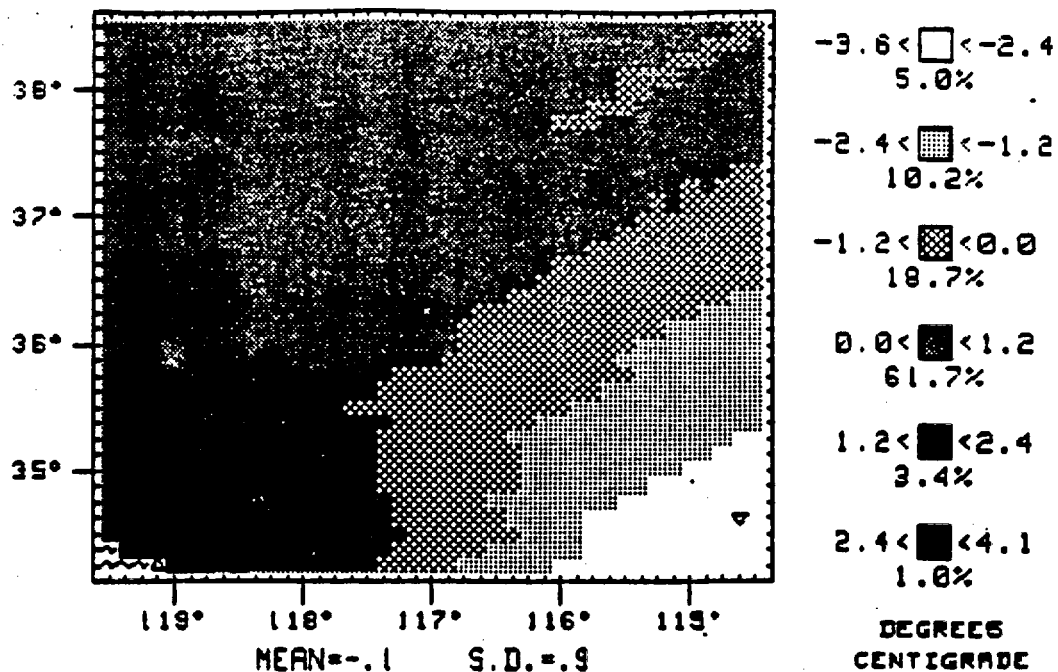


Figure 39. September temperature change (top) and precipitation change (bottom).

LGM MINUS MOD OCTOBER TEMPERATURE



LGM MINUS MOD OCTOBER PRECIPITATION

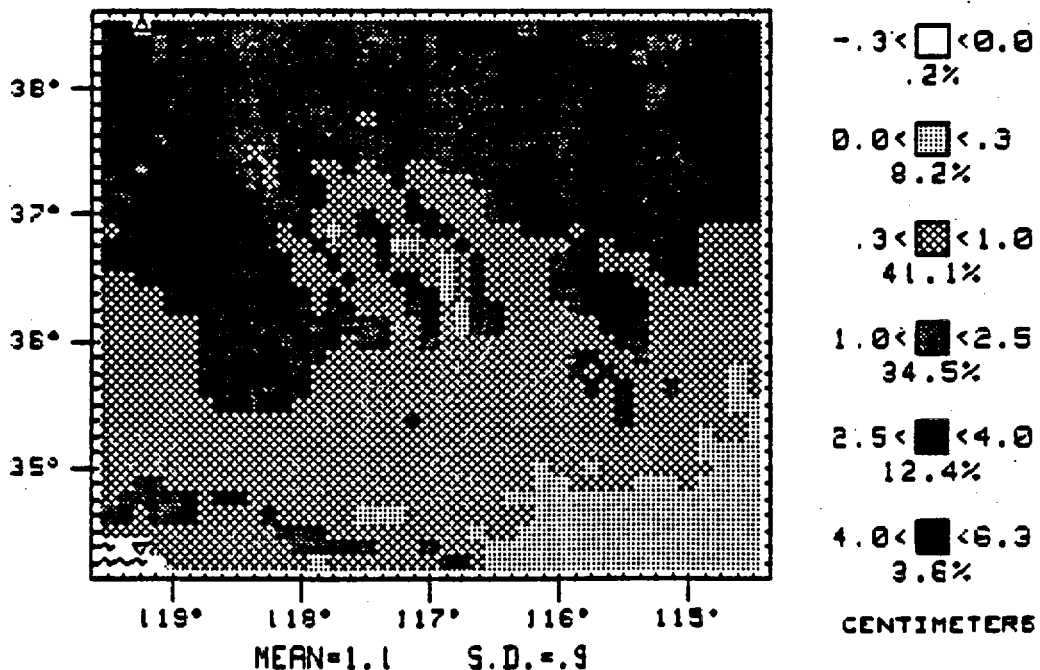


Figure 40. October temperature change (top) and precipitation change (bottom).

Table 9. Statistical summary of regression testing for a linear relation between mean monthly change in the precipitation and the standard deviation of that change.

$$H_0: b_0 = \bar{y}, b_1 = 0$$

$$F_{1, 10} = 148.08^{**}$$

$$b_0 = 0.38, \quad t = 2.76^*$$

$$b_1 = 0.57, \quad t = 12.17^{**}$$

$$r^2 = 93.67\% \quad \sigma_e^2 = 0.29$$

* Significant at the 5% level

** Significant at the 1% level

The dominant role of the Sierras in the overall pattern of precipitation change continues through the spring. A number of minor ranges, including the Inyos and the Panamints, show slight changes, mostly decreases. This could produce a stress on the endemic vegetation during its usual period of rapid growth and propagation. By May the increase in precipitation due to the increased strength of the Great Basin low during the LGM is as important as the Sierra elevations in determining precipitation change.

During the summer months, especially July and August, changes appear to most closely correspond to changes in the sea surface temperature patterns between the present and LGM. There are slight increases in the northwest, slight decreases in the southeast. A similar pattern prevails until September or October at which point the elevational control again dominates predicted changes. It should be noted that changes in summer precipitation amounts are generally so minor as to be essentially imperceptible with available geologic data.

By November, the pattern typical of all winter months - great increases in the Sierras, uniformly minor changes elsewhere - again has been established. The greatest increases are again at the crest of the Sierras. Very minor decreases (less than 1cm) occur at sporadic localities within these mountains. Again, within the Great Basin and in the San Joaquin Valley, changes are so minor as to be almost negligible.

SOLUTION OF TOTAL RUNOFF

Using the Blaney-Criddle equation we have estimated evapotranspiration in each of the twelve months from the available temperature data. The Blaney-Criddle procedure requires information concerning the consumptive use coefficient, K. This coefficient was assumed to vary slightly as a function of elevation so that at lower elevations the consumptive use coefficient is higher. The assumed values of K are given in Table 10. Estimated modern values of evapotranspiration for February, August and yearly totals are illustrated in Figures 45-47. Because the patterns so closely follow temperature other months are not included.

It should be noted that the values reported in Figures 45-47 represent potential evapotranspiration. The actual values (true evapotranspiration) applied are commonly lower, especially in areas of low precipitation. On a monthly basis actual evapotranspiration never is allowed to exceed available moisture (precipitation for that month). Furthermore, since at each point the computed potential evapotranspiration is linearly proportional to the temperature and the constant of proportionality changes only slightly from point to point, one would expect the evapotranspiration maps to closely correspond to the temperature maps. This is in fact the case as can be seen clearly in comparing

Table 10. Values of the consumptive use coefficient, K, used in the Blaney-Criddle equation to estimate evapotranspiration.

<u>Elevation</u> <u>(m)</u>	<u>K</u>
1000	.75
2000	.70
3000	.65
4000	.60
5000	.55

IN

6 <  < 3.7
3.8%

7 <  < 4.6
8.9%

6 <  < 5.5
23.7%

5 <  < 6.4
20.5%

4 <  < 7.3
23.3%

3 <  < 8.4
19.8%

IN METERS

<  < 3.7
3.5%

<  < 4.6
3.3%

3 <  < 5.5
3.3%

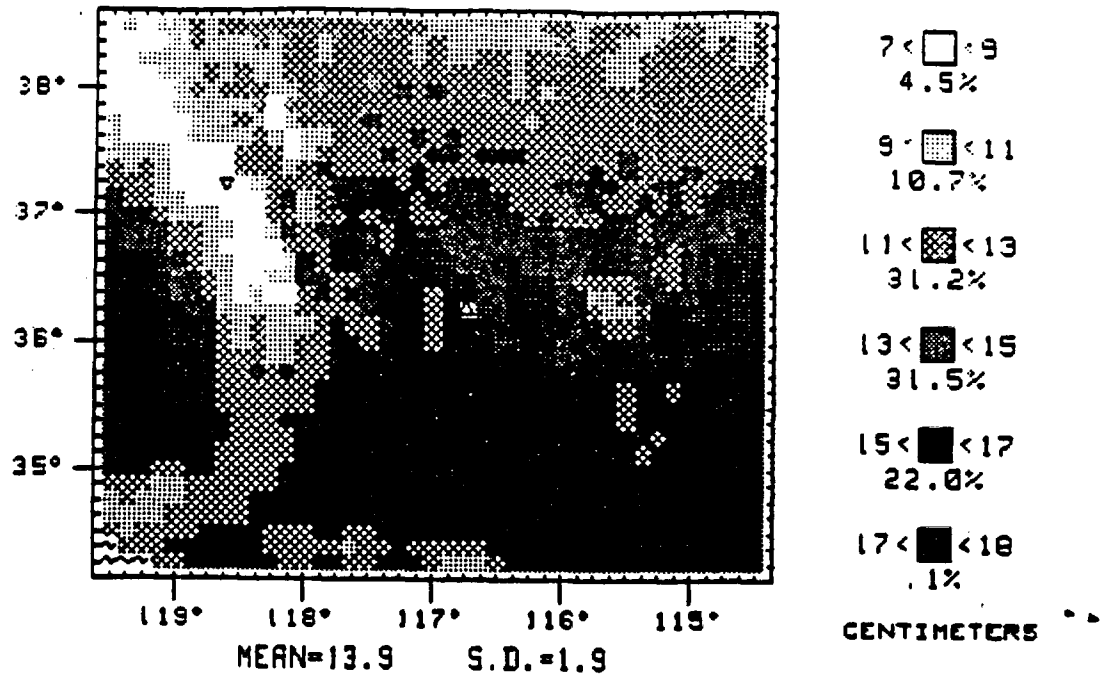
4 <  < 6.4
4.8%

5 <  < 7.3
5.3%

6 <  < 8.3
1.8%

IN METERS

MODERN AUGUST EVAPOTRANSPIRATION



L.G.M. AUGUST EVAPOTRANSPIRATION

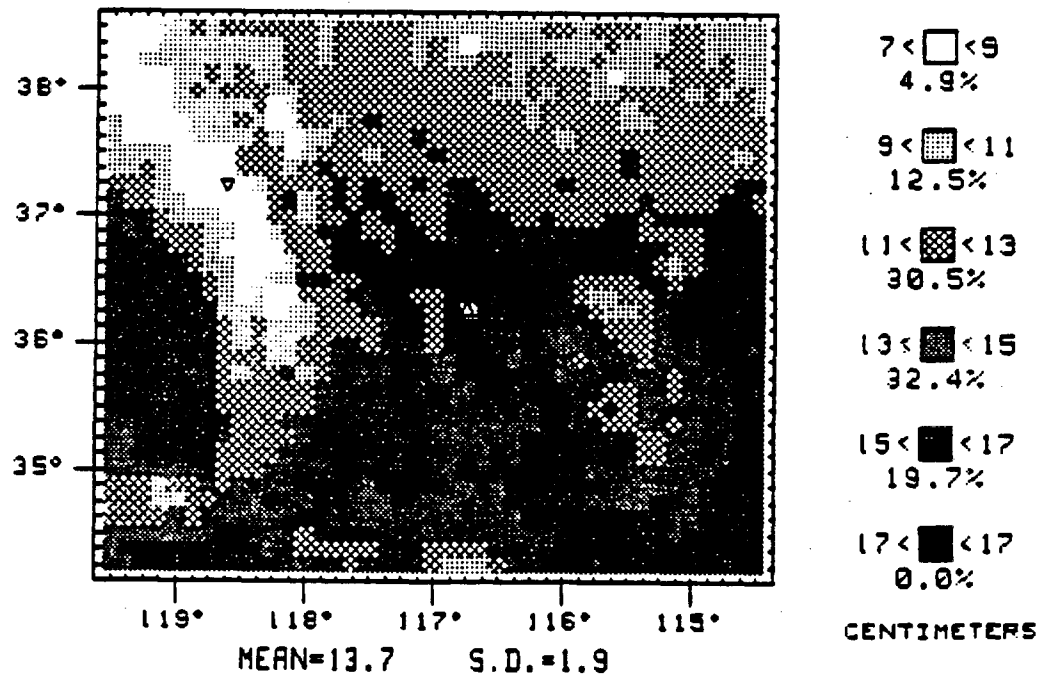
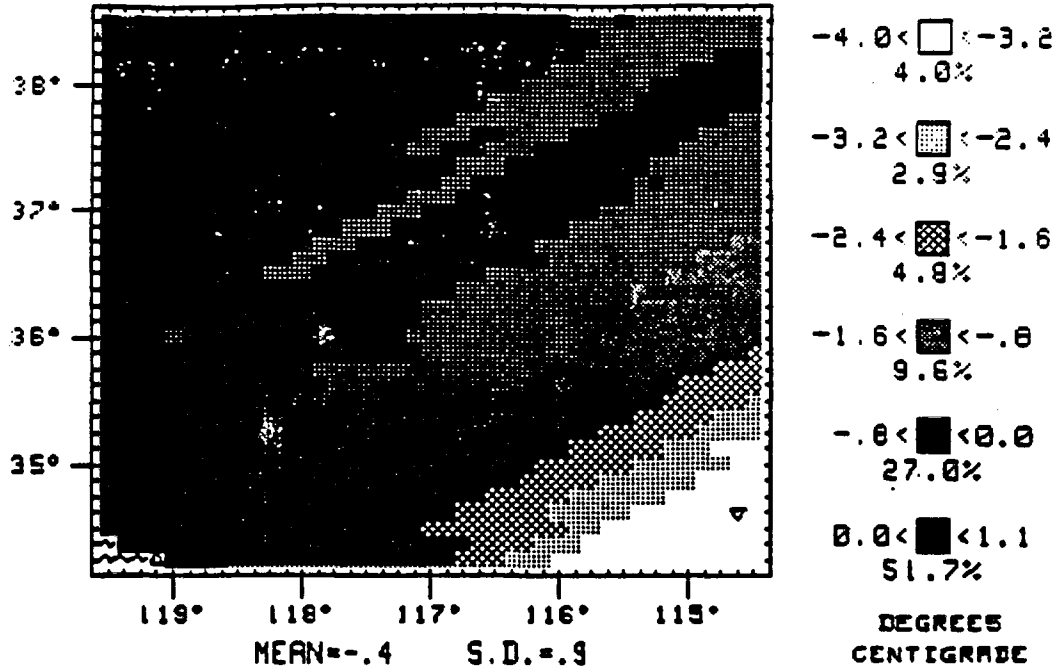


Figure 46. August modern (top) and last glacial maximum (bottom) evapotranspiration.

LGM MINUS MOD NOVEMBER TEMPERATURE



LGM MINUS MOD NOVEMBER PRECIPITATION

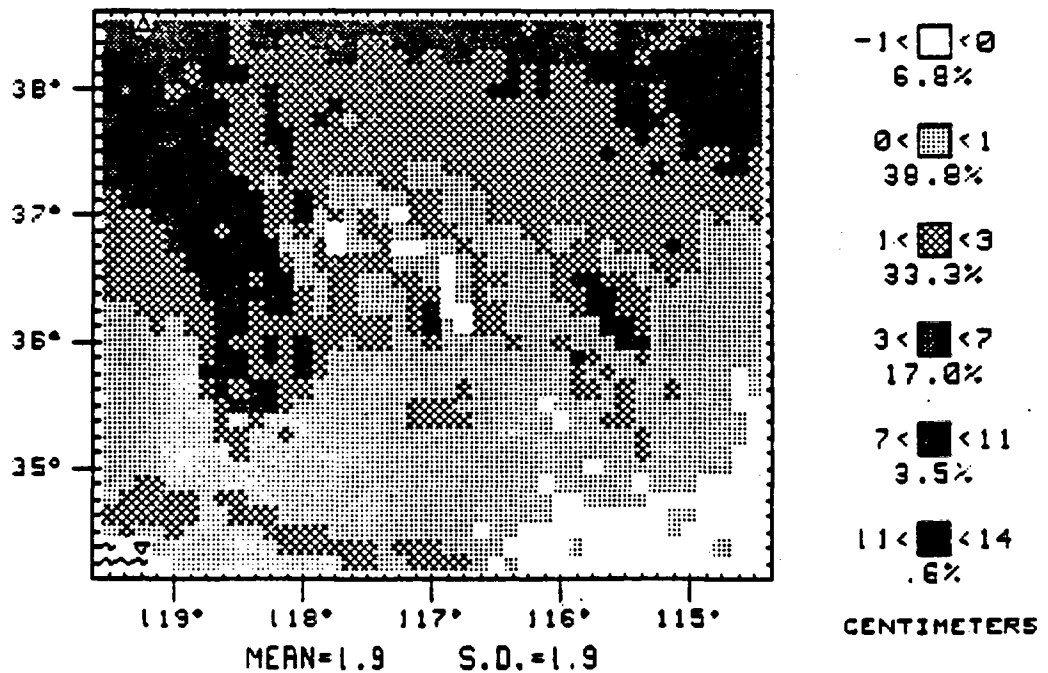
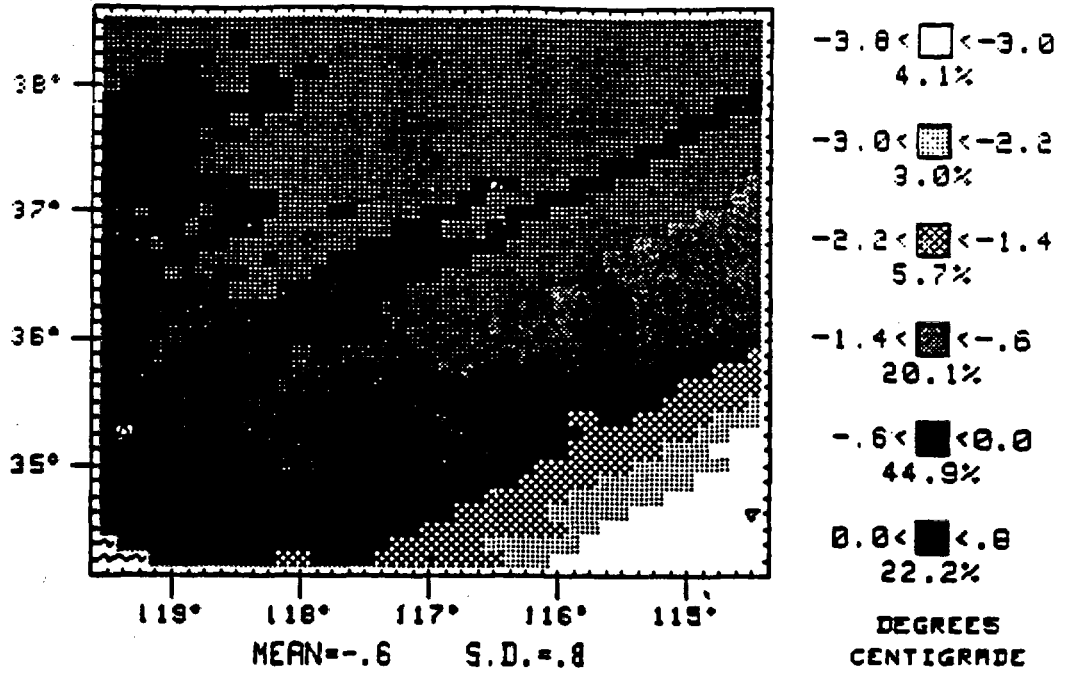


Figure 41. November temperature change (top) and precipitation change (bottom).

LGM MINUS MOD DECEMBER TEMPERATURE



LGM MINUS MOD DECEMBER PRECIPITATION

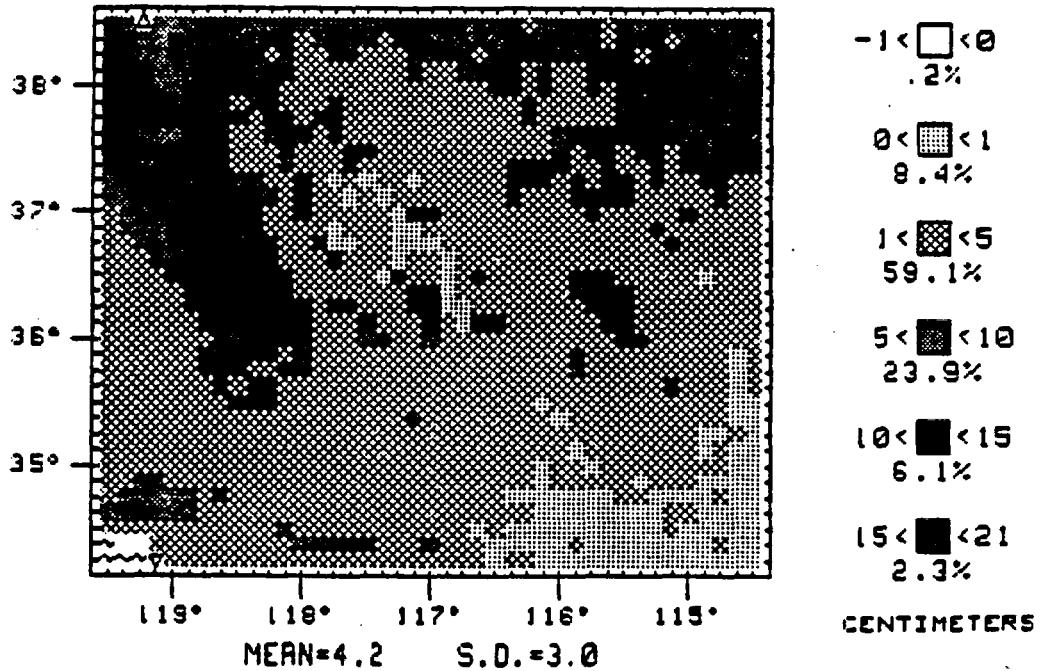


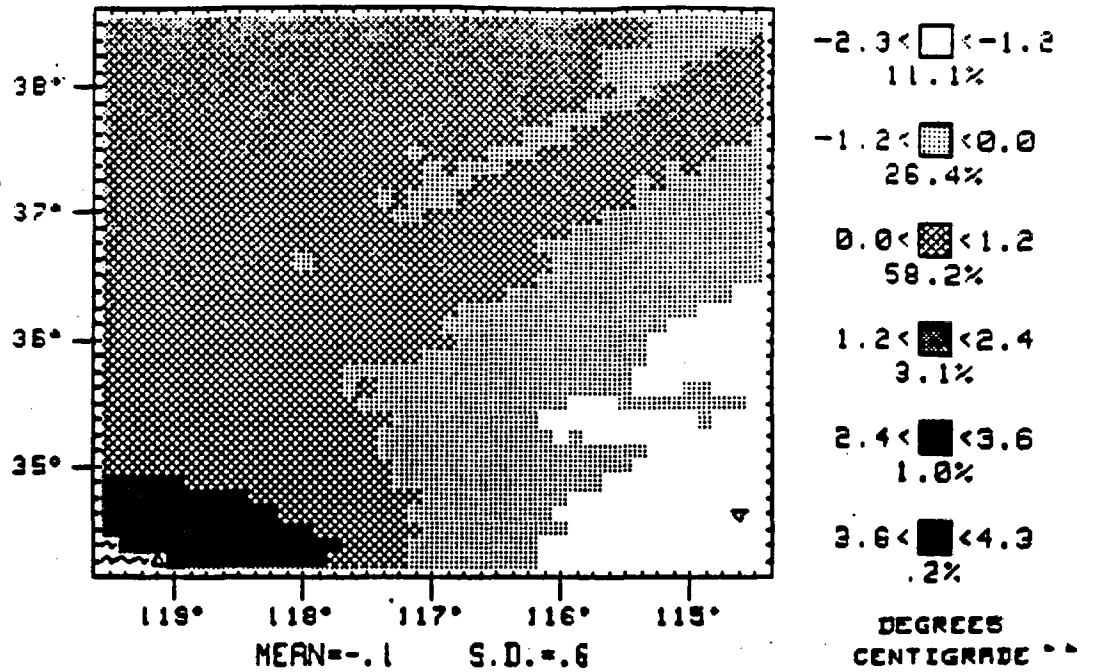
Figure 42. December temperature change (top) and precipitation change (bottom).

SOLUTION OF TOTAL RUNOFF

Using the Blaney-Criddle equation we have estimated evapotranspiration in each of the twelve months from the available temperature data. The Blaney-Criddle procedure requires information concerning the consumptive use coefficient, K. This coefficient was assumed to vary slightly as a function of elevation so that at lower elevations the consumptive use coefficient is higher. The assumed values of K are given in Table 10. Estimated modern values of evapotranspiration for February, August and yearly totals are illustrated in Figures 45-47. Because the patterns so closely follow temperature other months are not included.

It should be noted that the values reported in Figures 45-47 represent potential evapotranspiration. The actual values (true evapotranspiration) applied are commonly lower, especially in areas of low precipitation. On a monthly basis actual evapotranspiration never is allowed to exceed available moisture (precipitation for that month). Furthermore, since at each point the computed potential evapotranspiration is linearly proportional to the temperature and the constant of proportionality changes only slightly from point to point, one would expect the evapotranspiration maps to closely correspond to the temperature maps. This is in fact the case as can be seen clearly in comparing

LGM MINUS MOD MEAN TEMPERATURE



LGM MINUS MOD TOTAL PRECIPITATION

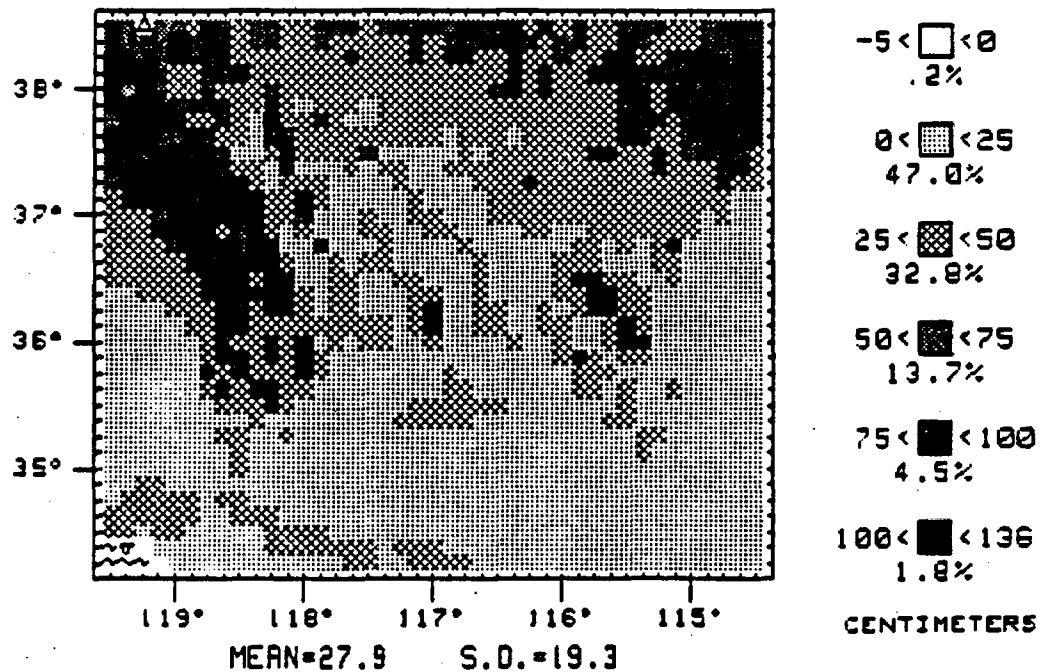


Figure 43. Annual temperature change (top) and precipitation change (bottom).

Table 7. Summary of our estimates of temperature change in the Southwest at the Last Glacial Maximum.

Month	Modern (°C)		Last Glacial Maximum (°C)		Nature of the Last Glacial Maximum			
	\bar{T}	σ	\bar{T}	σ	ΔT^*	$\sigma_{\Delta T}$	$\Delta T/\text{mod.}T$	$\Delta\sigma$
Jan.	8.0	3.6	7.7	3.2	-0.4	0.7	-4%	-0.4
Feb.	9.5	4.0	9.3	3.7	-0.2	0.6	-2	-0.3
Mar.	12.2	4.6	12.5	4.3	0.3	0.6	+2	-0.3
Apr.	16.5	4.8	16.8	4.6	0.2	0.6	+2	-0.2
May	20.4	5.0	21.0	4.7	0.6	0.6	+3	-0.3
Jun.	25.4	5.1	26.5	4.8	1.1	0.7	+4	-0.3
July	29.2	4.8	28.5	4.8	-0.6	1.1	-2	0.0
Aug.	28.3	4.8	27.9	4.7	-0.4	0.9	-1	-0.1
Sept.	25.8	4.5	25.5	4.2	-0.2	0.9	-1	-0.3
Oct.	19.7	4.2	19.6	3.8	-0.1	0.9	-1	-0.5
Nov.	13.3	3.7	12.9	3.2	-0.4	0.9	-3	-0.5
Dec.	9.5	3.3	9.0	2.8	-0.6	0.8	-5	-0.5
Annual	18.1	4.3	18.1	4.0	-0.1	0.6	-1%	-0.3

* Values reported here are mean differences of all of the points within the Death Valley drainage system. This is not the differences in the means although the two are equal except for roundoff (± 0.1) error. The value reported is the more accurate one.

Precipitation

At the last glacial maximum precipitation increased by a factor of 94%. This proportionate change was fairly uniform throughout the area although there are second order patterns that make such generalizations less useful. For example, in nearly every month there are points that do not receive any precipitation or receive less than 2cm. Furthermore, there are some points where precipitation actually decreases. Some specific features of the LGM precipitation patterns (Figures 18-30) are described below.

February precipitation amounts at the LGM, as with modern precipitation, are greatest of all the months. Within the Sierras not only has the absolute amount of precipitation increased but also the relative area of high precipitation zones has expanded. Thus about four times as large an area is now included in the highest precipitation class.

Within the Great Basin areas, the spatial variability of precipitation in January has greatly increased. Thus, although the limits on the lowest precipitation class have increased there are more points in the higher classes than are seen at present. However, along the Coast Ranges in the southwestern portion of the area variability has decreased markedly. Here some points actually receive less precipitation.

The pattern of elevation influence is still dominant. Highest precipitation is in the Sierras, lowest in basins

such as Death Valley. Besides the Sierras two other ranges are predicted to receive significant precipitation; they are the White Mountains and the Spring Mountains. A secondary high is in the Panamint Range, another in the Sheep Range. The gradual increase in elevation on the west flanks of the Sierras is reflected in the gradual increase in precipitation as one moves northeast from the San Joachin Valley. In contrast, the steep east flank is mirrored in the sharp contact between the highest precipitation class on the crest of the Sierras and lowest precipitation class found in the Owens Valley. Even the plateau-like volcanic tableland of Bishop tuff at the northern end of the Owens Valley is represented in the higher precipitation there compared to the rest of the Owens Valley. This could also be seen in the predictions for the modern precipitation, especially in May and September. Those familiar with the area will recognize that this prediction corresponds well to actual conditions today.

Precipitation amounts at the LGM decline very slowly through March, April and May. The general pattern of precipitation changes only slightly. In the desert areas precipitation decrease is least; it also becomes considerably more variable. At some of the higher elevations there, precipitation actually increases slightly through March. This pattern is only vaguely discernable in estimates of modern precipitation. Such a phenomenon would explain the incursion

of more moisture demanding plant species into this area as has been recorded in a number of pollen studies.

With the end of spring the variability of precipitation in the deserts declines while in the northern portions of the Great Basin it shows a relative increase (although an absolute decrease). The typical summer convective storm pattern begins to develop. This pattern - dominated by the Great Basin low centered roughly at the northeastern edge of the area - continues to control precipitation throughout the area until the end of summer. Throughout some of this period (May-September) the greatest precipitation is still found in the Sierras and the Spring Mountains. Lesser peaks occur on the White and Panamint Mountains. However, in July and August it is almost unrelated to topography. This is of course as would be anticipated from intense convective storms. A similar pattern is seen today in these months. The slight changes appear to be most closely related to the fact that the coastline is now farther away. Retreat was most extreme in the area of most gentle bathymetry (the southwestern corner) and this retreat is reflected in the patterns of July precipitation, modern vs. LGM. It is the summer months that show the least overall increase in precipitation amounts (always less than 5cm). Indeed in nearly one-half (the southeastern half) the precipitation amounts actually decrease by as much as 2.5cm.

Fall precipitation, beginning in September, once again begins to reflect the influence of elevation. The Sierras are lightly sprinkled (no more than 4cm). However the highest rainfalls are still in the northeast, related to the lingering Great Basin low. That area receives up to 5cm of rain.

By November the last inkling of that low has disappeared. The Sierras again dominate the scene and the peaks along the crest of the Sierras receive up to 36cm, over 50% more than today. Precipitation amounts are much more variable at those high elevations than is the case today. Over the remainder of the study area precipitation is uniformly low, although still roughly 50% greater than today.

As was the case with the predictions of temperature, the comparison of data for individual months is more readily achieved through the presentation of difference maps (Figures 31-43). Again, we subtract present from LGM so that positive values indicate an increase at the LGM. Those difference maps are presented using the same configuration and symbolism as used before. We use the lightest symbols to represent the greatest increase. The darkest symbol denotes the smallest increase (in some cases actually a decrease). To facilitate comparisons we make the upper limit of this (negative) class equal to zero. Thus areas of increased precipitation can readily be distinguished from areas of decrease.

The range of changes (and standard deviation) is lower in the colder months suggesting a proportional effect is at work (Table 8). To further illustrate this relation between mean and variance we plot in Figure 44 these values for all 12 months. A least squares regression line is shown. The linear relation is significant as judged by an F-test (Table 9) and the slope of that line is significantly different from zero. These results imply that the changes are heteroscedastic, a logarithmic transformation may be appropriate before further analysis of changes in precipitation. We assume that the logarithms of the precipitation change data are normally distributed. Thus the proportionate change is a more meaningful description of differences between modern and last glacial maximum conditions. Those values are also reported in Table 8.

Except in the drier months (in which all changes are minor) the most outstanding change observed is the very large increase in precipitation in the Sierras. In a number of sites the increase reaches as much as 22cm. The increase is by no means uniform, even within the Sierras there is considerable variability in the amount of increase. The vast majority of the region shows very little absolute change in precipitation amounts. Other than the Sierras, the largest change is a decrease in the southwest reflecting the decline in the maritime influence as sea level drops and the coastline moves westward.

Table 8. Summary of our estimates of precipitation change in the Southwest at the Last Glacial Maximum

Month	Modern (cm)		Last Glacial Maximum (cm)		Nature of the Last Glacial Maximum			
	\bar{P}	σ	\bar{P}	σ	ΔP^*	$\sigma_{\Delta P}$	$\Delta \bar{P}/\text{mod.}\bar{P}$	$\Delta \sigma$
Jan.	4.8	4.9	8.6	7.6	3.9	3.0	+79%	+2.7
Feb.	4.8	4.3	10.3	7.2	5.4	3.1	115	2.9
Mar.	4.8	4.8	9.5	7.4	4.6	2.9	98	2.6
Apr.	2.4	3.0	4.7	4.5	2.3	1.6	96	1.5
May	1.1	1.3	4.0	3.1	2.9	1.9	264	1.8
June	0.4	0.4	1.4	1.0	1.0	0.6	250	0.6
July	0.9	0.5	1.1	0.8	.2	0.5	22	0.3
Aug.	1.2	0.5	1.3	0.6	.1	0.7	8	0.1
Sept.	0.9	0.4	1.3	0.6	.3	0.3	44	0.2
Oct.	1.5	1.6	2.6	2.4	1.1	0.9	73	0.6
Nov.	2.3	3.6	4.2	5.4	1.9	1.9	83	1.8
Dec.	4.6	4.8	8.8	7.5	4.2	3.0	91	2.7
Total	29.8	28.3	57.7	46.0	27.9	19.3	94%	0.4

* Values reported here are mean differences of all of the points within the Death Valley drainage system. This is not the differences in the means although the two are equal except for roundoff (± 0.1) error. The value reported is the more accurate one.

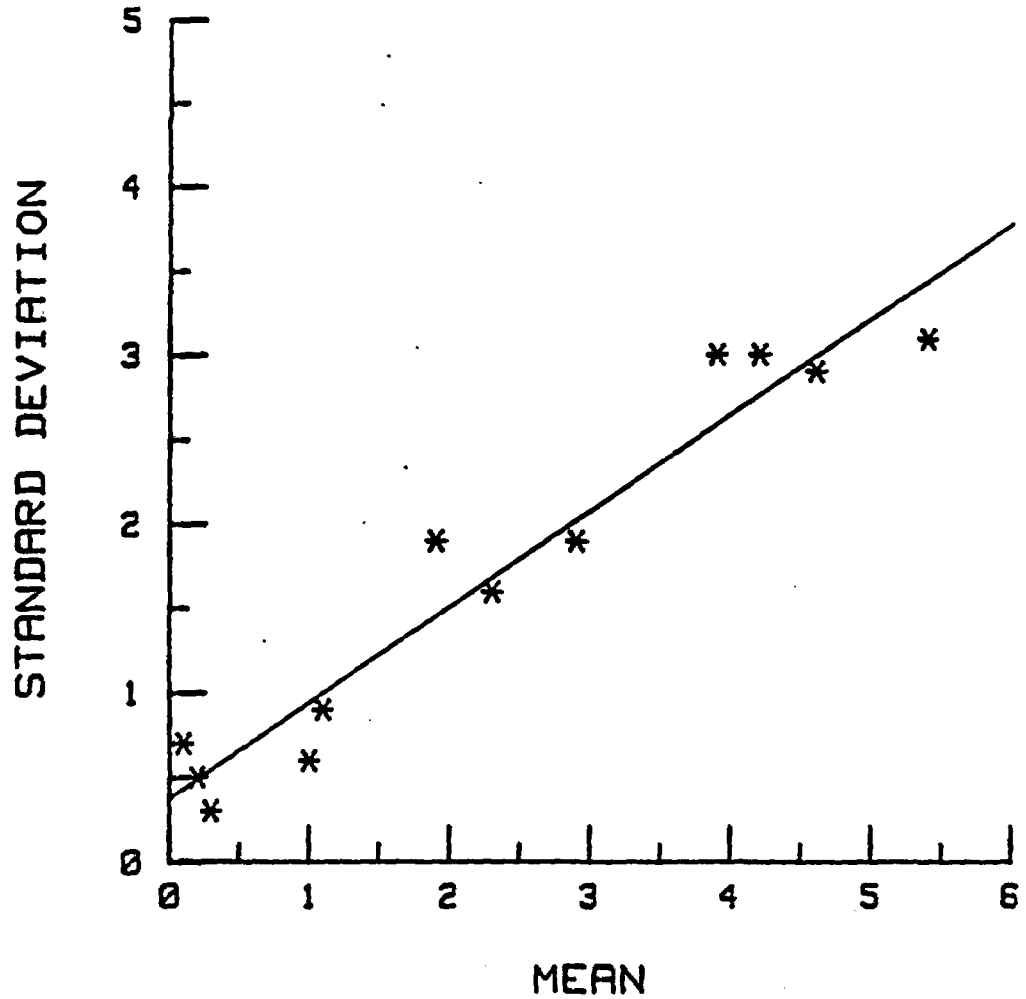


Figure 44. Relation between the monthly mean change in precipitation and standard deviation of that change. Change is measured between the present and last glacial maximum. The least squares line fitting these data is shown.

Table 9. Statistical summary of regression testing for a linear relation between mean monthly change in the precipitation and the standard deviation of that change.

$$H_0: b_0 = \bar{y}, b_1 = 0$$

$$F_{1, 10} = 148.08^{**}$$

$$b_0 = 0.38, \quad t = 2.76^*$$

$$b_1 = 0.57, \quad t = 12.17^{**}$$

$$r^2 = 93.67\% \quad \sigma_E^2 = 0.29$$

* Significant at the 5% level

** Significant at the 1% level

The dominant role of the Sierras in the overall pattern of precipitation change continues through the spring. A number of minor ranges, including the Inyos and the Panamints, show slight changes, mostly decreases. This could produce a stress on the endemic vegetation during its usual period of rapid growth and propagation. By May the increase in precipitation due to the increased strength of the Great Basin low during the LGM is as important as the Sierra elevations in determining precipitation change.

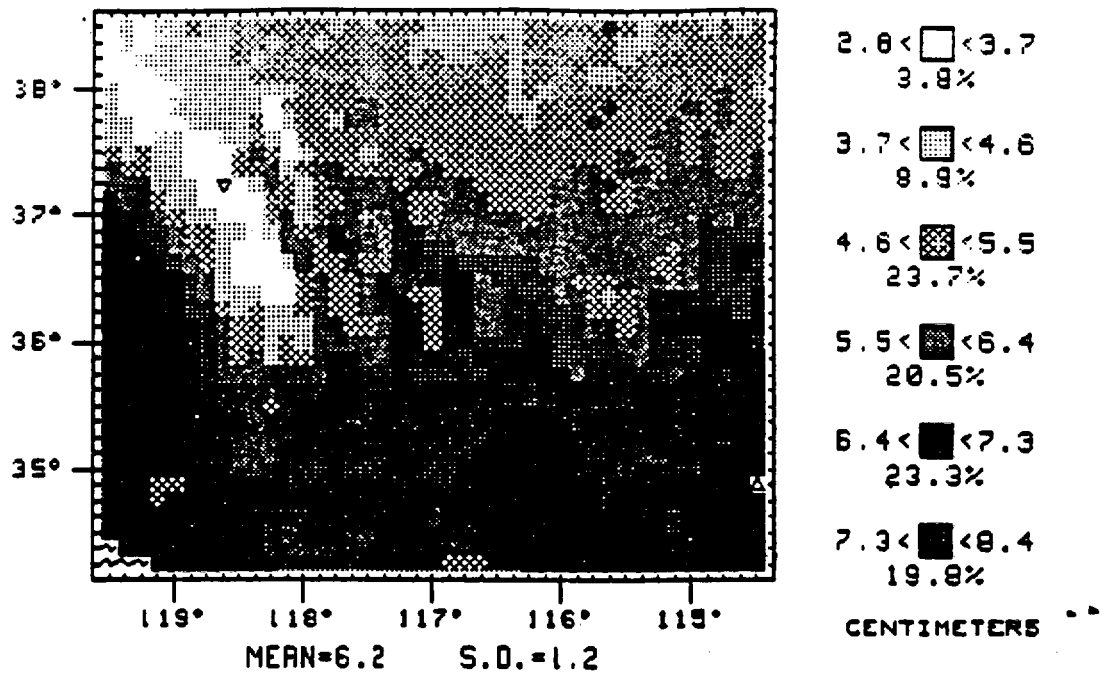
During the summer months, especially July and August, changes appear to most closely correspond to changes in the sea surface temperature patterns between the present and LGM. There are slight increases in the northwest, slight decreases in the southeast. A similar pattern prevails until September or October at which point the elevational control again dominates predicted changes. It should be noted that changes in summer precipitation amounts are generally so minor as to be essentially imperceptible with available geologic data.

By November, the pattern typical of all winter months - great increases in the Sierras, uniformly minor changes elsewhere - again has been established. The greatest increases are again at the crest of the Sierras. Very minor decreases (less than 1cm) occur at sporadic localities within these mountains. Again, within the Great Basin and in the San Joaquin Valley, changes are so minor as to be almost negligible.

Table 10. Values of the consumptive use coefficient, K, used in the Blaney-Criddle equation to estimate evapotranspiration.

<u>Elevation</u> <u>(m)</u>	<u>K</u>
1000	.75
2000	.70
3000	.65
4000	.60
5000	.55

MODERN FEBRUARY EVAPOTRANSPIRATION



L.G.M. FEBRUARY EVAPOTRANSPIRATION

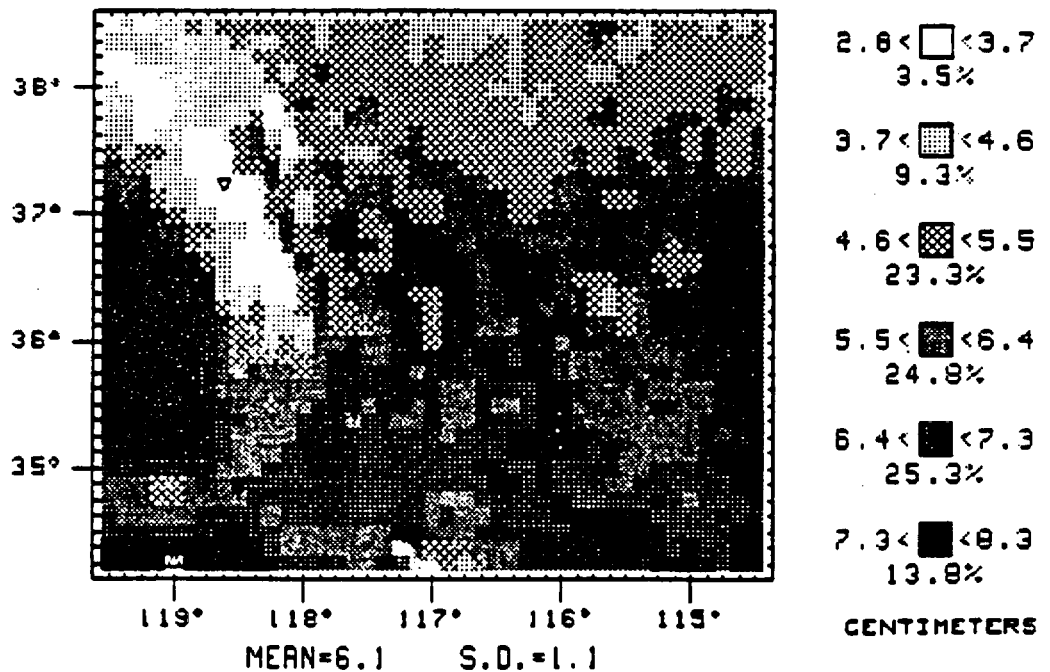
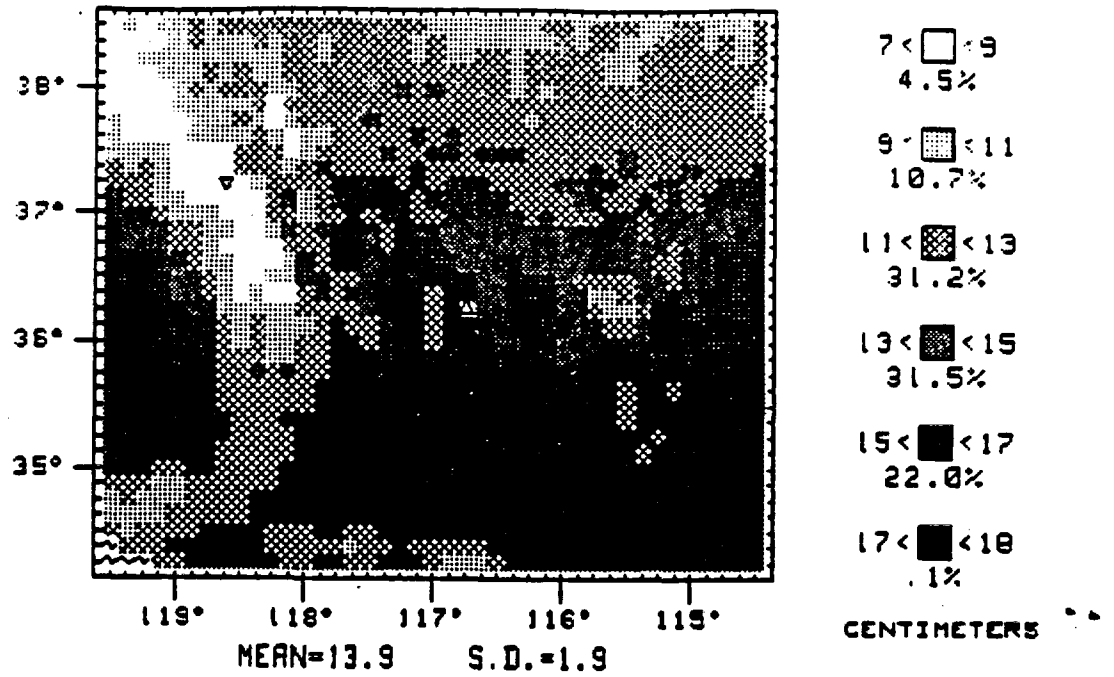


Figure 45. February modern (top) and last glacial maximum (bottom) evapotranspiration.

MODERN AUGUST EVAPOTRANSPIRATION



L.G.M. AUGUST EVAPOTRANSPIRATION

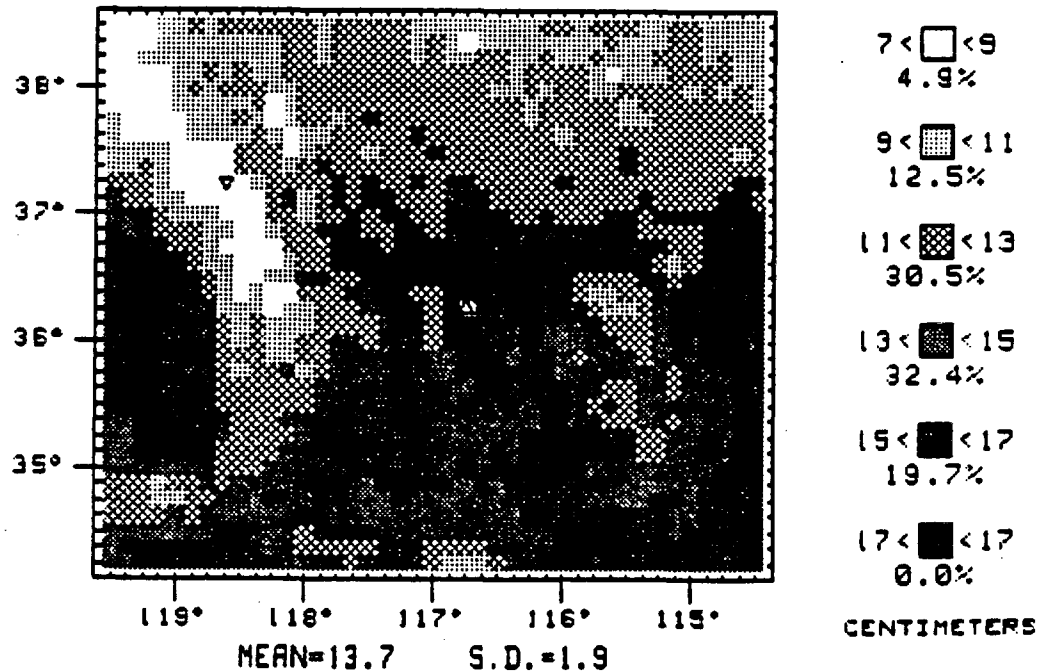
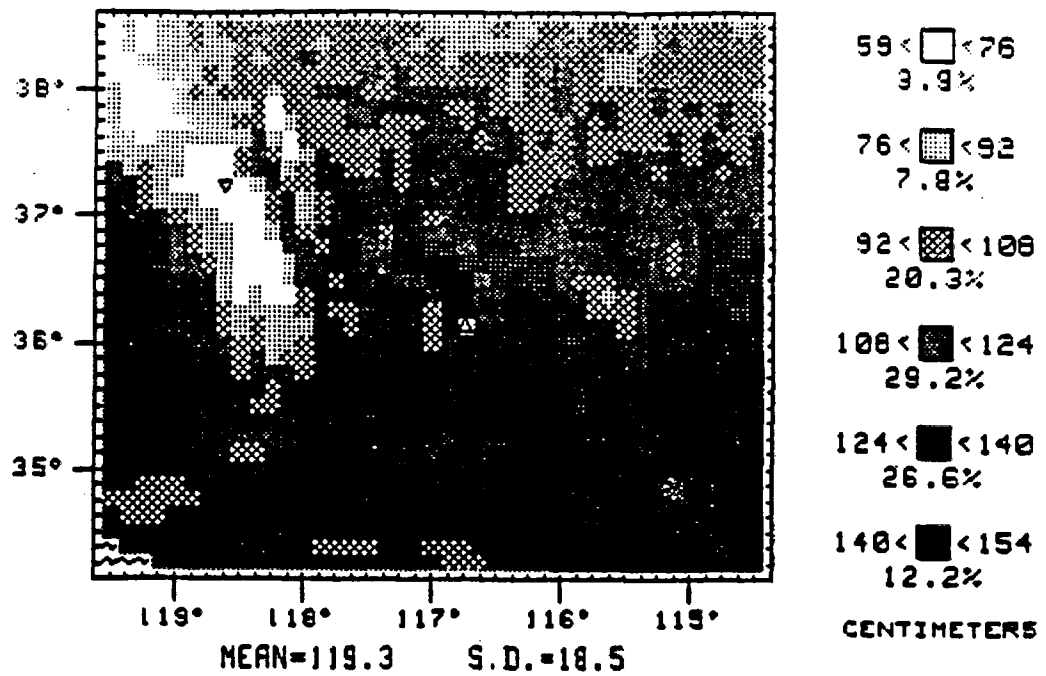


Figure 46. August modern (top) and last glacial maximum (bottom) evapotranspiration.

MODERN TOTAL EVAPOTRANSPIRATION



L.G.M. TOTAL EVAPOTRANSPIRATION

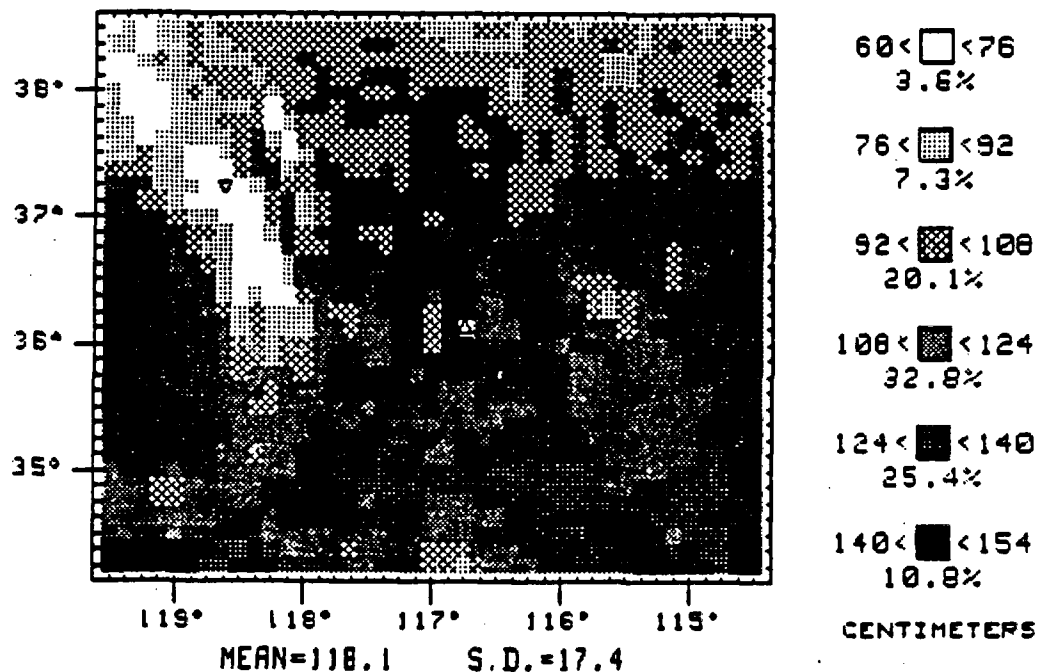


Figure 47. Annual modern (top) and last glacial maximum (bottom) evapotranspiration.

Figures 45-47 with 6, 12 and 17. This correspondence holds for all months; thus we do not discuss plots of evapotranspiration except the yearly total. That is the value most frequently reported in the literature and so allows comparison of our predictions to published observations.

Of all the variables studied it is evapotranspiration that is least certain. Very few actual observations of this variable are reported in the literature, especially for this area. Most estimates that are made are based upon an assumed extrapolation from pan evaporation data. Such extrapolation is fraught with difficulties. There is some suggestion that evapotranspiration varies with depth to the water table (Tanner, 1957, figure 7). It also varies with vegetation, of course. Because we do not yet have models of the vegetation distribution that are useable in this simulation effort it is not practical to represent the variation of evapotranspiration with vegetation.

The relation of evapotranspiration with depth to the water table is an inverse one. Tanner (1957) reports values as shown in Figure 48. As can be seen the values roughly vary from 16cm for a shallow water table to 1cm for a relatively deep one. Because it can be expected that the water table will be more shallow in regions of discharge, and because those usually are found at lower elevations, we assume that the depth to water tables will

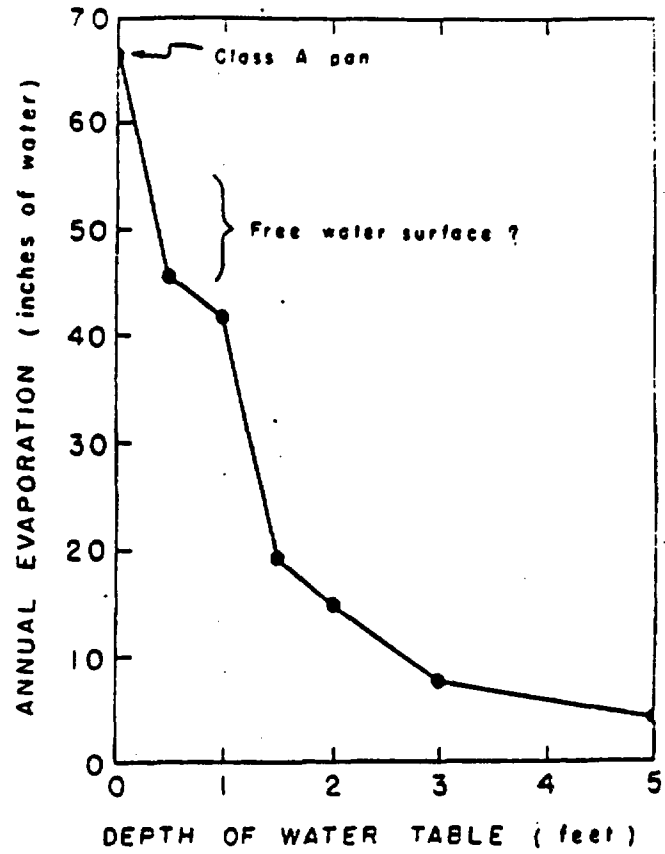


Figure 48 . Relation between evapotranspiration and depth to the water table (from: Tanner, 1957, figure 7).

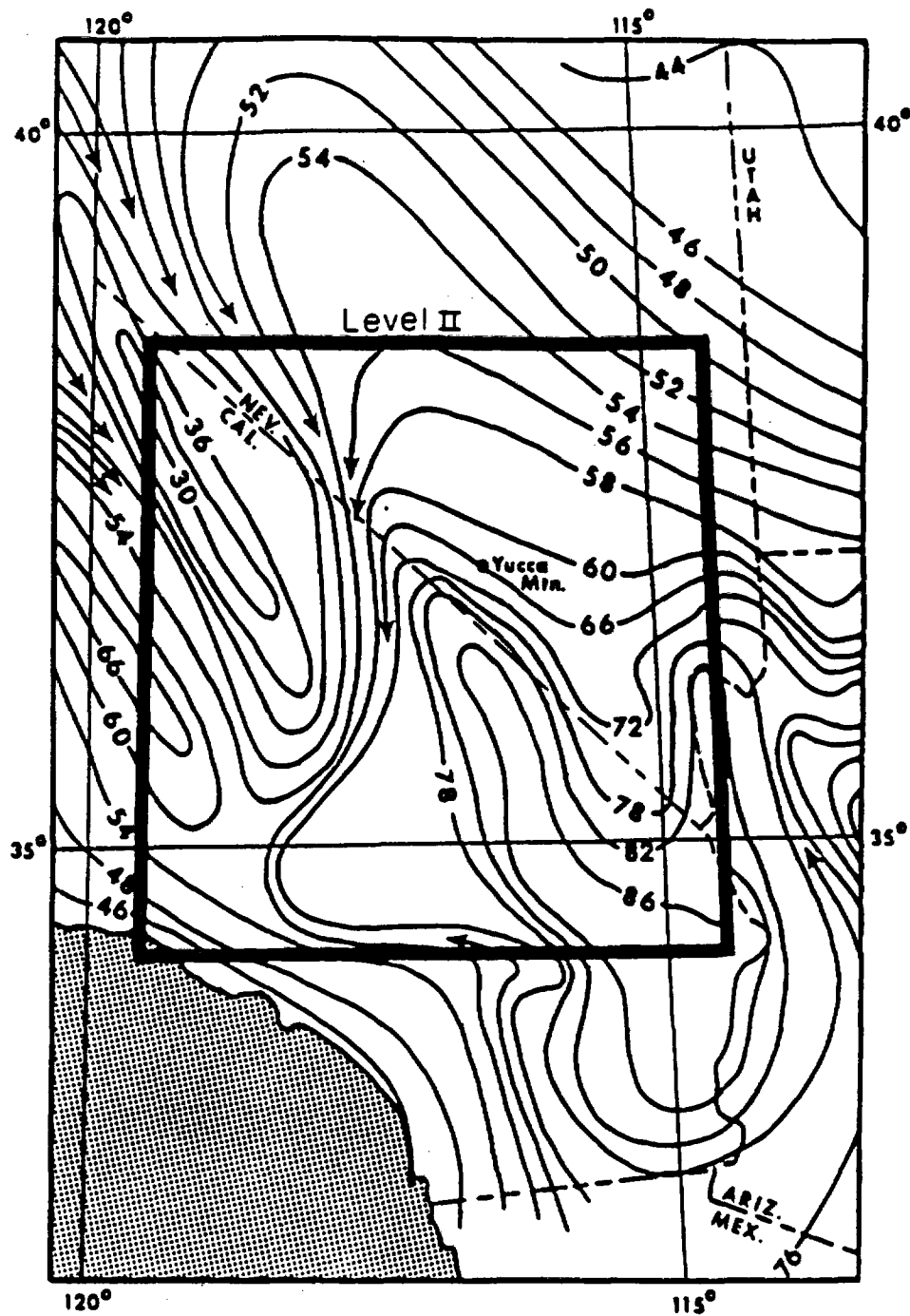


Figure 49. Annual potential lake evaporation for the area as reported by the Department of Commerce (1968, plate 2). Contours are in inches. The level II area and Yucca Mtn. are shown for orientation. The Pacific Ocean is shaded.

decrease as elevation decreases. Thus the consumptive use coefficient will be slightly larger; this assumed relation is that which is reported in Table 10.

As would be expected, evapotranspiration in the warmer months is greater than in months such as February. Comparing Figures 45 and 46 we see that evapotranspiration is approximately doubled in August (maximum = 18cm) compared to February (maximum = 8.4cm). Comparing Figures 19 and 45 we see that precipitation in February exceeds evapotranspiration at most points; there is surplus water nearly everywhere. On the other hand, in August precipitation nowhere exceeds 4.6cm but August evapotranspiration is everywhere greater than 7cm. Thus no surplus occurs anywhere in the entire area. Because precipitation behaves in an inverse fashion to temperature the seasonality is highly amplified when runoff is computed.

The yearly potential evapotranspiration values reported in Figure 47 do not seem out of line. The Department of Commerce (1968, Plate 2) estimates potential lake evaporation for the area (reproduced here as Figure 49). Those values range from less than 30" (76cm) in the Sierras to greater than 86" (218cm) in the Mojave Desert. The values we report from the same area range from 57cm to 155cm following very closely that pattern seen in the Climate Atlas. The lake evaporation values are larger

than ours by about 50%. This seems reasonable in that evaporation from lakes will nearly equal the potential evaporation in an area since water is constantly available. Evaporation from soils and transpiration from vegetation is limited to available water. Other factors also lower evapotranspiration; these include protective adaptations of vegetation, insulation effects of soil cover, slope azimuth and inclination, and shadowing effects. For these reasons evapotranspiration can be expected to be markedly lower than lake evaporation (Tanner, 1957).

Over a smaller range of elevations (270m to 2600m) Armstrong and Stidd (1967, figure 2) show a range of evapotranspiration estimates of about 12" (30cm) to 35" (89cm) for the American River watershed in the Sierra Nevada. This range of values very closely matches our predicted range of values over the same elevations. Thus, although there is certainly a wide latitude for improvements to be made in the current model of evapotranspiration, the results correspond fairly well to observed values and first approximation results are very encouraging.

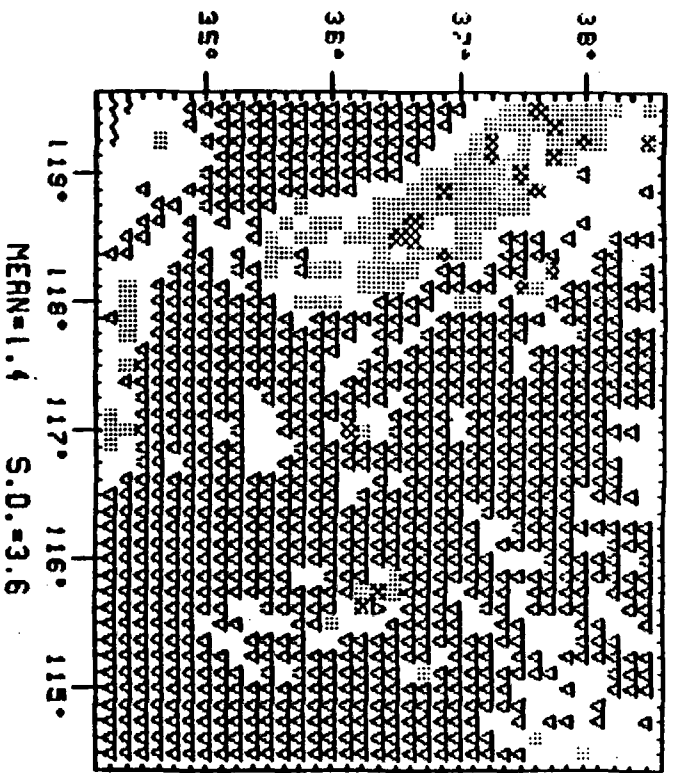
We have assumed that the groundwater recharge and discharge conditions remain in equilibrium throughout the time of study so that the discharge equals the recharge. We have also assumed that storage remains constant during

this time. Under those assumptions we have solved for runoff since runoff equals total precipitation minus evapotranspiration. This of course further assumes that the surface water basins correspond to groundwater basins. The evapotranspiration estimates, when subtracted from the previously available precipitation estimates, yield runoff estimates that are illustrated at the top in Figures 50 through 52. Estimates of runoff were made on a monthly basis so that for any points in those months where potential evapotranspiration exceeds precipitation, the runoff is adjusted to zero. This avoids the problem of a negative balance in one month being artificially carried over to some other month.

Few data on observed modern runoff values are available. Recording stations are mostly limited to the west-flowing Sierran streams in the western portion of the study area. The most comprehensive summary is that of McGuinness (1964). That study showed annual runoff and is reproduced as Figure 53. We have shown the same area for comparison in Figure 52 using our own equations.

As can be seen the agreement is quite close, both in the pattern and in absolute values. Because McGuinness' map is more generalized (it covers the whole U.S. at a scale of 1:5,000,000) exact comparisons are difficult. For

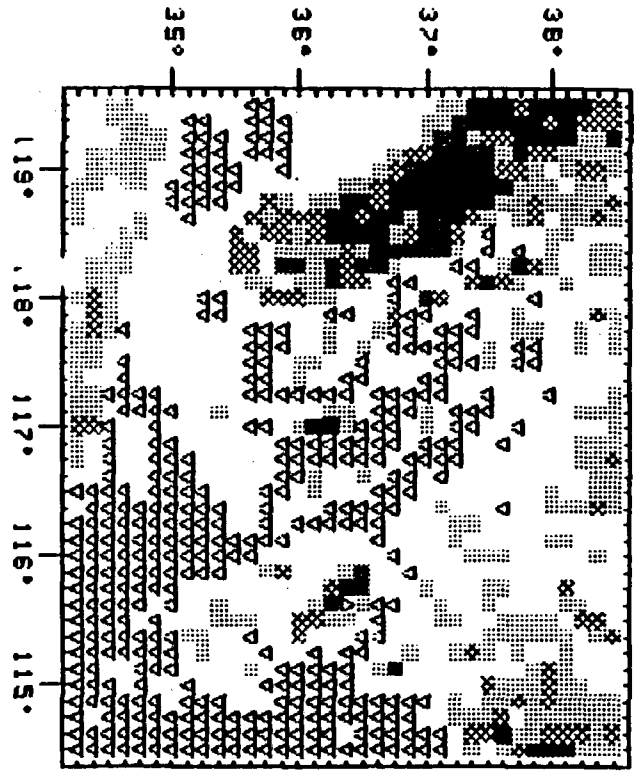
MODERN FEBRUARY RUNOFF



MEAN=1.4 S.D.=3.6

- 0 < □ < 8
 - 91.1%
 - 0 < ▤ < 16
 - 7.5%
 - 16 < ▩ < 24
 - 1.3%
 - 24 < ■ < 32
 - .1%
 - 32 < ■ < 40
 - 0.0%
 - 40 < ■ < 47
 - 0.0%
- CENTIMETERS

L.G.M. FEBRUARY RUNOFF

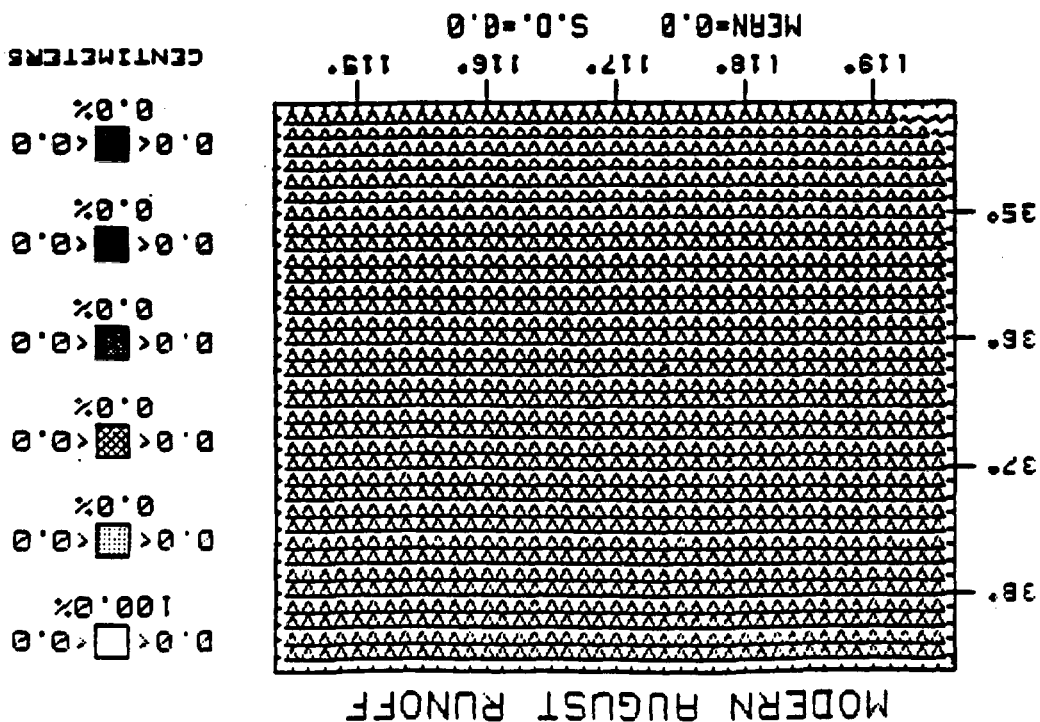
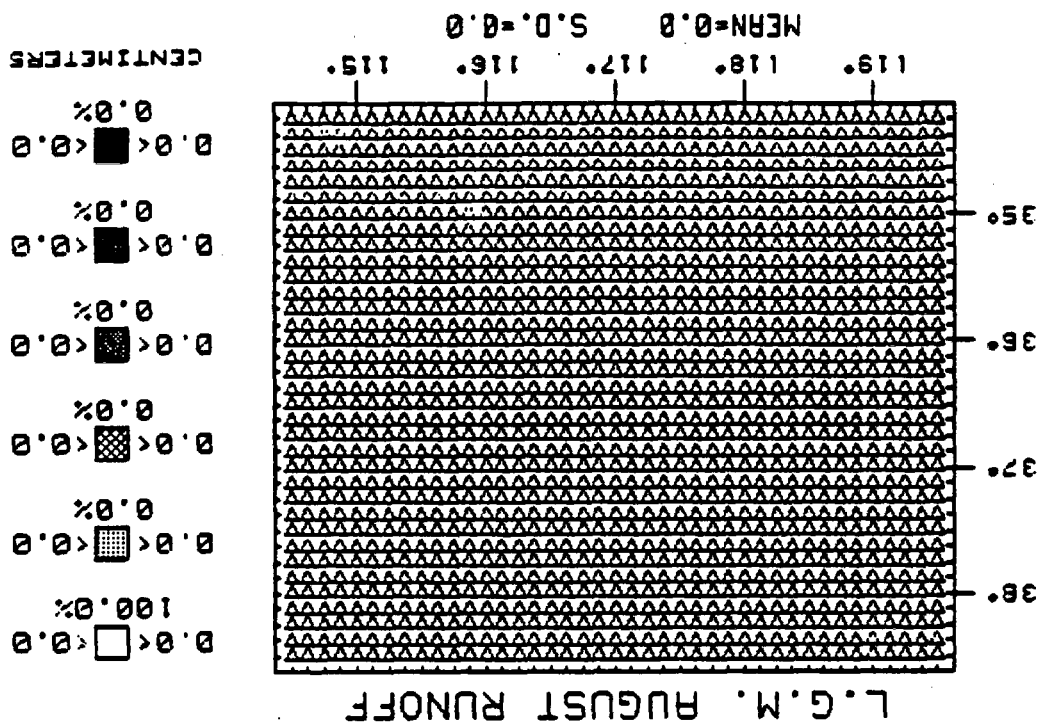


MEAN=5.0 S.D.=7.2

- 0 < □ < 8
 - 70.9%
 - 0 < ▤ < 16
 - 17.1%
 - 16 < ▩ < 24
 - 5.9%
 - 24 < ■ < 32
 - 4.4%
 - 32 < ■ < 40
 - 1.6%
 - 40 < ■ < 47
 - .1%
- CENTIMETERS

Figure 50. February modern (top) and Last Glacial maximum (bottom) runoff.

Figure 51. August modern (top) and last glacial maximum (bottom) runoff.



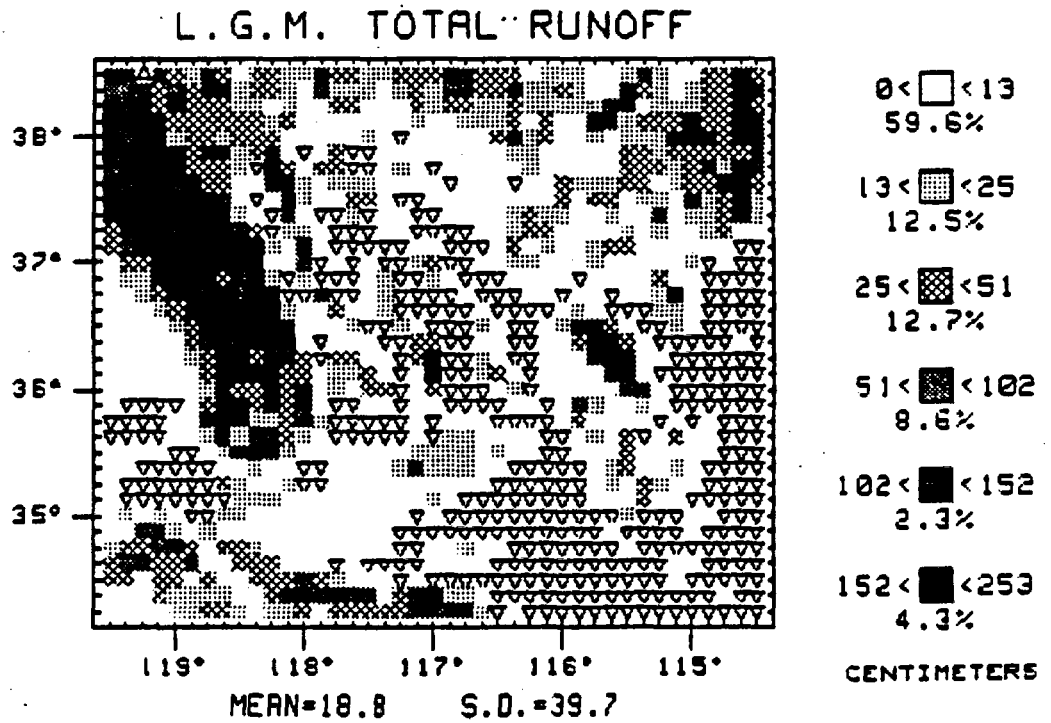
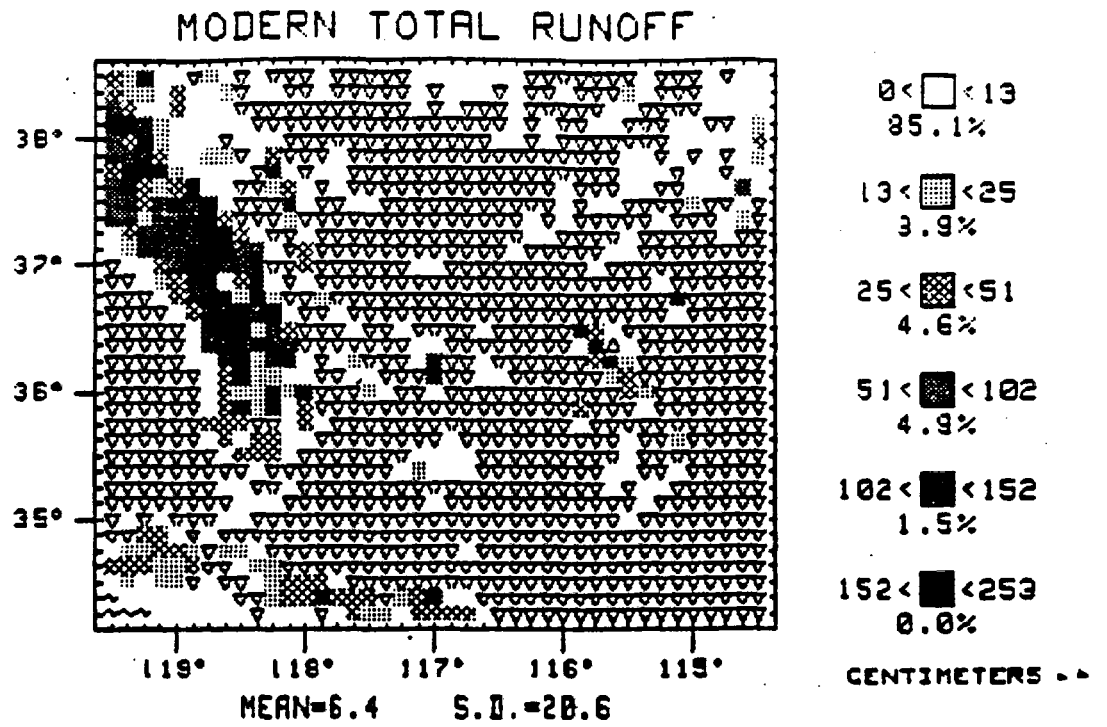


Figure 52. Annual total modern (top) and last glacial maximum (bottom) runoff.

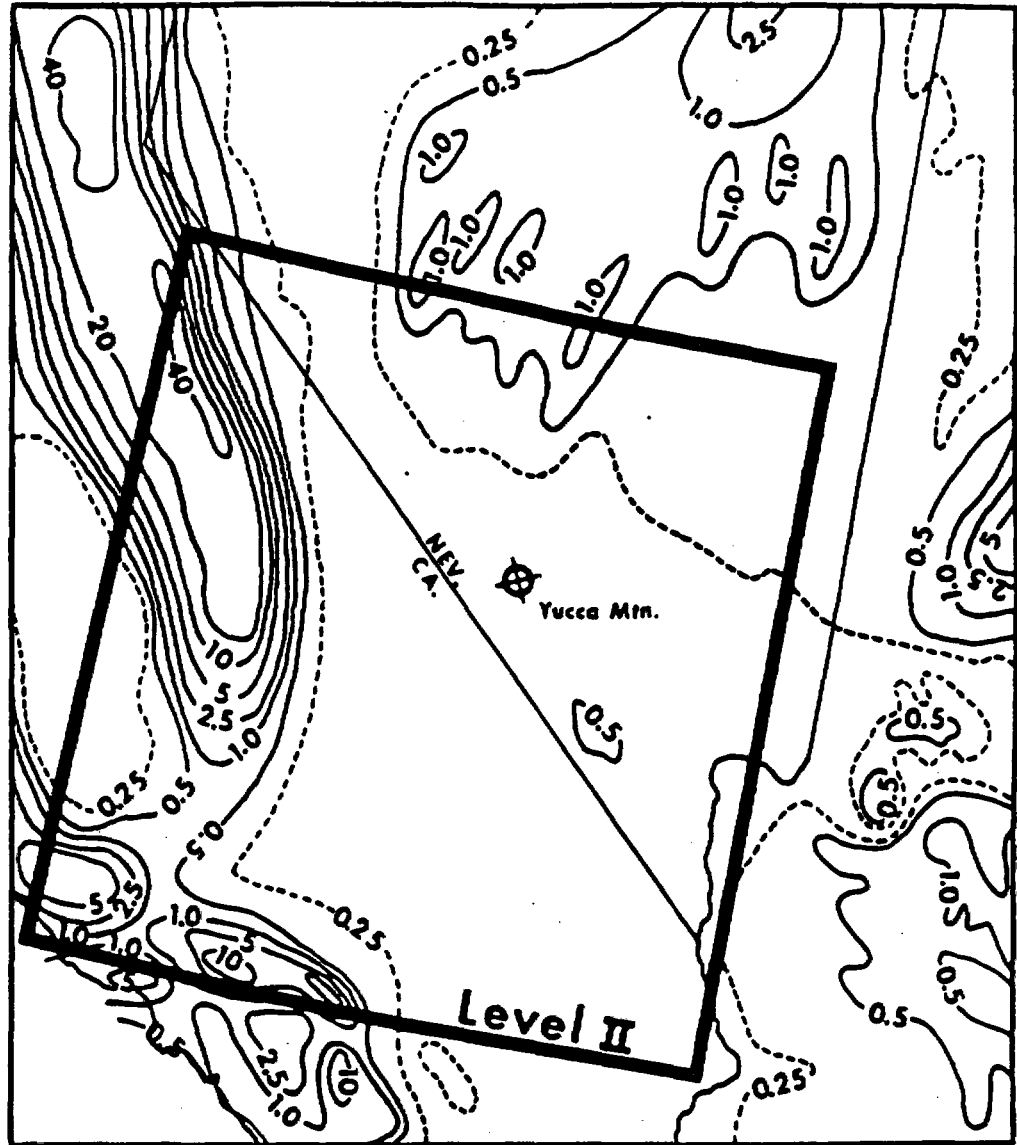


Figure 53. Observed values of runoff under present climatic conditions in the Southwest. Contours are in inches. The level II area of this study is outlined. The high values of the Sierras can be seen on the left. Data from: McGuinness (1964).

example it is not clear what value he would assign as a maximum in the Sierras. Because a 20" contour interval is used there, and the largest value reported is a closed contour at 40" (101.6cm), we assume the observed maximum would be a little less than 60" (152.4cm), based on the contour spacings. Our computations yield a maximum of 142cm and show a long narrow zone of precipitation in the 96cm to 120cm range where McGuinness shows the 40" (101.6cm) to less than 60" (less than 152.4cm) band. Thus our estimates in the most important zone - that of the highest runoff values - are extremely close to those of McGuinness.

Throughout most of the Great Basin proper within this area McGuinness infers values less than 0.25" (0.635cm). Our own estimates give a runoff of zero. Since there are a few points of slightly higher runoff (up to 25cm) we believe that, if generalized over broader areas as McGuinness did, the correspondence would again be quite close. Indeed, in light of the uncertainties in both of these estimates we suggest that (1) the answers cannot be considered significantly different (2) our own estimates are likely to be closer to correct if there is a difference and (3) our estimates are more useful because they contain greater detail.

In conclusion we can say that the entire modelling procedure has yielded estimates of available moisture in

the level II area that are at least as good as any others available. They can be expected to yield useful estimates of quantities such as total precipitation, mean annual temperature, total evapotranspiration and total runoff that reflect the available knowledge of such parameters as closely as currently possible. With these, estimates of hydrogeologic quantities such as infiltration and recharge should be improved over those provided by other means. Estimated values of runoff as reported in these figures have been totalled and are input to the computer code that solves lake configurations.

SOLUTION OF LAKE CONFIGURATIONS

Modern

This code was described in our previous report (Craig and Singer, 1983). The configurations were examined over a one thousand year period at ten-year time steps to determine the lake configuration that will be in equilibrium with the assumed runoff values. We used a ten-year time step to minimize approximation errors in the relation between net lake evaporation and the surface area - depth of lake function. This time step appears to produce smooth results (Figure 54). Lake configurations resulting from our predictions of modern runoff are reported in Figure 55.

These values of lake configuration have been adjusted at each step to account for lake evaporation as estimated within the area from available data and approximated with a quadratic equation (Figure 56). This equation was developed from modern observed lake evaporation measurements using a stepwise regression procedure. Although we had originally hoped to use the equations of Benson (1981) to estimate lake evaporation using an energy balance approach, this was impractical due to uncertainties in his formulation that remain unresolved.

As can be seen from examination of Figure 57, the predicted lake configurations solved using our climate equations correspond quite well to those actually observed today.

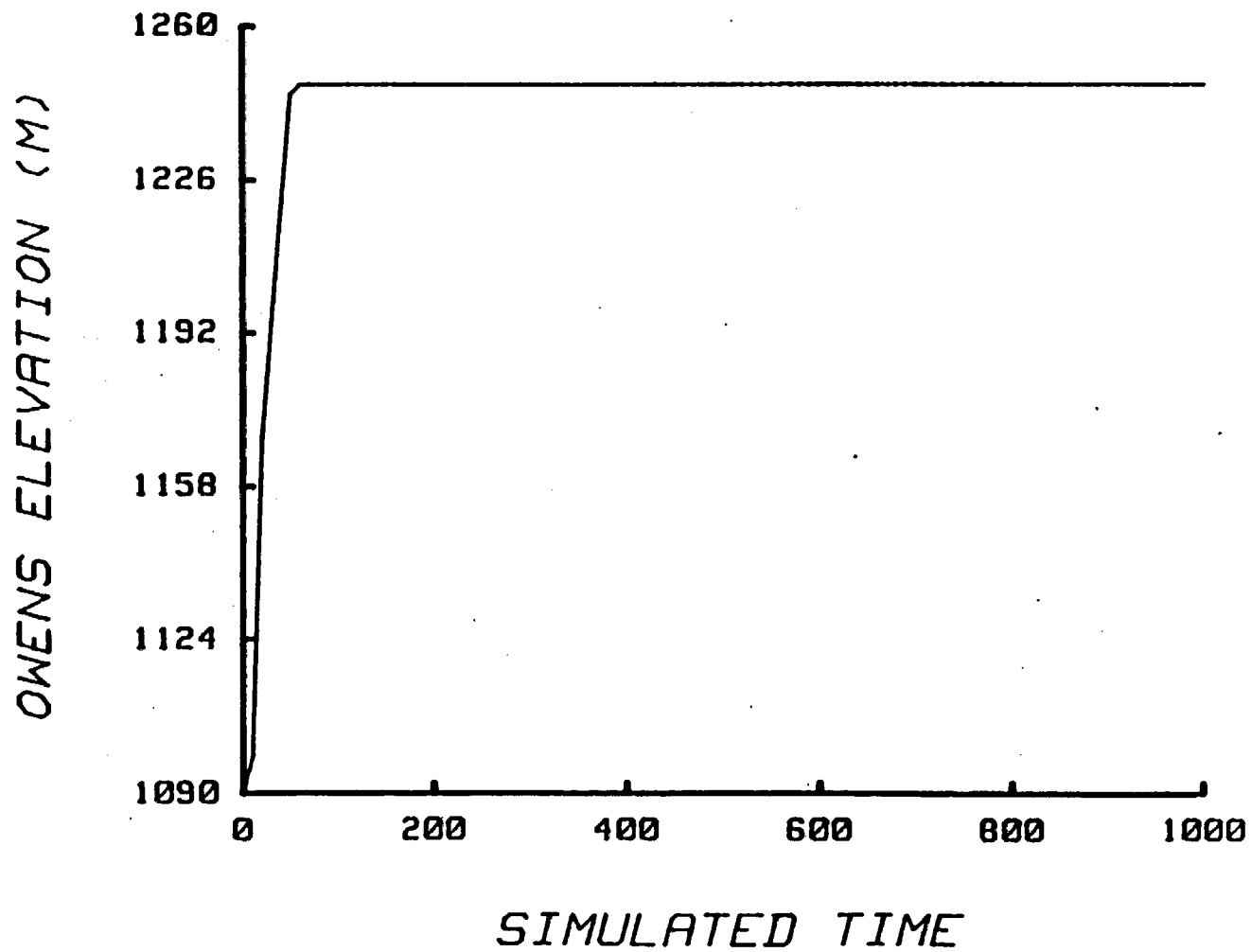


Figure 54. Convergence to an equilibrium configuration of lakes illustrated by the water surface elevation of Lake Owens at each 10 year time step of a 1000 year simulation.

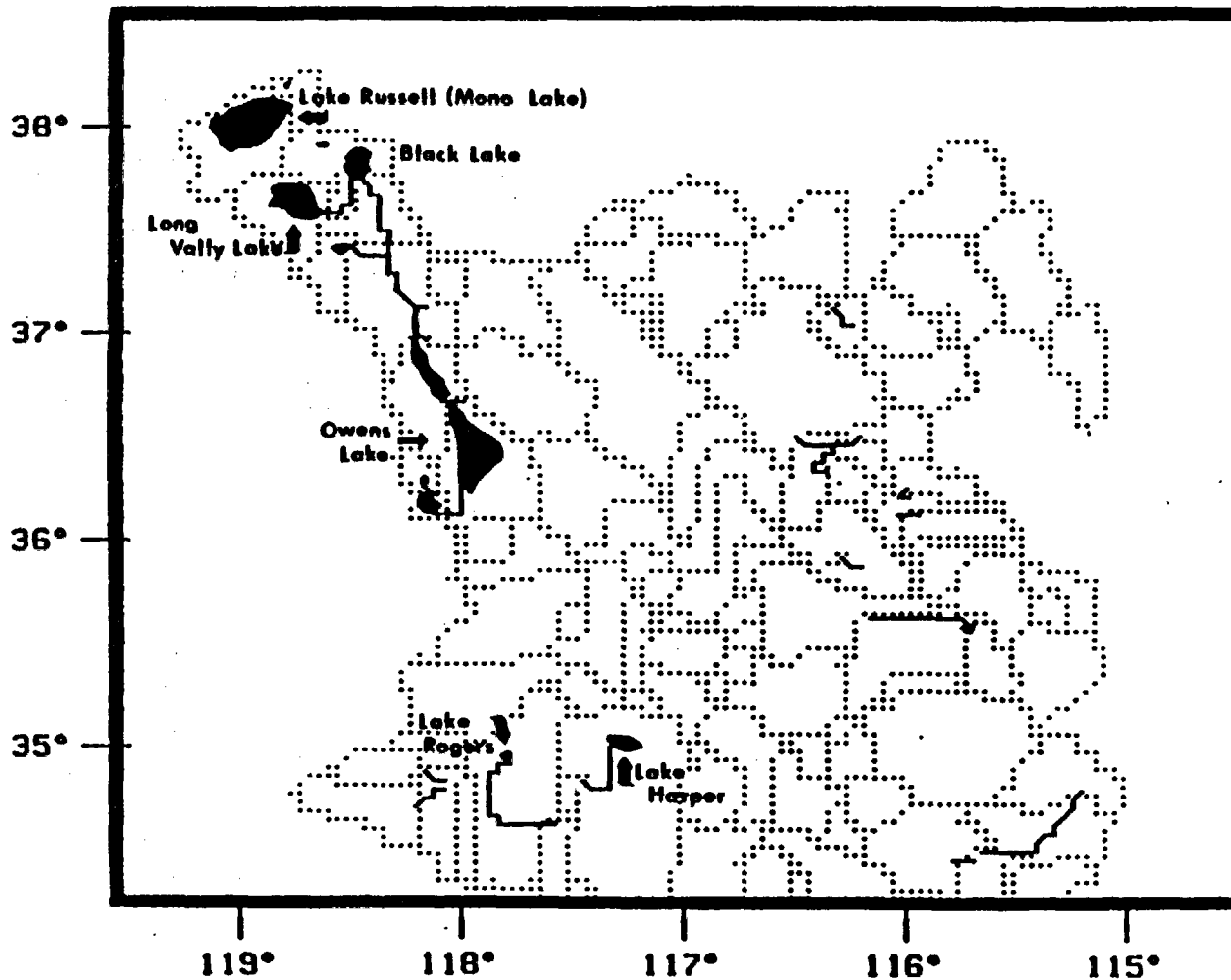


Figure 55. Configuration of lakes in the Death Valley drainage system that are in equilibrium with the estimated modern runoff computed with our climate equations. Dotted lines mark drainage divides. Solid lines mark overflow channels.

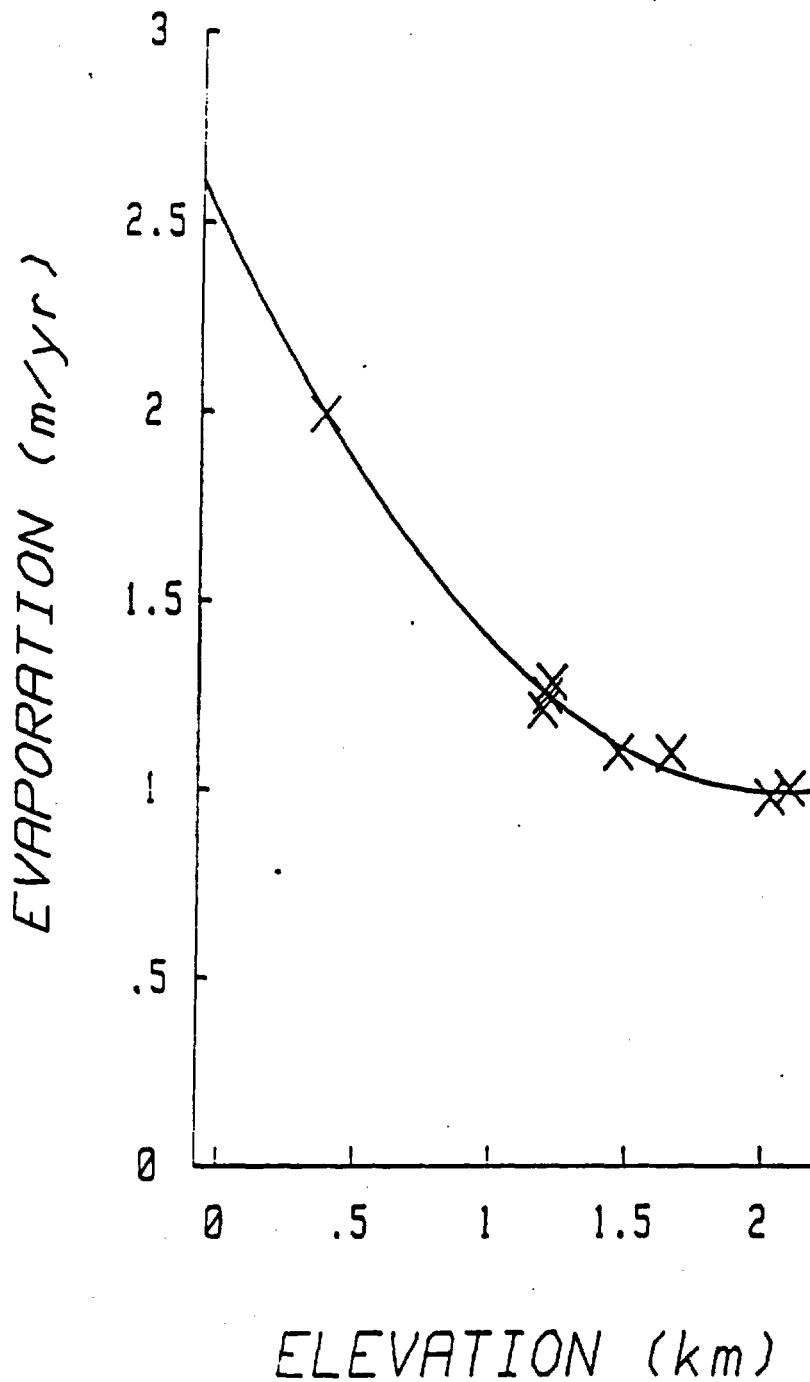


Figure 56. Relation between lake evaporation and elevation. These values are from Mifflin and Wheat (1979). The line shown is a best-fit (least squares) quadratic equation ($Ev=248-1.46(Elev/10)+0.0036(Elev^2/100)$). Evaporation in the equation is in cm/yr, elevation is in meters. The coefficient of determination (R^2) is 99%. Standard error of the estimate is ± 3.84 .

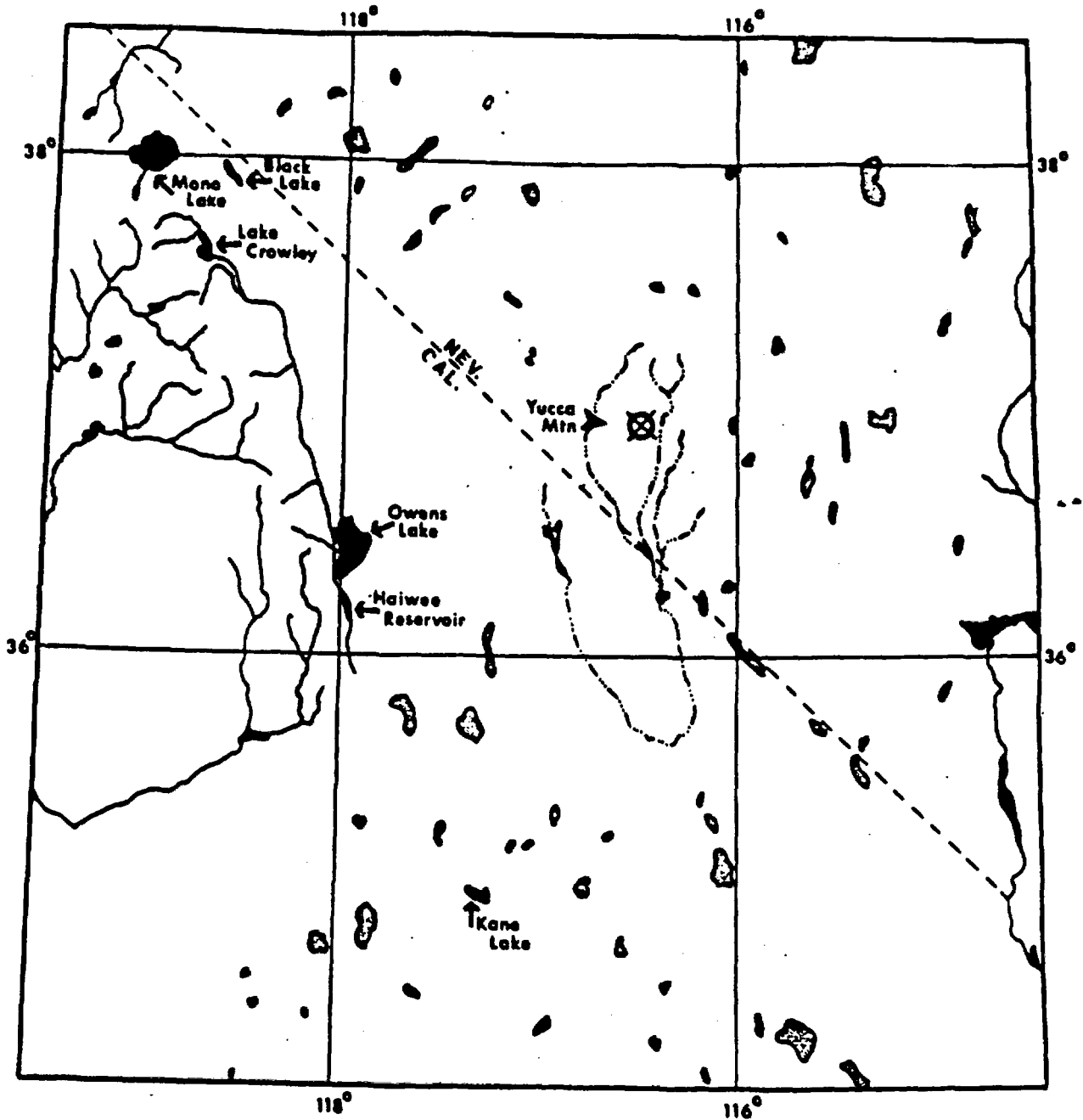


Figure 57. Locations of lakes within the level II area today. Existing lakes, including some man-made lakes, are shown in dark shading. Playas presently dry and only intermittently receiving water are shown with light shading.

Only Owens Valley contains major lakes. The largest is Mono Lake; others include Lake Crowley (in the Long Valley caldera depression), a small lake in the Adobe Valley (Antelope Lake, River Spring Lakes and Black Lake are seen today) and Owens Lake itself. Two small lakes are predicted in the Mojave Desert, the larger of these, Lake Harper is shown on modern (U.S.G.S.) hydrologic unit maps of the State of California. The other, Lake Rogers on the site of the Edwards Air Force Base, is frequently wet. Indeed, such a condition delayed landing of NASA's Space Shuttle in 1983.

Minor intermittent streams in the area of Ash Meadows are also predicted. Occasionally today the Amargosa River does flow at approximately this location. From the close correspondence between the modern day observed and predicted configurations we conclude that the model provides a satisfactory and acceptable estimate of the present runoff characteristics of this region when considered over ten to one hundred year time spans.

LAST GLACIAL MAXIMUM

We have made similar computations of evapotranspiration for each month of the year using estimated temperatures in each month at the last glacial maximum. It should be noted that the Blaney-Criddle consumptive use coefficient at each point changes slightly, using the same values as reported in Table 10, since elevation at each point increases by 104 meters (due to sea level drop) during a glacial maximum. These values of evapotranspiration for several months were illustrated in Figures 45 through 47.

Using the same assumptions as in the computation of present-day runoff we have computed runoff at the last glacial maximum as precipitation minus evapotranspiration. Our estimated values of runoff at each point in the level II study area are illustrated at the bottom in Figures 50 and 51. Finally we have summed the monthly values to compute total runoff throughout the year (Figure 52) at the last glacial maximum and those values of runoff have been input to the lake code to estimate equilibrium configurations.

At the last glacial maximum a much larger portion of the area received sufficient water to yield some non-zero runoff on an annual basis. Only about 40% of the area had no runoff at all (net deficit of moisture) compared to nearly 80% of the area today. It is reasonable to assume that this additional available water would encourage plant growth and immigration of new plant (and animal) species into these areas. The largest region so affected includes the Nevada portion of the study area, including the NTS.

Greatest runoff occurs in the winter months, just as is true today. Surprisingly, the highest runoffs in winter months such as February (Figure 50) occur in the Spring Mountains, not in the Sierras. Of course the total volume of runoff from the Sierras is much larger than that of any other source. The aridity of Death Valley and the lower Mojave remains important. Even the relative dryness of the Owens Valley is clear through the winter months. Regional runoff for February (in the Death Valley drainage system) increases to 5.0 cm per cell. This is an increase of 3.6 times over that of the present. In the summer months such as August (Figure 51) no runoff occurs anywhere in the area, as is the case today. Thus, it can be expected that summer remains a time of stress on the endemic vegetation and will limit the introduction of new species into the area.

Total runoff reaches a maximum of 2.53m, compared to a maximum of 1.42m today. Data reported by Armstrong and Stidd (1967, fig. 2) show runoff of 1.07m in the American River watershed of the Sierras at an elevation of 1945m. Projection of their relations of runoff and evapotranspiration with elevation would suggest a runoff of about 1.30m at an elevation of 3352m. Since our elevations in fact reach over 4000m it appears reasonable to predict a modern maximum runoff of 1.42m.

Between today and the last glacial maximum runoff increased from a mean of 6.4cm per cell to a mean of 18.8cm^{*} per cell. This indicates that, on the average, runoff increased by a factor of 2.9 times. By comparison, for runoff sufficient to fill Lake Searles without causing Lake Panamint to grow, Smith and Street-Perrott (1983, p. 200, table 10-2) suggest that runoff must have been three to six times the modern amount. Our own solutions of lakes (next section) suggest that this is the lake configuration that would result from our LGM predictions. Thus our 2.9x's increase is at the low end of Smith and Street-Perrott's estimate. Of course the 2.9 factor is computed for the entire Death Valley drainage system which includes some points where runoff remained zero at the LGM. Considering the Owens drainage only (as reflected in the number Smith and Street-Perrott report) it is likely our factor of increase would be considerably higher. Conceivably it might

be at the high end of the range they report. Modifications of our computer code would allow direct reporting of such changes in runoff.

Again, to more clearly show the changes we predict between modern and LGM conditions we show in Figure 58 the differences in the two predictions. Most strikingly, we see that in certain of the lowest elevations runoff actually decreases. This happens in 31% of the entire level II area. These decreases are very minor, nowhere exceeding 4cm. However, since runoff in these areas was never large such decreases are very significant. Stress on endemic plants would have been greater in these areas at the LGM. This may explain the continued occurrence of desert plants in these areas. Such "...altered species associations were, in a sense biotic refugia under Wisconsin climatic conditions" (Spaulding, et al., 1983, p. 285).

The greatest part of the area (almost 46%) experiences only slight increases (0cm to 26cm) and these are usually the middle elevation points. The most dramatic increases occur at high elevations including the Panamint Mountains, Spring Mountains and especially in the Sierras. Increases in the Sierras are almost all greater than 64cm. Thus it can be anticipated that almost all the increased runoff that would feed growth of Lake Searles would originate in the Sierras. Although the points of significant large

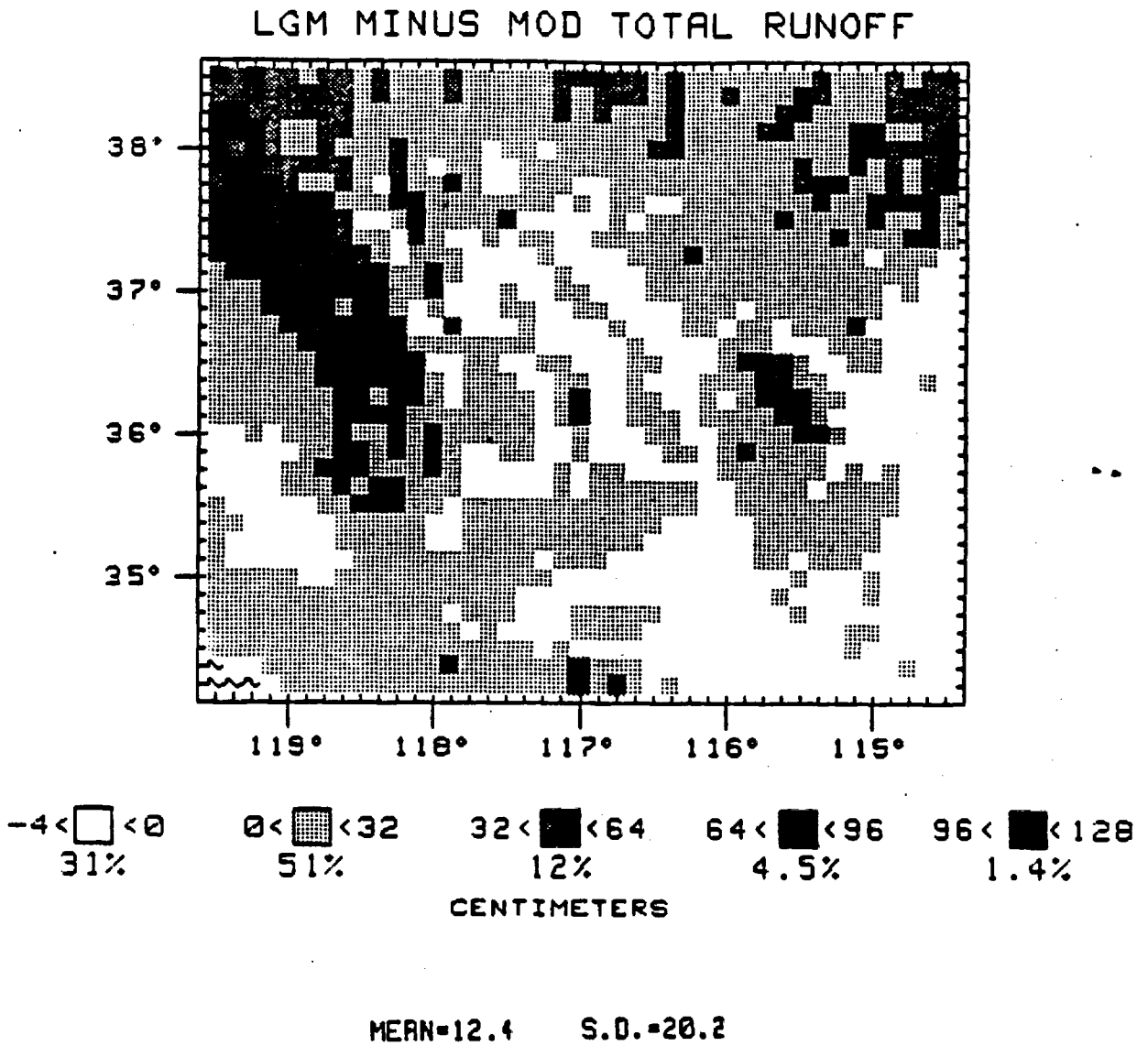


Figure 58. Change in total annual runoff between the present and the last glacial maximum. Positive values indicate an increase at the last glacial maximum.

absolute increases in runoff comprise no more than 6% of the total area of the Death Valley drainage system their contribution was able to swell the downstream Lakes Owens and Searles to their maximum levels.

Again lake level computations were run for a one thousand year time period at ten year time steps to reach overflow. In general we note that equilibrium is reached within approximately 100 years (Figure 59). The equilibrium configuration at the last glacial maximum as estimated with our runoff values and assuming the present lake evaporation rates is reported in Figure 60.

The correspondence to the geologic record is probably within the limits of error of that record itself. As can be seen by comparison of Figures 55 and 59 the greatest predicted change from modern to last glacial maximum configurations is by creation of Lake Searles. All authors agree that Searles was full and overflowing at the last glacial maximum (Smith and Street-Perrott, 1983, p. 193). Lake Searles is predicted to have received its water almost exclusively from Lake Owens; this also agrees with the geologic record (Smith and Street-Perrott, 1983, p. 199). Our model also predicts that the overflow from Lake Searles will result in a small lake in the Panamint Valley. However, it is not nearly as large as the largest lake which is documented to have existed at one time and certainly not deep enough to overflow to Lake Manly.

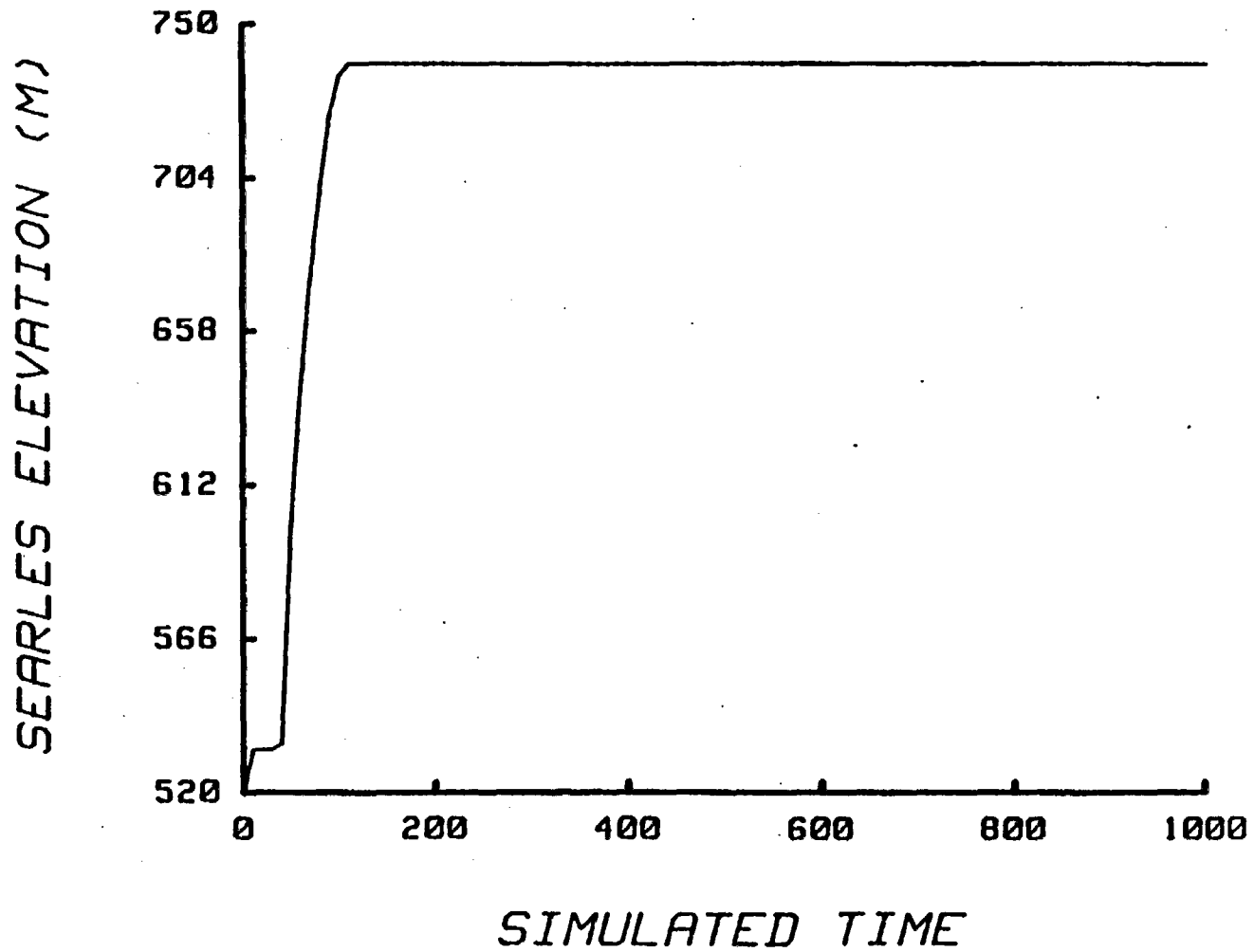


Figure 59. Convergence to an equilibrium configuration of lakes illustrated by the water surface elevation of Lake Searles at each 10 year time step of a 1000 year simulation.

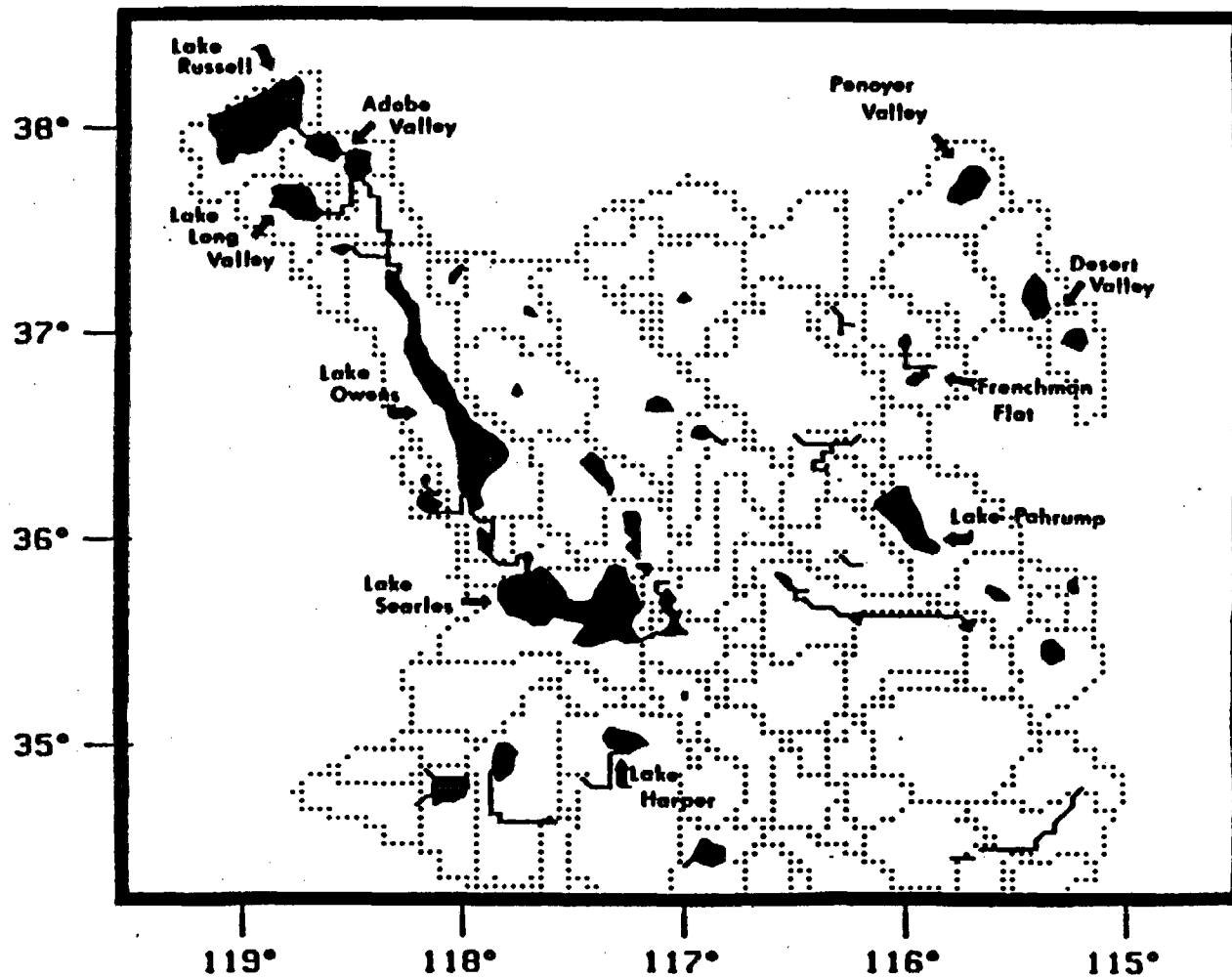


Figure 60. Configuration of lakes in the Death Valley drainage system that are in equilibrium with the climate equations reported here and solved using boundary conditions representative of the last glacial maximum.

This configuration also agrees with the most recent interpretations of the geologic record. Smith (Smith and Street-Perrott, 1983, p. 199) claims that the highest shoreline in Panamint Valley predates the last glacial maximum, having occurred over 25,000 yrs BP. He claims that the most recent lake (of the latest Pleistocene) was only 44m deep and must have been fed by overflow from Lake Searles. The lake we predict for the Panamint Valley was 51m deep.

There is some discrepancy in the literature about the size of the late Pleistocene lake that occupied Death Valley. Hooke (1972, p. 2086-87) claimed that a lake 90m deep existed about 11,000 yr BP. Although Smith (Smith and Street-Perrott, 1983, p. 199) agrees that the sedimentologic evidence suggests the presence of a lake in Death Valley between 12,000 yr BP and 21,000 BP, he claims the evidence points to lakes which, "were small and substantially less than 90m deep." Our own results agree quite closely with this latter interpretation. We find two lakes, one near Stovepipe Wells and the other near Furnace Creek Ranch. Both of these lakes are quite shallow with small surface areas.

Little information is available about the configurations of lakes in the Mojave. The data of Smith and Street-Perrott (1983, p. 200) do suggest that some lakes

did exist in this area at the last glacial maximum and that Silver Lake "had a major pluvial episode ending about 14,500 B.P." Our own model does not suggest a lake there but does predict another (Silurian Lake) downstream of it in this drainage system of the eastern Mojave. In the western Mojave we predict growth of Lake Kane, Lake Harper and Lake Rogers (a part of Lake Thompson).

A set of small lakes and intermittent drainage in Nevada is also predicted. Although this includes a sizeable lake in the Pahrump Valley; it did not overflow to Ash Meadow where minor perennial drainage is seen. Small lakes also form in Yucca Flat, and Frenchman Flat. A few lakes also form north of the Sheep Range but these do not overflow either. Overall the lakes throughout this area do not appear to develop to sizes substantial enough to directly influence the regional groundwater potentiometric surface.

PLUVIAL MAXIMUM

Under the assumption that lake evaporation would decrease during a glacial maximum, due perhaps to increased cloud cover (Benson, 1981), we have computed the equilibrium configuration under an assumed 27% reduction in lake evaporation from that of modern values. The equilibrium configuration of lakes under these assumed values is illustrated in Figure 61. As can be seen these values are sufficient to produce a significant lake within Death Valley at an elevation of approximately 192 meters.

Under such conditions substantial changes occur in all portions of the pluvial system. Several points are of interest in these changes. Although the Owens Valley remains the major source of overflow for the growth of lakes in downstream basins - including Lake Manly - it is not the sole supply. Measurable influxes come from both the Mojave Desert - by way of Soda Lake - and from the Amargosa Valley. The latter overflow is fed by runoff from the Spring Mountains. This runoff enlarges Lake Pahrump until it overflows to Ash Meadows. The lake in Ash Meadows is also fed by a stream in Fortymile Wash. This in turn receives its major supply from overflow of a small body of water in the Timber Mountain caldera. A tiny ponded area forms in the Amargosa Desert

before this overflow reaches Ash Meadows. From Ash Meadows overflow fills Lake Tecopa and hence continues southward into Death Valley. Another minor supply comes west down the Kingston Wash.

The suggestion is strong that runoff is significant across virtually the entire study area. Accompanying such a radical shift in the fluvial system we can expect major modification of the groundwater. Recharge will probably increase significantly. Most notably for our purposes we can expect a rise in the potentiometric surface at Timber Mountain and probably throughout flowlines extending beneath Yucca Mountain and the lower Amargosa Basin. Because of the lake in Ash Meadows, the potentiometric surface in this area would be considerably elevated. This will most likely further modify flowlines from Yucca Mountain toward the south and west. Diversion of those lines to a more westerly direction might be anticipated.

Coupled with this will be an increase in the potentiometric surface at the Death Valley discharge points. This might tend to lower flow rates along the trans-Yucca Mountain flowlines. In turn the potentiometric surface could rise a corresponding amount (recall that the rise in Death Valley is nearly 200m). Such potential for changes cannot be ignored when one is considering the stability of the groundwater system beneath Yucca Mountain.

These reconstructions are based upon calculations assuming a 27% decrease in rates of evaporation from lakes in the study area. This value was chosen because it is the value which, when combined with our solutions of runoff under last glacial maximum climatic conditions (predicted temperature and precipitation), will produce a lake in Death Valley as large as is documented in the geologic record of the Late Pleistocene (Hunt and Mabey, 1966). Several authors have published estimates of the percent decrease in evaporation over lakes in closed basins of the southwest during a full glacial event; these are reproduced in Table 11.

There is some considerable uncertainty in these estimates. Indeed two authors have published revised estimates involving increases of 4 and 13 percentage points respectively. We note that the mean of the 15 known estimates is 31.7% with a standard deviation of 10.13%. This yields a standard error (uncertainty in the mean) of 2.6%. Thus our determination of the degree of decrease in lake evaporation required to produce the maximum documented stand of Lake Manly is well within the uncertainty bounds of published estimates. Indeed, prudence would dictate that we consider the effects of decreases in the range of 37.3% to 26.1%. Such a range is appropriate if we assume that each of these researchers has produced an independent,

Table 11. Estimates of change in climate at the time of the last maximum pluvial event as reported in the literature.

Reference	%E*	Location	Source**
Antevs, 1952	-34	Lahontan	SS
Antevs, 1952	-30	Lahontan	SLV
Brackenridge, 1978	-42	Estancia	SS
Brackenridge, 1978	-43(?)	Spring Valley	SS, SLV
Broecker and Orr, 1958	-30	Lahontan	SS, SLV
Galloway, 1970	-45***	Estancia	SS
Leopold, 1951	-34	Estancia	SS
Leopold, 1951	-38	Estancia	SS
Leopold, 1951	-23 to -50 (-36.5)	Estancia	SLV
Mifflin and Wheat, 1979	-16	Lahontan	SS
Mifflin and Wheat, 1979	-10	Nevada Statewide	SS, SLV
Reeves, 1965, 1966	-27	Southern High Plains	SS, SLV
Reeves, 1973	-40	Southern High Plains	SS
Snyder and Langbein, 1962	-30	Spring Valley, Nevada	SS, SLV
Weide, 1976	-20	Warner, Oregon	SS
N = 15	means -31.7	$\sigma = \pm 10.13$	$\sigma / \sqrt{n} = \pm 2.62$

* %E is computed as $\Delta E / \text{modern } E$ following SLV

** The references listed are taken from two compilations SS = Smith and Street-Perrott, 1983, Table 10-1, p. 195; SLV = Spaulding, Leopold and VanDevender, 1983, Table 14-6, p. 288.

*** SLV provide a value of -51, however this appears to correspond to the value of ΔE in cm that SS report.

unbiased estimate of the same mean and that the true values of lake evaporation change are normally distributed.

Whether such assumptions are warranted can be tested in several ways. Independence of estimates is suggested by the fact that of three re-estimates by the same author (one by Leopold and two by Reeves), new values were offered in two cases. We note also that an identical set of values occurs in only one other case (the estimates of Antevs, 1952; Broecker and Orr, 1958 and of Snyder and Langbein, 1962). The value these authors present, 30%, is close to the mean of all estimates. So it is not surprising that it should form a mode.

The assumption of normality can be tested more exactly; we compute Fisher's estimates of skewness and kurtosis from these 15 samples. Standardized values are: $g_1 = 1.12$ and $g_2 = -0.26$. Both of these values are well within the 95% confidence limits for samples from a normal population. They provide no reason to question the assumption of normality.

There is no suggestion that estimates made from points farthest from the study area (Death Valley) deviate more than the mean value. For example, the very largest deviation, 21%, is from an estimate for the entire state of Nevada and so would include much of the study area. The

second largest deviation, 15%, is for the Lahontan system, probably the closest analog to the Lake Manly system. For the four systems for which multiple estimates have been made, the group means for these systems vary from the grand mean by 1.8% for the most distant (Southern High Plains, Texas) to 7.4% for the next most distant (Lake Estancia, New Mexico). The mean of estimates for the Lahontan system differs by 4.2% and for Spring Valley by 4.8%. None of these deviations are out of line with the estimated uncertainty in the mean (± 2.6 = one standard error of the mean based upon fifteen samples).

It appears reasonable to assume that the mean lowering of evaporation rates was the same throughout the area encompassed by these estimates. A further conclusion which appears justified is that evaporation rates within even a small area (such as that of Spring Valley) can vary spatially ($\pm 10.1\%$). Over short time spans, under the same climatic regime, basin-wide evaporation rates can also vary about the regional mean ($\pm 2.6\%$ if only fifteen points are being considered). In general, the degree of deviation would depend upon the total number of points under consideration. For example, if we consider the entire level II study area (about 10,000 points) the variation in grand mean from one independent time step to another would be $\pm 0.1\%$ if the value at each point is independent of that at all others.

CONCLUSIONS

From the work we have completed to date and the analyses that have been performed we are able to reach a number of important conclusions about climatic change in the study area. These conclusions fall into two classes. First, recognizing that this entire procedure represents a new strategy in geologic analyses, we reach several conclusions concerning the modelling procedure itself. Second, using this modelling procedure, we can reach several conclusions concerning the climatic changes that can be anticipated during a glacial event.

We have found it possible to construct statistically-based models that allow us to predict temperature and precipitation under modern regional climatic regimes quite precisely. These predictions can be tested by comparison with previously created maps of these variables. Tests are also available by combining such predictions with the pluvial lakes code that we have created in order to study the impact of this climate upon the drainage system of the area. Both of these tests suggest that no systematic biases occur. Climate can be predicted equally well throughout the area.

These predictions have been successfully generalized to allow estimates to be made under changed global boundary conditions of sea surface temperature, sea level and wind patterns. The success of the generalization methodology can

be tested by examining the impact of these climatic predictions upon the fluvial system. Specifically we have tested the predictions for the last glacial maximum and have found the degree of correspondence to be quite acceptable.

Predictions of evapotranspiration made using the Blaney-Criddle equation are acceptable for our purposes. This equation allows estimates using only temperature on a monthly basis as input. The equations we have used, when combined with our climatic predictions, yield estimates of evapotranspiration that are in close correspondence with other published estimates. The estimates appear to be well within the range of uncertainty of our knowledge of this variable within the area.

We have found that the methodology can yield predictions of the lake configurations for the last glacial maximum that are in excellent agreement with the available geological evidence. The most sensitive tests are provided by the predicted configurations of Lake Searles, Lake Panamint and Lake Manly. Predictions for each of these three lakes are in close accord with the most recently published geological interpretations.

Using these models we are able to predict that during a glacial event precipitation will increase markedly throughout the region of interest. In absolute terms the

greatest increase will occur at the highest elevations of the Sierra Nevada Mountains. It is the increased precipitation here that will, by way of runoff, eventually result in growth of lakes within the Death Valley system. However, precipitation increases will occur in equal proportion throughout the study area. Thus we can expect changes in the runoff-recharge values at all points. We note the pattern of change is highly erratic on a spatial scale so that second and third order variability is an important component of the observed patterns.

In a similar way we can use the equations developed to provide estimates of temperature during a glacial event. With these we find that temperatures will not change very much. Temperature change is also erratic and difficult to describe in simple terms. We do not expect that changes in temperature will themselves produce significant effects upon the hydrologic system.

Using the climatic estimates that we have derived, and with no change in lake evaporation rates, we find that no large lakes will form within Death Valley during a climatic change of an extent comparable to that of the last glacial maximum. Several small playa lakes do form, but these in themselves should have no significant effect upon the groundwater flow system of the region. However, they reflect increased available moisture that could affect the groundwater system, as noted below.

If lake evaporation rates decrease by 27% a major lake will form in Death Valley. This lake will be of an extent comparable to the highest recorded stand of Lake Manly during the Wisconsin. This estimate agrees closely with available geologic estimates of the amount of lake evaporation change that occurred. It also agrees very closely with the geologic evidence concerning the size of Lake Manly.

We believe that because of the increase in precipitation that is predicted during a glacial event, recharge rates, and so groundwater flow conditions, will change significantly during a glacial event. Such changes are of an extent that they should be considered when evaluating the overall geologic stability of a proposed nuclear waste repository to be built under Yucca Mountain, Nevada. It is premature at this point to state whether such a change could significantly decrease the repository stability there.

RECOMMENDATIONS FOR FUTURE WORK

The equations we have described here seem to be quite successful in describing the climatic characteristics of the region as seen today. They pass the most stringent tests we are able to apply, including their ability to predict the modern configurations of lakes. They have greater predictive ability than any known alternatives. These equations were purposefully constructed to allow solution also under boundary conditions independently established as representing the last glacial maximum. With those boundary conditions the solutions are quite plausible. They do not appear to diverge from estimates made from paleoclimatic evidence. The most encompassing and sensitive test of the entire procedure - the ability to predict lake configurations of that time, as documented by geological evidence - yields impressive success. On this score we cannot 'rate' the quality of the approach vis à vis other methods. Alternatives are not available.

Potential applications of these equations are many and diverse. Thus it would appear prudent and fruitful to devote some additional energies to refining the model. A long list of 'finishing touches' can be suggested and some are listed next. The data base used to develop our equations was limited. Only 124 climate stations with complete data sets could be used and the records only extended to about 1960.

With an additional 20 years of record, and with records covering more stations, we could improve our confidence in the model. Results to date emphasize the critical importance of the points of highest elevation, especially the Sierra Nevada. A concerted effort should be made to obtain climate records from a large number of stations in that area.

Our estimates of wind vectors are quite primitive at this point. More detailed models of topographic control upon local circulation could be achieved. This should provide increased predictability. We also should develop more close links to GCM generalized wind vectors. This is especially important in defining other boundary conditions. In conjunction with these we can and should define methods to make more complete use of the available sea surface temperature information. Integrating the sea-surface temperature history of an air mass for several hundred kilometers before it passes inland is one obvious need.

Another major improvement could be obtained through more exact representation of evaporation from lakes. Energy-balance equations, such as those described by Benson (1981) could be used to advantage. Considerable refinement over Benson's formulation is possible since we already have the requisite information to estimate the advection term which he ignored. His own results suggested the importance of that term.

More thorough analysis of the statistical aspects of this model is appropriate. We need a complete 'all possible regressions' analysis to be assured that the model is the most appropriate that can be obtained (Draper and Smith, 1966). A bootstrap or jackknife analysis of the regression coefficients would be useful to establish the best estimate of uncertainty in those. Such estimates, along with estimates of uncertainty in the other components of the model, should be evaluated in a full Monte Carlo simulation procedure. With this available a sensitivity analysis - to identify those components responsible for changes in paleoclimate - could form the basis of a rigorous site stability assessment.

The dominant influence of the Sierras suggest the need to evaluate the impact of lag effects induced by growth of perennial snowpacks and glaciers as climates change. Fairly useful models of such phenomena are now possible. The two critical components, monthly temperature and monthly precipitation, are available. The most challenging aspect of this study would be linking accumulation to meaningful flow models that would incorporate the influence of complex terrain. Refined models of ablation would also be required.

We have some suggestion that the usefulness of our predictive model could be considerably improved if it were linked to a finer grid of elevation data. Such a finer grid is available and could be used with only minor modifications

to our program. It is also desirable to extend the elevation data set to the south several degrees of latitude. This would allow more complete use of wind vector information and available climate stations. We recommend a thorough evaluation to choose the most appropriate grid spacing.

Because of the many potential applications of such a model it is reasonable to structure the present computer realization of that model to encourage and simplify its application. A number of ideas for such a task are described here. Application by others would be most easily achieved if it were set up in an interactive manner. In this way the user could be given the option of detailed specification of the boundary conditions to be considered. The code could be refined to allow examination of the predicted characteristics of selected areas within the context of the entire system. A variety of features of the resulting predictions can be reported, depending upon the interests of the individual investigator. For example, one researcher might be interested in the relative volumes of local vs. 'alien' water within a specific lake basin. Another could be interested in the percentage change in precipitation at a specific point. Many such items could be made available at the user's choice and each will play a role in the overall evaluation of the model.

Such a capability would be enhanced by designing graphical and other auxiliary output to enhance the clarity of the predictions. Pseudo-three-dimensional color displays of the results of a model run will make evaluation and comprehension of these results much easier. This capability will become more important as persons only peripherally acquainted with the work begin to utilize the results. Personnel of a number of government agencies and the public at large will eventually need these predictions explained in understandable terms. Graphical displays will be important for this.

Since the climate has direct impact upon the groundwater system - a major point of concern in site stability - efforts should be made to link our model directly to finite difference or finite element groundwater models. This could be a fairly straight-forward step.

With a model available to a select group of knowledgeable users, it becomes practical to design and execute a number of significant and detailed tests. These could allow important refinements of the model and would in the end provide a professional certification of the method. This will be important as the model is applied to specific analyses of nuclear waste repository stability. Such an evaluation should be planned.

Second generation models can be envisioned. Such developments can proceed along two lines. First, we currently have achieved only static views of the climate system at two specific boundary conditions, those representative of modern conditions and those characterizing conditions at the last glacial maximum. We will ultimately want to extend these. First, we could interpolate our results to represent intermediate boundary conditions. In this way transitions from one climate state to another could be examined. Such transitions could be controlled by estimates of the global climate state made from Milankovitch-based predictions as described in the original "conceptual model" report prepared by Craig (1982). With such a control we could also consider limited extrapolations beyond the two sets of boundary conditions.

Such interpolations and extrapolations can be integrated with available paleoclimatic reconstructions of sea-surface temperature in the North Pacific Ocean off the California coast. A small number of deep-sea cores have been obtained and continuous oxygen-isotope and microfossil-based paleoclimate reconstructions have been obtained for periods of several hundred thousand years. Where estimates of sea-surface temperature are available these could be used as constraints to direct climate histories. Such historical reconstructions would provide an order-of-magnitude more sensitive test of the model. Predicted lake histories could

be compared with temporal reconstructions from geological evidence such as the cores of lacustrine sediments covering comparable time spans - these are available from Searles and China 'lakes'.

A longer-term development that can be suggested - extension of the modelling procedure so that other regions could be studied in comparable detail - will require considerably more work and a long-term commitment. On the basis of our present understanding we suggest that the proposed nuclear waste repositories at the Paradox Basin, the Palo Duro Basin and the WIPP site would be most readily accommodated. Sites in salt domes in Texas and Louisiana would follow naturally after the models of Palo Duro Basin were available. The most difficult (conceptually) to model will be the Hanford site. The close proximity of the edge of the Cordilleran Ice Sheet - with its attendant dramatic shifts in air circulation - has few, if any, well-documented modern analogs. For this, further development of our ability to integrate global circulation models with our models will be needed. If such are to be available for use in site selection, work should proceed immediately.

ACKNOWLEDGEMENTS

In a study such as this where an attempt is made to integrate the work of many geologists who have worked before us we must acknowledge the great assistance of a number of people who have been a great help in the definition and study of the problems involved. Of especial help has been Dr. Michael Foley of the Battelle Memorial Institute Pacific Northwest Labs. Mike was of great help in initiating the program for the work at the Nevada Test Site and it is he who first got us involved in this project. Mike has been very instrumental in arranging the support for the program and in encouraging our continuing work on this project.

Charlie Hunt (Salt Lake City) was a great help to us in our orientation to the study area. Charlie acted as a consultant to the project in its early stages and was involved in many discussions of the features of the area that would be of importance to us. Later Charlie made a very gracious host for us during a part of the field work in the Nevada area. Larry Benson of the U.S. Geological Survey (Denver) was of enormous help in a number of investigations of the question of lake evaporation. His frank discussions of the problems involved in such modelling was of a great help to us in understanding the procedures that should be applied. George Smith of the U.S. Geological Survey (Menlo Park) was of great help in the later stages of this project.

He has reviewed some of the lake configuration predictions that result from the climate equations we have developed. George has also helped us through the great encouragement he has provided to us in this program. Ike Winograd (U.S. Geological Survey) helped us early in the study by an in-depth discussion of the groundwater system and its characteristics in the area of the Nevada Test Site. He was also very encouraging in his support and suggestions. John Harbaugh (Stanford University) acted as a consultant on this project in its earliest stages and it was he who originally suggested the idea of modelling at multiple levels of detail as a function of the particular aspect being investigated.

A large number of people were involved in the modelling effort at Kent State University. Without their help this project could not have been completed. Among those involved included Sue McCauslin who was very useful in developing procedures for graphical representation of some of the modelling variables. She acted also to review certain chapters of this report. Sam Figuli was of great help summarizing various data that were produced during the modelling effort. Sam acted as a continuously available assistant in this project. Brian Hoyt was of great help at various stages as a consultant in programming and data base design problems. Brian acted as a systems analyst to aid us in the various problems that arose in making use of our computation facilities.

Lisa Cirbus was a great help in allowing us better understanding of the use of a global circulation model. She was also very useful in designing the layout of the final report and acted as a reviewer for certain chapters of this report. Dave Hose was of general assistance in various stages of the modelling effort. Jim Hanson acted as a reviewer for certain chapters of this report. Gregory Underberg was of great assistance to use by becoming involved in various discussions during the development of the model itself. Tom Dwyer drafted numerous figures in this report. He did an excellent job in his work and performed many tasks with rapid delivery. Ms. Dotty Thompson was of great service to us in preparing the final report including typing three drafts and many additional revisions to the final copy. Jane Anderson was instrumental in the early stages of this project in helping us to gather a large number of references that were required for use in the modelling effort. Julie Ellingson also helped us in drafting certain figures at early stages of the work.

This project began when Craig acted as consultant to Battelle Labs to develop the conceptual model for a comprehensive computer simulation of the geologic stability of the Nevada Test Site. Dr. Joseph Devary was liason at Battelle for that project and he did an excellent job of overseeing the effort. Work on the computer model itself began in November of 1982 under a contract from Battelle Labs with Harvey Dove as contract technical officer. We thank Dean Wenninger of the Office of Research and Sponsored Programs at Kent State University for

providing some funds to continue the work when funds were abruptly discontinued in this project half way through the contract period. We thank Barry Miller and Don Palmer of the faculty in the Geology Department for discussions at various times concerning aspects of the modelling effort. We also thank Dick Heimlich, Chairman of the Geology Department, for providing an assistantship to Barry Roberts to enable him to take part in this research effort.

Richard Craig was awarded two NORCUS Fellowships at Battelle Institute to facilitate development of this model. Both Mike Singer and Greg Underberg were also awarded fellowships early in the modelling period as was Jim Hanson. We appreciate the funding of the Department of Energy through these NORCUS Fellowships and Sandia National Laboratory through subcontract B-F7204-A-H for the early work that eventually led to preparation of this report. That contract provided an assistantship to Mike Singer to complete his portion of the study. At Sandia Labs, Regina Hunter was contract monitor and her encouragement and critical evaluations are greatly appreciated.

The model was conceived by Craig who supervised its construction. Roberts performed the statistical analyses leading to the climate prediction equations we report here. Singer constructed the computer code and performed the analysis of predicted runoff to obtain the lake configurations in equilibrium with these values. Errors that remain in this report are the responsibility of the senior author.

REFERENCES

- Antevs, Ernst, 1952, Cenozoic Climates of the Great Basin, Geol. Rdsch, v. 40, p. 94-108.
- Armstrong, C.F., and Stidd, C.K., 1967, A Moisture-Balance Profile on the Sierra Nevada, J. of Hydrology, v. 5, p. 258-268.
- Benson, L.V., 1981, Paleoclimatic Significance of Lake Level Fluctuations in the Lahontan Basin, Quat. Res., v. 16, p. 390-403.
- Brakenridge, G.R., 1978, Evidence for a Cold, Dry, Full-Glacial Climate in the American Southwest, Quat. Res., v. 9, p. 22-40.
- Broecker, W.S., and Orr, P.C., 1958, Radiocarbon Chronology of Lake Lahontan and Lake Bonneville, Geol. Soc. Am. Bull., v. 69, p. 1009-1032.
- CLIMAP Project Members, 1976, The Surface of the Ice-Age Earth, Science, v. 191, p. 1131-1137.
- Craig, R.G., et al., 1982, Conceptual Model of the Geologic Simulation Model of the Nevada Test Site, Report to: Battelle Memorial Institute, Pacific Northwest Laboratories.
- Craig, R.G., 1983, The Climate Submodel: Computer Code for the Simulation of Climate Changes in the Great Basin, Southwestern U.S., Report to: Battelle Memorial Institute, Pacific Northwest Laboratories.
- Craig, R.G., and Singer, M.P., 1983, The Pluvial Events Submodel: Computer Code for the Simulation of Growth and Dessication of Lakes in the Great Basin, Southwestern U.S., Report to: Battelle Memorial Institute, Pacific Northwest Laboratories.
- Denton, G.H., and Hughes, T. J., 1981, The Last Great Ice Sheets, N.Y., Wiley-Interscience, 484 p.
- Department of Commerce, 1968, Climatic Atlas of the United States, U.S. Department of Commerce, Environmental Science Services Administration, U.S. Government Printing Office, Wash., D.C., Plate 2.
- Dixon, W.J., 1981, BMDP Statistical Software, University of California Press, 725 p.

- Draper, N.R., and Smith, H., 1966, Applied Regression Analysis, John Wiley & Sons, Inc., N.Y., 407 pp.
- Galloway, R.W., 1970, The Full Glacial Climate in the Southwestern U.S., Am. Geographers Assoc. Annals, v. 60, p. 245-256.
- Gates, W.L., 1976, The Numerical Simulation of Ice-Age Climate with a Global General Circulation Model, J. of the Atmospheric Sciences, v. 33, p. 1844-1873.
- Hooke, R.L., 1972, Geomorphic Evidence for Late-Wisconsin and Holocene Tectonic Deformation, Death Valley, Calif., Geol. Soc. of Am. Bull., v. 83, p. 2073-2098.
- Houghton, J.G., 1979, A Model for Orographic Precipitation in the North-Central Great Basin, Mon. Weather Rev., v. 107, p. 1462-1475.
- Hunt, C.B., and Mabey, D.R., 1966, General Geology of Death Valley, California-Stratigraphy and Structure, U.S. Geol. Survey Prof. Paper, 494-A.
- Hunt, C.B., 1975, Death Valley: Geology, Ecology, Archaeology, Univ. of Calif. Press, p. 1-234.
- Imbrie, J., and Kipp, N.G., 1971, A New Micropaleontological Method for Quantitative Paleoclimatology: Application to a Late Pleistocene Caribbean Core, in Late Cenozoic Glacial Ages, ed. Karl Turekian, Yale Univ. Press, p. 71-181.
- Leopold, L., 1951, Vegetation of Southwestern Watersheds in the Nineteenth Century, Geographical Review, v. 41, p. 295-316.
- McGuinness, C.L., 1964, Generalized Map Showing Annual Runoff and Productive Aquifers in the Conterminous United States, U.S.G.S., Hydrologic Investigation Atlas, Ha-94.
- McIntyre, A., et al., 1981, Seasonal Reconstructions of the Earth's Surface at the Last Glacial Maximum, G.S.A. Map and Chart Series, MC-36.
- Mifflin, M.D., and Wheat, M.M., 1979, Pluvial Lakes and Estimated Pluvial Climates of Nevada, Nev. Bur. of Mines and Geology Bull., v. 94, 57 p.

- Morrison, R.B., 1965, Quaternary Geology of the Great Basin in Wright, H.E., Jr., and Frey, D.G., eds., The Quaternary of the U.S., Princeton, N.J., Princeton Univ. Press, p. 265-185.
- Nie, N.H., Hull, C., Jenkins, J.G., Steinbrenner, K., and Bent, D.H., 1975, SPSS: Statistical Package for the Social Sciences, 2nd ed., McGraw-Hall Book Co., 675 p.
- Reeves, C.C., Jr., 1965, Pleistocene Climate of the Llano Estacado, J. of Geology, v. 73, p. 181-188.
- Reeves, C.C., Jr., 1966, Pleistocene Climate of the Llano Estacado II, J. of Geology, v. 74, p. 642-647.
- Reeves, C.C., Jr., 1973, The Full-Glacial Climate of the Southern High Plains, West Texas, J. of Geology, v. 81, p. 693-704.
- Smith, G.I., and Street-Perrott, F.A., 1983, Pluvial Lakes of the Western United States in Late-Quaternary Environments of the United States, Wright, H.E., Jr., ed, vol. 1, The Late Pleistocene, S.C. Porter, Editor, Univ. of Minn. Press, p. 190-212.
- Snyder, C.T., and Langbein, W.B., 1962, The Pleistocene Lake in Spring Valley, Nevada, and Its Climatic Implications, J. Geophys. Res., v. 67, p. 2385-2394.
- Spaulding, W.G., Leopold, E.B. and Van Devender, T.R., 1983, Late Wisconsin Paleoecology of the American Southwest in Late Quaternary Environments of the United States, Wright, H.E., Jr., ed., vol. 1, The Late Pleistocene, S.C. Porter, Editor, Univ. of Minn. Press, p. 259-293.
- Tanner, C.B., 1957, Factors Affecting Evaporation from Plants and Soils, J. of Soil and Water Conservation, v. 12, p. 221-227.
- Tinkler, K.J., 1983, Post-glacial Temperature Anomalies and Glacial Isostasy, Quat. Res., v. 19, p. 293-301.
- Waddell, R.K., 1982, Two-Dimensional, Steady-State Model of Ground-Water Flow, Nevada Test Site and Vicinity, Nevada-California, U.S.G.S. Water Resources Investigations, 82-4085, 72 p.
- Weide, D.L., 1976, The Warner Valley, Oregon: A Test of Pluvial Climatic Conditions in American Quaternary Association, Fourth Biennial Conference, Abstracts, p. 23, Arizona State University, Tempe.

APPENDIX

Coefficients of the equations to predict
temperature and precipitation

Raw data used to derive the equations

Reported here are the final coefficients derived with the stepwise regression procedure to predict monthly temperatures and precipitation. In the following tables E signifies the exponent 10 thus .5E-3 is equivalent to $.5 \times 10^{-3}$ or .0005. Variable numbers correspond to those given in Tables 2 and 3 and defined in Table 1. These are also explained in more detail in that section. Variables not listed for a month did not enter the equation during the stepwise regression or entered but later were dropped out.

The regressions were performed using the BMDP stepwise regression package using the forward stepping option. The F-to-enter was set at 4.0 and F-to-remove at 3.9. These are the default values in the program. Minimum tolerance level was set at 0.01. Analysis of the regression equations included:

1. lists of all steps, examination for marginal entry of removal values,
2. lists of all residual values, examination of those exceeding two standard deviations,
3. plots of observed and expected versus each independent variable. This amounts to about 100 plots per regression,
4. consideration of the frequency distribution of residuals including the cumulative histogram, the

detrended cumulative histogram, raw histograms, summary statistics, and measures of skewness and kurtosis.

Presentation of all of these for all months and both variables would be prohibitively wasteful of space. Those steps are summarized in various tables and plots in the text of the report. Also, we include here the raw data that we used to make these regression equations and tests. Thus the interested reader could reproduce these analyses by use of any standard regression package such as BMDP (Dixon, 1981) or SPSS (Nie, et al., 1975). One could also compare these raw data to values computed by hand, using the computer programs we have presented in previous reports (Craig, 1982; Craig and Singer, 1983) or by other means.

We caution that the climate data we have used for these analyses are not a complete set. More recent data are available for all stations and additional stations may be available. Furthermore, we believe we have identified certain errors in the raw data supplied to us for certain (at least two and perhaps as many as six) climate stations and certain months. Correction of these data and inclusion

of additional data may allow some refinements of the estimates. We do not believe they will substantially change the resulting predictions, although that possibility should be tested.

Final coefficients of regression equations for temperature

<u>Variable No.</u>	<u>Coefficient</u>	<u>Variable No.</u>	<u>Coefficient</u>
January		June	
3	0.15244E-2	11	-0.53707
15	-0.55802E-3	28	0.27041
28	1.49466	40	0.78652
30	-0.39932	57	-1.37543
75	0.16563	b _o	9.20809
b _o	-2.58307		
February		July	
1	-1.25241	2	0.08883
3	-0.50070E-2	17	-0.44674E-3
10	0.52026E-2	28	-0.15292
22	-0.83026	40	1.09751
73	-0.18055	55	-0.23710E-3
b _o	70.26171	57	-0.41909
		63	-0.20677
March		78	0.49755E-3
28	0.53582	b _o	-9.87490
32	0.61758		
40	0.05716	August	
42	-0.17752	6	0.34499E-2
52	0.17949E-3	21	-0.02805
57	0.48135	28	1.01455
80	-0.21859E-3	54	0.15112E-2
b _o	-0.97075	69	9.84085
		75	3.43635
April		80	-0.00395
3	-0.51151E-3	b _o	-42.05649
4	0.39562E-3		
28	0.53413	September	
36	0.45721	21	-0.17759E-2
57	-0.22039	28	-0.43501
72	-0.08770	32	0.21311
74	-0.08859	40	0.37691
77	-0.65417E-3	44	0.81993
b _o	0.69628	63	0.33965
		83	-0.63967E-3
May		b _o	-0.07803
3	-0.30358E-3		
32	0.51128	October	
36	0.51359	3	0.12515E-2
44	-0.06212	20	-0.31169E-3
b _o	0.48320	22	-0.35002
		28	0.83366
		40	0.38271
		b _o	5.31792

Variable No. Coefficient

November

26	0.74983
32	-0.37324
44	0.64969
83	0.20072E-2
b _o	0.30101

December

3	0.33786E-3
26	1.05775
30	-0.31583
38	-0.05926
44	0.30092
57	-0.19660
75	0.10452
b _o	0.24821

Final coefficients of regression
equations for precipitation

<u>Variable No.</u>	<u>Coefficient</u>	<u>Variable No.</u>	<u>Coefficient</u>
January		May	
21	-0.63094E-3	10	-0.27504E-3
54	0.39377E-4	11	-0.07170
57	0.39691	58	0.40436
62	0.04728	59	0.60244
66	0.41610	65	0.55703
67	0.26366	66	-0.20169
73	0.01289	67	-0.43513
b _o	0.07667	84	0.19365E-3
		b _o	0.84864
February		June	
11	-0.12938	21	0.60374E-3
16	0.13761E-2	60	0.57737
20	-0.32716E-3	64	0.23267
52	-0.43489E-3	70	-0.04105
54	-0.70560E-3	b _o	-0.05022
71	-0.14340		
82	-0.10125E-2	July	
84	0.25133E-2	7	0.92302E-3
b _o	4.12944	16	0.12544E-3
March		28	-0.03782
1	-0.04761	63	0.72698
2	0.02708	b _o	0.52807
54	0.81306E-4	August	
56	0.39798	2	-0.25091
57	0.35189	21	-0.54608E-3
59	0.26139	22	-0.24157
69	0.06997	73	-0.04202
84	-0.54150E-3	b _o	34.66157
b _o	-1.84313		
April		September	
20	0.72470E-4	18	0.80319E-3
28	0.04778	62	0.27719
30	-0.05156	65	0.35155
56	-0.24043	b _o	0.29022
57	0.74007		
64	-0.18387		
66	0.70602		
67	-0.30941		
69	0.14388		
75	0.05557		
84	-0.24869E-3		
b _o	-0.50187		

Variable No. Coefficient

October

4	-0.41913E-4
10	0.42019E-3
20	0.79071E-4
42	-0.00613
63	0.11542
66	0.46758
67	0.21338
b _o	0.11731

November

1	0.05638
3	-0.10247E-3
38	-0.00557
57	0.59226
63	0.17305
78	0.32961E-3
84	-0.37950E-3
b _o	-1.61396

December

46	0.01459
52	-0.76070E-4
57	0.00784
66	0.54190
74	-0.02230
75	-0.02385
b _o	0.11094

RAW DATA

Listed on the following six pages are the raw data used to develop the regression equations. These are the "orographic" variables as listed in Table 1 of this report. Note that the variables latitude, longitude, elevation and slope are listed twice, first under the data for February and again under the data for August. The remaining variables are unique to the wind vector for that particular month. We do not list the climate data since they can be obtained from any standard climatic atlas.

=====
 | DATA FOR FEBRUARY |
 =====

LAT (deg.)	LONG (deg.)	ELEV (m.)	MAXIMUM		MINIMUM		SLOPE (m.)	COAST DIST	SST (C.)
			ELEV	DIST	ELEV	DIST			
34.07	117.77	260.6	740	192	138	22	+7	284	13.
36.07	119.02	119.8	351	173	54	79	+18	278	12.
35.37	117.65	1075.9	1881	67	903	20	-17	405	12.
34.05	117.18	401.7	760	186	138	76	+166	337	13.
37.48	122.23	9.5	312	13	9	3	+303	49	11.
33.97	117.33	309.4	578	208	187	75	-33	326	13.
37.03	122.10	190.5	191	5	191	5	-21	81	11.
34.13	117.27	342.9	1366	83	337	21	+1	341	13.
34.27	118.47	294.1	578	98	129	84	-1	216	13.
37.78	122.42	15.9	76	8	16	5	+60	31	11.1
37.62	122.38	2.4	195	11	2	1	+193	36	11.1
33.78	116.97	475.8	557	39	476	4	+46	228	14.1
37.35	121.90	21.3	312	45	12	26	+27	66	11.1
35.30	120.67	91.4	132	20	78	9	-13	42	13.1
33.75	117.87	35.1	54	49	2	24	-29	71	14.1
34.43	119.70	30.5	0	8	0	8	+8	8	14.
36.98	122.02	38.1	288	26	4	21	-17	46	12.
34.02	118.50	4.6	5	2	5	2	-5	12	14.6
37.98	120.38	557.8	558	2	558	2	-118	282	11.1
37.50	119.63	1560.6	1561	0	1561	0	-331	318	11.1
37.97	121.38	3.4	124	131	8	18	+4	177	11.1
35.03	118.75	434.3	805	88	196	25	+334	233	13.1
33.62	116.17	-36.6	1562	56	-37	4	+131	384	14.1
35.78	117.38	516.6	2464	93	517	3	+138	429	12.1
34.13	116.03	602.0	2363	79	602	3	+543	457	13.1
34.13	117.68	560.8	886	187	169	136	-264	298	13.8
38.37	122.00	53.3	345	26	53	1	+63	134	11.2
34.53	117.30	871.1	1929	183	735	79	+90	358	13.4
36.33	119.30	107.9	742	178	51	81	-19	285	12.2
33.28	116.63	969.3	1204	25	846	23	+96	118	15.1
36.93	121.77	29.0	29	6	29	6	-17	21	12.3
37.75	119.58	1214.6	1884	15	1215	4	+589	343	11.2
36.90	116.75	1010.1	3512	182	699	57	-32	582	11.4
35.98	114.85	769.6	3537	338	19	202	-93	723	11.8
36.43	115.37	890.0	3374	287	22	172	+440	674	11.6
37.62	118.02	1516.4	3149	20	1516	2	+587	586	11.1
36.58	115.67	955.9	3512	284	699	159	+150	685	11.4
36.17	115.13	611.4	3274	312	19	172	+78	788	11.7
36.53	114.43	371.9	3388	410	372	6	+124	886	11.3
37.27	117.02	1225.3	3184	215	1225	3	+47	589	11.2
35.47	114.92	1079.0	2551	313	148	161	-46	785	12.1

=====

| DATA FOR FEBRUARY |

=====

LAT (deg.)	LONG (deg.)	ELEV (m.)	MAXIMUM		MINIMUM		SLOPE (m.)	COAST DIST	SST (C.)
			ELEV	DIST	ELEV	DIST			
36.85	121.40	36.9	288	82	4	77	+167	103	12.1
37.23	119.22	2139.7	2140	3	2140	3	-690	344	11.5
36.42	120.67	807.7	1043	9	808	6	+235	132	12.4
33.73	116.25	3.4	2066	49	3	2	+138	429	13.8
35.65	117.82	743.7	1653	30	744	6	+275	399	12.5
34.13	115.13	231.0	1644	365	269	26	+187	566	13.3
35.47	118.79	295.7	743	256	70	83	+115	289	12.8
36.87	120.88	154.8	947	143	155	7	+87	190	12.5
36.28	121.13	97.5	947	48	98	6	+176	95	12.5
34.25	117.18	1596.5	1925	54	701	18	-527	349	13.6
34.78	118.15	716.9	1644	80	717	6	+26	281	13.3
37.65	121.78	166.1	348	9	166	4	+174	89	11.6
34.47	117.75	1154.3	1929	145	681	82	+262	295	13.5
38.12	121.28	12.2	337	181	0	19	-3	282	11.2
33.77	118.28	18.4	0	5	0	5	+0	5	14.8
34.85	118.23	95.1	283	68	14	26	-68	188	14.3
37.85	120.85	38.1	466	115	38	6	+165	162	11.9
36.97	120.87	82.3	303	145	25	88	-17	234	11.9
35.88	119.38	207.3	885	23	207	5	+253	176	13.2
37.97	122.18	84.7	215	14	85	4	+130	95	11.4
33.55	116.83	-53.3	1569	44	-53	6	+89	245	14.6
37.38	120.48	51.5	793	115	20	47	-14	287	11.7
35.58	119.82	244.3	776	16	245	5	+531	168	13.8
37.65	121.80	27.7	340	81	19	11	-9	180	11.5
37.33	121.65	1282.9	1283	5	1283	5	-684	103	11.8
34.23	118.87	1748.1	1740	6	1740	6	-1311	253	13.8
34.77	114.62	278.3	1881	351	278	2	+283	689	12.7
33.68	117.88	2.4	2	3	2	3	-1	23	14.9
37.87	120.87	65.5	143	181	0	57	-24	216	11.3
37.88	122.18	134.1	134	7	134	7	-121	51	11.6
34.45	119.25	228.6	1328	38	229	6	+134	141	13.8
34.18	119.17	13.7	14	7	14	7	-14	18	14.4
34.58	118.12	889.2	1929	188	889	5	+218	284	13.4
33.82	116.53	125.3	2066	21	125	7	+488	482	13.8
33.35	116.87	1698.1	1698	3	1698	3	-872	128	14.9
36.53	120.45	128.8	926	27	128	6	+541	141	12.4
34.28	114.17	224.9	1631	487	285	19	+7	688	13.1
34.15	118.13	263.4	379	58	93	23	-145	148	14.1
35.63	120.68	213.4	495	42	213	5	+88	75	13.1
38.23	122.63	4.9	143	22	5	2	+119	57	11.3
36.48	121.18	398.4	632	24	179	18	+1	79	12.4
35.67	121.28	5.5	5	6	5	6	-5	18	13.1

=====

| DATA FOR FEBRUARY |

=====

LAT (deg.)	LONG (deg.)	ELEV (m.)	MAXIMUM		MINIMUM		SLOPE (m.)	COAST DIST	SST (C.)
			ELEV	DIST	ELEV	DIST			
33.60	114.53	88.4	2172	224	88	4	+13	684	13.6
35.18	114.05	1015.9	2464	402	265	206	-296	737	12.1
34.15	114.30	123.4	1530	411	118	19	+10	666	13.1
38.02	121.77	8.5	296	20	9	3	+146	121	11.1
36.48	118.83	517.6	621	224	50	141	+5	349	12.6
37.08	119.48	611.1	748	185	20	139	-151	299	11.7
33.35	118.33	0.0	95	16	0	5	+95	28	14.9
34.95	118.18	806.2	1631	35	806	7	+15	300	13.1
35.42	119.05	158.6	571	111	91	42	-41	238	13.0
34.98	117.02	652.9	1631	137	653	3	+184	432	13.0
33.93	116.98	796.4	796	6	796	6	-259	249	14.1
37.87	122.25	76.2	163	46	7	11	-69	67	11.5
37.20	119.25	1502.1	1772	29	970	23	-52	343	11.5
37.37	118.37	1252.1	3388	47	1252	1	+488	443	11.3
33.62	114.60	81.1	2172	218	81	2	+10	597	13.6
33.28	116.35	198.5	1444	28	191	4	+631	144	15.1
34.18	118.30	207.3	379	42	93	9	-114	124	14.1
35.48	119.47	81.7	776	49	82	4	+204	188	13.1
38.28	120.32	1431.3	1431	6	1431	6	-620	319	10.9
38.25	120.85	200.6	363	216	0	69	-104	272	11.0
38.42	121.53	4.3	363	154	0	18	-4	210	11.0
36.15	120.35	204.5	947	117	158	85	+294	164	12.5
33.87	117.57	216.4	448	17	216	5	+224	172	14.3
34.93	119.62	682.8	1248	13	683	6	+565	116	13.5
34.87	116.78	585.8	1470	151	586	3	+301	454	13.0
38.53	121.75	15.5	529	80	15	11	-1	192	10.9
36.45	116.87	-51.2	3274	153	-51	6	+70	542	11.7
33.80	115.45	296.6	1693	148	141	86	+250	513	13.7
33.67	117.33	391.7	715	29	247	28	+245	86	14.8
33.12	117.08	201.2	201	4	201	4	-48	53	15.3
34.70	118.43	932.7	1929	77	922	26	+95	257	13.3
36.78	119.70	100.9	621	140	48	86	-35	268	11.9
36.73	118.97	2005.6	2006	3	2006	3	-1068	336	11.9
38.43	122.88	64.0	149	23	21	22	-1	44	11.2
36.13	117.95	1165.9	2551	30	1166	5	+999	407	12.2
37.48	122.45	18.3	18	5	18	5	-18	16	11.9
38.07	122.52	.9	188	21	1	6	+84	57	11.4
36.33	119.67	73.8	755	134	60	19	-13	217	12.3
33.70	115.63	417.6	1320	371	141	72	+287	500	13.7
33.23	116.77	823.0	846	10	823	3	+23	107	15.1
37.95	119.78	1179.6	1893	27	1180	6	+427	347	11.1

=====
 | DATA FOR AUGUST |
 =====

LAT (deg.)	LONG (deg.)	ELEV (m.)	MAXIMUM		MINIMUM		SLOPE (m.)	COAST DIST	SGT (C.)
			ELEV	DIST	ELEV	DIST			
34.07	117.77	260.6	268	11	261	5	+7	76	17.4
36.07	119.02	119.8	776	109	63	59	+18	198	16.7
35.37	117.65	1075.9	1333	158	718	34	-17	210	17.7
34.05	117.18	401.7	728	45	402	8	+166	89	17.5
37.48	122.23	9.5	312	13	9	3	+303	37	15.8
33.97	117.33	389.4	546	29	276	16	-33	83	17.5
37.83	122.10	190.5	195	42	8	26	-21	62	14.8
34.13	117.27	342.9	546	43	213	36	+1	97	17.5
34.27	118.47	294.1	294	4	294	4	-1	48	17.4
37.78	122.42	15.9	195	19	16	5	+60	34	14.8
37.62	122.38	2.4	195	11	2	1	+193	25	14.9
33.78	116.97	475.8	633	41	412	31	+46	85	17.6
37.35	121.98	21.3	466	23	21	4	+27	59	15.2
35.38	120.67	91.4	91	7	91	7	-13	27	16.7
33.75	117.87	35.1	35	8	35	8	-29	27	17.5
34.43	119.78	38.5	8	8	8	8	+0	8	17.2
36.98	122.02	38.1	38	3	38	3	-17	15	15.3
34.02	118.58	4.6	5	2	5	2	-5	12	17.2
37.96	120.38	557.8	803	129	19	76	-118	286	15.4
37.58	119.63	1560.5	1561	8	1561	8	-331	253	15.9
37.97	121.38	3.4	446	107	3	6	+4	142	15.1
35.03	118.75	434.3	1807	38	434	3	+334	117	17.2
33.62	116.17	-36.6	1444	50	-37	4	+131	149	18.1
35.78	117.38	516.6	1807	188	517	3	+138	266	17.2
34.13	116.03	602.8	1562	79	141	43	+543	177	17.7
34.13	117.68	568.8	561	5	561	5	-264	67	17.4
38.37	122.00	53.3	163	77	1	52	+63	86	14.6
34.53	117.38	871.1	1599	34	871	6	+98	148	17.5
36.33	119.30	107.9	571	107	35	56	-19	196	16.5
33.28	116.63	969.3	1065	12	969	3	+96	188	18.2
36.93	121.77	29.8	34	22	12	11	-17	29	15.4
37.75	119.58	1214.6	1804	15	1215	4	+589	273	15.8
36.98	116.75	1010.1	2464	177	195	37	-32	433	17.1
35.98	114.85	769.6	1925	318	320	141	-93	488	17.2
36.43	115.37	898.8	2139	48	898	6	+448	437	17.3
37.62	118.02	1516.4	3512	77	1367	42	+587	374	16.3
36.58	115.67	955.9	1939	28	956	6	+158	434	17.2
36.17	115.13	611.4	1462	38	611	5	+78	417	17.4
36.53	114.43	371.9	1429	394	341	208	+124	483	17.3
37.27	117.02	1225.3	3182	148	528	87	+47	428	16.7
35.47	114.92	1079.0	2084	233	558	101	-46	358	17.5

 | DATA FOR AUGUST |

LAT (deg.)	LONG (deg.)	ELEV (m.)	MAXIMUM		MINIMUM		SLOPE (m.)	COAST DIST	SST (C.)
			ELEV	DIST	ELEV	DIST			
36.95	121.40	86.9	572	14	87	4	+167	75	15.7
37.23	119.22	2139.7	2140	3	2140	3	-690	255	16.7
36.42	120.67	807.7	1043	9	808	6	+235	105	16.7
33.73	116.25	3.4	1569	26	3	2	+138	134	17.8
35.65	117.82	743.7	1929	156	286	112	+275	244	17.7
34.13	115.13	281.0	1444	162	-13	108	+187	260	18.7
35.47	118.78	295.7	1248	110	92	49	+115	200	17.4
36.07	120.08	154.8	788	28	155	7	+87	123	16.4
36.20	121.13	97.5	743	34	98	6	+176	50	16.8
34.25	117.18	1586.5	1586	5	1586	5	-527	111	17.5
34.70	118.15	716.9	1062	22	717	6	+26	119	17.4
37.65	121.78	166.1	446	52	12	35	+174	86	15.2
34.47	117.75	1164.3	1619	16	1164	3	+262	96	17.2
38.12	121.28	12.2	348	59	0	23	-3	144	15.8
33.77	118.20	10.4	0	5	0	5	+0	5	17.4
34.05	118.23	95.1	95	6	95	6	-68	41	17.4
37.05	120.85	38.1	698	92	38	6	+165	136	15.8
36.97	120.07	82.3	881	151	50	29	-17	187	16.8
35.08	119.38	207.3	1248	41	207	5	+253	131	17.4
37.97	122.10	84.7	215	14	85	4	+138	62	14.7
33.55	116.03	-53.3	1196	73	-53	6	+89	163	18.2
37.30	120.48	51.5	650	74	34	40	-14	179	15.2
35.50	119.82	244.9	776	16	245	5	+531	111	16.9
37.65	121.08	27.7	803	63	19	11	-9	148	15.4
37.33	121.65	1282.9	1283	5	1283	5	-684	74	15.3
34.23	118.07	1740.1	1740	6	1740	6	-1311	57	17.2
34.77	114.62	278.3	1569	215	141	189	+283	322	17.8
33.60	117.88	2.4	2	3	2	3	-1	16	17.6
37.87	120.87	65.5	803	86	19	36	-24	164	15.3
37.80	122.18	134.1	195	34	1	20	-121	51	14.9
34.45	119.25	228.6	363	13	229	6	+134	35	17.2
34.18	119.17	13.7	14	7	14	7	-14	10	17.4
34.58	118.12	809.2	1114	15	809	5	+210	113	17.5
33.82	116.53	125.3	1562	22	125	7	+488	120	17.7
33.35	116.87	1690.1	1690	3	1690	3	-872	64	17.8
36.53	120.45	128.0	1043	32	128	6	+541	128	16.2
34.28	114.17	224.9	1502	266	-70	187	+7	357	18.5
34.15	118.13	263.4	263	3	263	3	-145	55	17.4
35.63	120.68	213.4	412	16	213	5	+80	49	16.5
38.23	122.63	4.9	188	16	5	2	+119	41	14.6
36.48	121.18	398.4	881	38	158	13	+1	74	16.8
35.67	121.29	5.5	5	6	5	6	-5	10	16.4

 | DATA FOR AUGUST |

LAT (deg.)	LONG (deg.)	ELEV (m.)	MAXIMUM ELEV.	DIST	MINIMUM ELEV.	DIST	SLOPE (m.)	COAST DIST	SST (C.)
33.60	114.53	88.4	1037	203	-31	104	+13	285	18.5
35.18	114.85	1015.9	1562	294	141	258	-296	393	17.7
34.15	114.30	123.4	1502	248	-70	167	+10	338	18.5
38.02	121.77	8.5	340	19	9	3	+146	95	14.9
36.48	118.83	517.6	571	151	49	98	+5	248	16.7
37.08	119.48	611.1	1043	138	51	78	-151	226	16.0
33.35	118.33	8.0	95	16	0	5	+95	19	18.1
34.95	118.18	886.2	1183	46	720	10	+15	134	17.3
35.42	119.05	150.6	1248	88	92	26	-41	176	17.4
34.90	117.82	652.9	1925	89	653	3	+184	178	17.2
33.93	116.98	796.4	796	6	796	6	-259	94	17.6
37.87	122.25	76.2	76	1	76	1	-69	52	14.8
37.28	119.25	1502.1	1502	6	1502	6	-52	251	16.0
37.37	118.37	1252.1	3512	36	1252	1	+480	331	16.4
33.62	114.60	81.1	1149	191	-49	118	+10	281	18.6
33.28	116.35	198.5	1196	31	191	4	+631	120	18.3
34.18	118.30	207.3	207	8	207	8	-114	36	17.2
35.48	119.47	81.7	869	48	82	4	+284	137	17.1
38.28	120.32	1431.3	1431	6	1431	6	-620	231	15.2
38.25	120.85	208.6	348	114	0	63	-184	184	15.0
38.42	121.53	4.3	215	78	0	10	-4	130	14.7
36.15	120.35	204.5	683	21	205	4	+294	109	16.4
33.37	117.57	216.4	448	17	216	5	+224	58	17.5
34.93	119.62	682.8	1358	23	683	6	+565	93	17.4
34.87	116.78	585.8	1925	104	586	3	+301	202	17.4
38.53	121.75	15.5	163	105	1	79	-1	114	14.6
36.45	116.87	-51.2	1798	130	-51	6	+70	403	17.4
33.88	115.45	296.6	1196	132	-68	61	+250	222	18.3
33.67	117.33	391.7	637	17	392	7	+245	51	17.6
33.12	117.88	281.2	281	4	281	4	-48	41	17.9
34.78	118.43	932.7	1028	8	933	7	+95	100	17.3
36.78	119.78	188.9	821	111	51	42	-35	198	16.3
36.73	118.97	2085.6	2086	3	2086	3	-1068	246	16.4
38.43	122.88	64.0	64	6	64	6	-1	29	14.4
36.13	117.95	1165.9	2464	41	1166	5	+999	314	17.3
37.48	122.45	18.3	18	5	18	5	-18	16	14.9
38.87	122.52	.9	163	22	1	6	+84	38	14.7
36.33	119.67	73.8	788	73	54	20	-13	178	16.4
33.78	115.63	417.6	1196	112	-68	41	+287	204	18.2
33.23	116.77	823.0	846	10	823	3	+23	79	18.1
37.95	119.78	1179.6	1719	12	1180	6	+427	237	15.4